Mathematical Models of Depth Perception in Weakly Electric Fish

Babak Pourziaei

A Dissertation Submitted To The Faculty Of Graduate Studies In Partial Fulfillment Of The Requirements For The Degree Of

Doctor of Philosophy (PhD)

Mathematics & Statistics

York University

Toronto, Ontario

June 2013

Abstract

Weakly electric fish use electrolocation - the detection of electric fields - to sense their environment. The task of electrolocation involves the decoding of the third dimension – depth – from a two-dimensional electric image. In this work we present three advances in the area of depth-perception. First, we develop a model for electrolocation based on a single parameter, namely the width of the electric image. In contrast to previous suggested algorithms, our algorithm would only require a single narrow tuned topographic map to accurately estimate distance. This model is used to study the effects of electromagnetic noise and the presence of stochastic resonance. Second, considering the problem of depth perception from the perspective of information constraints, we ask how much information is necessary for location disambiguation? That is, what is the minimum amount of information that fish would need to localize an object? This inverse problem approach gives us insight into biological electrolocation and provides a guide for future experimental work. Our final contribution is to provide a mathematical foundation for two of the most accepted depth perception models currently in use.

To my mother Jila, who has never left my side. This work is as much mine as hers for she suffered along with me every step of the way.

Acknowledgements

From the formative stages of this thesis, to the final draft, I owe an immense debt of gratitude to my supervisors, Drs. Huaxiong Huang and Greg Lewis. Their sound advice and careful guidance have been invaluable. I would also like to thank Dr. John Lewis who worked behind the scenes to make sure we did not deviate from the biology. Finally, I would be remiss without mentioning my committee members, Drs. Hugh R. Wilson and Tom Salisbury whose helpful advice and input kept this work congruent. To each of the above, I extend my deepest appreciation.

Contents

List of Tables

List of Figures

LIST OF FIGURES

1

Introduction

The electric sense, the biological ability to perceive natural electrical stimuli, has fascinated scientists and non-scientists for decades. Although its function remained a mystery, the presence of an electric organ in weakly electric fish had been known since the nineteenth century. Termed pseudoelectric these fish did not produce the strong fields required for prey capture and predator avoidance as did their strongly electric cousins. The first indication for the true function of these fish's electric organ came in the 1950's. Hans Lissmann found [1] that the fish could discriminate between a porous porcelain container with aquarium water and one in which 20% of the liquid was distilled water-and that discrimination could not have been possible by chemical, mechanical, or visual clues but must have been the result of electrical conductivity of the fish's organ discharges. Since Lissmann's instrumental work, a long series of research has been devoted to understanding this new sense modality.

We now know that weakly electric fish are comprised of two orders of freshwater teleost, the South American Gymnotiformes and the African Mormyriformes. These fish inhabit aquatic environments in which visual cues are limited, and have evolved the ability to generate and detect weak electric fields in order to both perceive their environment and communicate with conspecifics. In addition to these "active" electric fish, possessing the ability to generate electric fields, we have learned that other aquatic species such as sharks, rays and catfish can detect low frequency fields (less than 20 Hz) even though they lack the electric organ. Termed "passive", these fish sense natural electric fields from sources other than the electric organs.

All aquatic animals generate weak electric fields as a result of the uneven distribution of ions between the interior of the animal and its environment [2]. Such biological sources of electrical potential serve as important cues for predatory fish, and hence there is a great premium in being able to detect such fields. Low frequency electrosensory systems, responsible for the detection of such signals, are found in all electrosensory fish. In addition to this low frequency sensitive ampullary system, active electric fish possess tuberous electroreceptors. Tuberous receptors are tuned to frequencies within or near the electric organ discharge frequency of the respective species.

The self-generated electric field produced by the electric organ is perturbed by objects whose electric properties differ from that of the surrounding water. These perturbations are sensed by the tuberous receptors, and constitute an electric image on the surface of the fish. The electric image is analyzed to extrapolate information about the particular object. In addition to prey detection, the electric sense is used for sex and species recognition, courtship, aggression and appeasement [3, 4].

1.1 Electrogenesis

Electrogenic fish, defined as those capable of producing electric fields, can be categorized according to the strength of the field they produce. Strongly electric fish have been known to man for centuries, as the strength of their field makes them painful to handle. The strong electric field is used as a weapon for both prey capture and predator avoidance. Recognition of weakly electric fish only occurred in the 20th century [5], a delay due to the imperceptibility of their weak discharges. In weakly electric fish, the generated field is a part of the electrosensory system, utilized for both environmental perception and communication.

1.1.1 Electric Organ

In both weak and strong categories, specialized cells called electrocytes are configured in series and in parallel (in accordance to the particular species) to form the electric organ (EO), a specialized organ for the production of the electric field outside the body. Electrocytes are modified muscle cells, and are electrically excitable much like other

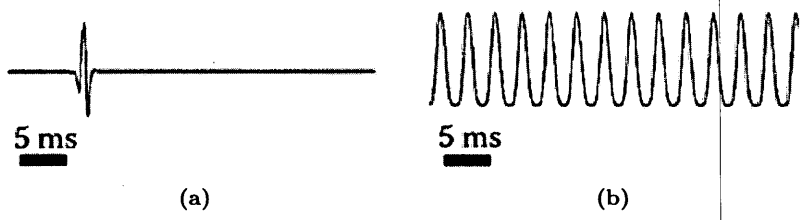

Figure 1.1: EOD waveforms - (a) Pulse-type EOD waveform from *Gymnotus varzea.*(b) Wave-type EOD waveform from *Eigenmannia cf. virescens* (from [7]).

electrogenic cells such as neurons. The cells are flattened and are innervated by an electrocyte stalk. The stalk in some cases penetrates the cells to innervate on the opposite side.

The EO is usually found in the tail, though it can be located anywhere (for example, in the strongly electric rays, the electric organ is located in the head region). The geometry of the EO, innervation of the cells and non-electrogenic tissue determine the firing pattern and thus the field shape. Strongly electric fish produce monophasic electric organ pulse discharge resulting from simultaneous activation of the electrocytes. The electric organ discharge (EOD) generated by weakly electric fish can be monophasic, diphasic, triphasic or more complex [6]. Such pulses can be separated by either a long or short intervals. Weakly electric fish can be categorized according to these interpulse intervals. The EOD of pulse-type fish consists of individual pulses followed by relatively long and often highly variable intervals of silence (figure 1.1a). The duration of pulses emitted by wave-type fish are as long or longer than the intervals between them resulting in a quasi-sinusoidal discharge pattern (figure 1.1b). Wave EODs are usually of constant frequency and amplitude.

1.1.2 Function

Electrocytes function on the same general principle as ordinary nerve and muscle cells. Potentials result from selective permeability and passive movement of ions down their concentration gradients. The EOD is controlled by a set of neurons, the command nucleus, located in the brain stem. Discharges of the command nucleus trigger a relay structure that projects to the spinal structures which in turn transform the series of

command impulses into a series of stereotyped EODs [8]. Several mechanisms exist for the control and synchronous activation of the electrocytes. Synchronization is achieved by equally lengthed nerve fibers running from the command nucleus to different parts of the EO. This translates to fibers which take meandering paths to nearby parts of the EO and more direct paths to more distant parts. A second mechanism involves varying the conductivity of the fibers. With distant parts of the EO being reached by more conductive and nearer parts by less conductive fibers, the time that a signal would take to reach different parts of the EO can be equalized.

1.1.3 Electric Field

Recent advances have been made in understanding the spatiotemporal pattern of the EOD field and its interaction with objects in the environment [9]. The field generated in the exterior of the fish by the EO of weakly electric fish resembles an elongated dipole [10]. Measured close to the fish's body, field amplitudes of weakly electric fish are generally on the order of a few hundred millivolts per centimeter [8]. As we travel through one cycle of the EOD wave, the head-to-tail potential difference begins with the head taking a positive potential relative to the tail (figure 1.2). This positive potential travels down the fish body to the trunk and then the tail, at which point the head becomes negative relative to the tail.

1.1.4 Electric Image

Objects whose electrical properties (ohmic resistance and/or capacitive reactance) differ from that of the surrounding water distort the field produced by the fish. The distortion, constitutes an "electric shadow" or electric image (EI) on the surface of the fish. The electric image is an area in which the density of the current lines defining the fish's electric field has changed. Objects with lower impedance than the surrounding water attract the field lines and cause more current to flow through them. Higher impedance values repel field lines and decrease current flow (figure 1.3). Changes in current flow are sensed by specialized electroreceptor organs.

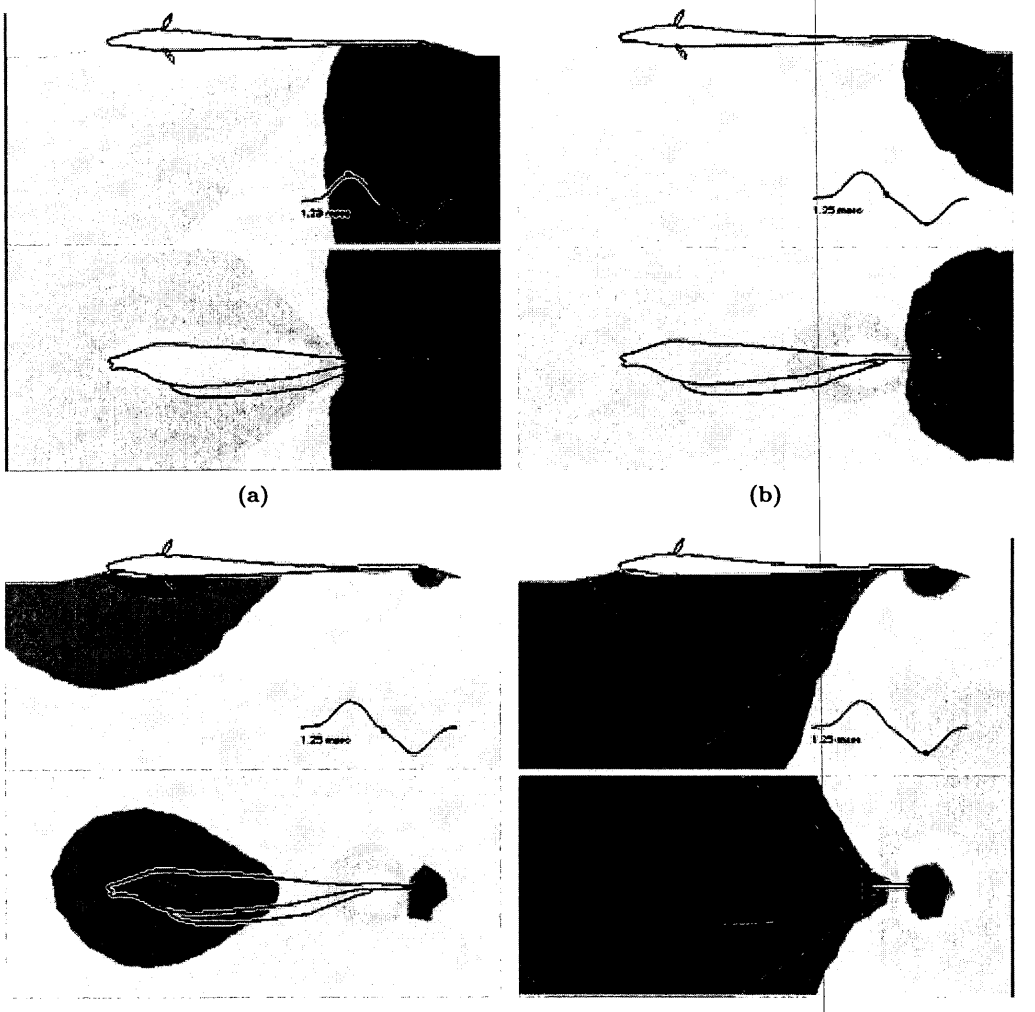

Figure 1.2: Spatiotemporal EOD pattern - (a)–(d) Electric field generated by EOD of *Apteronotus leptorhynchus* at different points along the EOD cycle, depicted by the black curve (inset). Light blue representing zero; green - yellow - red represent successively greater positive values; and blue - dark blue - violet representing successively negative values of the potential and field magnitude. In each figure the top pannel represents a view from the top down and the bottom pannel a lateral view of the fish, (from [11]).

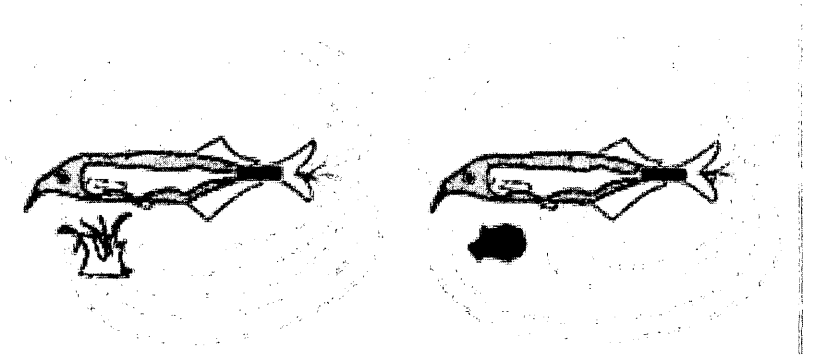

(a) (b)

Figure 1.3: Field distortion by dielectric objects - (a) Distortions of the electric field caused by objects with differing impedances. Objects with low impedance "attract" the electric field lines and result in more current flowing through the electroreceptor organs in that part of the body located opposite to the object. (b) Objects with higher impedance than the surrounding water reduce the current flow in the corresponding electroreceptors as compared with the flow in the absence of the object. (From [12]).

1.2 Electroreception

Soon after the discovery of electrolocation capabilities of weakly electric fish, electroreceptors, the organ responsible for the detection of electric fields was identified [13, 14]. Active electric fish possess two types of electroreceptors, each designed to extract different signal information. Ampullary receptors are sensitive to low-frequency stimuli, and act primarily as passive sensors of natural electric fields from sources other than electric organs. They are present in all electroreceptive fish. In contrast, tuberous receptors, which are unique to fish possessing an electric organ, respond to the high frequency components of the EOD (from tens of Hertz to more than one kilohertz), and are insensitive to DC signals. These receptors have evolved independently in two groups of freshwater fish; the Gymnotiformes of South America and the Mormyriformes of Africa. None of the common ancestors of these two groups is capable of electrogenesis or electroreception.

1.2.1 Physiology

Considerable anatomical differences exist between tuberous receptors in different species. However, all tuberous receptors follow the same basic physiological design. One to tens of sensory cells are housed within a jelly-filled intra-epidermal chamber. The chamber is covered by a plug of loosely packed epidermal cells, (figure 1.4). Supporting cells situated below the sensory cells are thought to be involved with the production of the jelly which fills the chamber. Only a small part of the basal face of the sensory cells is anchored to the supporting cells. The apical and basal membranes are electrically and chemically isolated from each other by means of tight junctions [15]. The apical membrane of each sensory cell is covered by a large number of microvilli which are believed to act as a coupling capacitor [16], allowing AC signals to pass through while at the same time blocking DC signals.

All sensory cells in an organ are innervated by a single nerve fiber that divides to form several synaptic connections on the basal membrane of individual sensory cells [15]. Each fiber innervates from one to tens of closely clustered electroreceptor organs. The spatial receptive field of afferent fibers is large, contributing to the blurredness of electric images.

The apical face of the sensory cells is passive and low resistance while the basal surface through which current is funneled acts as the voltage sensor and contributes to transduction [17]. Flow of current depolarizes the basal membrane changing the amount of released neurotransmitter and hence the firing rate of the afferent fiber.

Tuberous electroreceptors are distributed widely over the animal surface with higher concentration being found in the rostral region. Here the receptors of Gymnotiformes fish have a density from nine to fifteen organs/mm^2, while, over the operculum region, their density falls to seven to nine receptor organs/mm^2 [18]. On the trunk, the absolute densities are far lower than on the head, ranging between 0.6 and 3.4 tuberous electroreceptor organs/mm^2.

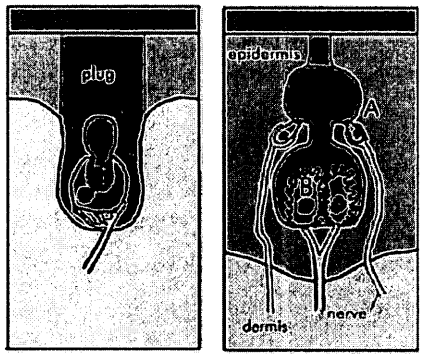

Figure 1.4: Tuberous electroreceptor organ - (a) Schematic drawings of tuberous electroreceptors of a *Gymnarchus* and (b) mormyrid fish. (From [19]).

1.2.2 Function

Tuberous receptors are specialized into subcategories, usually two in each species, differing in the dynamics of response and hence in their functional roles. Time-coding tuberous electroreceptors encode the temporal characteristics of the EOD pattern while amplitude-coding receptors encode amplitude information. All weakly electric fish irrespective of their particular EOD pattern (wave/pulse) possess both types of receptors.

Amplitude Coding

The amplitude of a signal carries information about the size, distance and resistivity of an object. The afferent fibers of wave type fish fire action potentials in a probabilistic manner. Signal amplitude is encoded by an increase in the firing rate of the fibers [20], (figure 1.5). The afferent fibers of pulse type fish, termed burst-duration coders, fire bursts of action potential of varying duration to represent the local amplitude of the EOD [21].

Time Coding

The temporal features of stimuli convey information about the capacitance of objects, as well as the waveform of the EOD. Time coding is important in behavioral functions such as electrolocation and jamming avoidance response (JAR). The time coding afferent

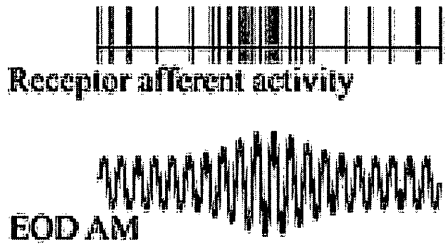

Figure 1.5: AM transduction - Transduction of EOD amplitude modulation (AM) to electrical impulses. Top panel depicts the modulation of the EOD amplitude by a dielectric object. Bottom panel shows how this amplitude modulation is encoded by and increase in the firing rate of the the amplitude coding receptors.

fibers of wave-type fish, termed tonic time coders, fire one action potential for each cycle of the EOD, thereby maintaining a continuous one-to-one firing pattern with the EOD. In pulse-type fish, time coding afferents, termed pulse markers, also fire a single action potential for each EOD cycle. It is interesting to note that both tonic time coders as well as pulse markers show varying degrees of amplitude-dependent latency changes and as such entail time-amplitude ambiguity [21, 22, 23].

Frequency Tuning

Time coding tuberous electroreceptors of wave type fish are sharply tuned to the particular frequency of the fish's EOD, showing a V-shaped threshold tuning curve [24] (figure 1.6). In pulse type species, the frequency components of the pulse, rather than its repetition frequency are important [25]. Using Fourier analysis Bastian has shown that the EOD pulse is comprised of broad spectra with peaks roughly matching the best frequency of receptor tuning [21, 26].

1.2.3 Processing Pathways

Amplitude information undergoes substantial processing in the electrosensory lateral line lobe (ELL), an anatomical structure in the hindbrain. The ELL consists of several different zones that receive input from different types of primary afferent fibers.

In Gymnotiform fish the fibers make synaptic connections with pyramidal cells, which

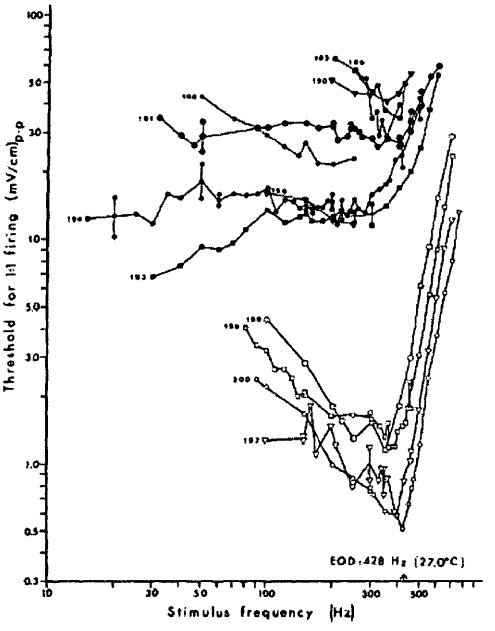

Figure 1.6: Tuberous tuning curves - Tuning curves for tuberous electroreceptors from a single *Eigenmannia*. Peak-to-peak thresholds were determined by measuring the minimum electric field required to elicit one spike on each stimulus period. The arrow shows the fish's EOD frequency prior to the experiment. *Filled circles:* amplitude-coding P-type afferent; *open circles:* time-coding T-afferents (from [24]).

in turn extract features such as increases and decreases in amplitude. The ELL of Gymnotiform fish can be segmented into three distinct regions; lateral, centromedial and centrolateral. Amplitude-coding afferent fibers map onto each of the zones [27]. Physiological differences such as the different rates of convergence reflect differences in function [25]. Neurons in each segment are topographically organized to form a spatial map of the electrosensory periphery [18]. These neurons respond maximally for one location, with their activity decreasing for locations away from this preferred location; hence neuronal responses are described by bell-shaped tuning curves.

The width of the tuning curves within each of the ELL segments differ. Neurons in the lateral map have a large or coarse receptive field and are the most sensitive of the three maps, responding to high-frequency amplitude modulations. Centromedial neurons have the smallest and most precise receptive field, and respond to low-frequency amplitude modulations. The centrolateral map consists of neurons with intermediate spatial and temporal characteristics [25]. Estimates of the physiological range of the tuning curve width are between 0.3 and 0.7 cm depending on the particular ELL map [28].

It has been shown that different electric image features are best estimated using different tuning curve widths. For example wider tuning curves can more accurately estimate the peak amplitude of the electric image, whereas, to encode image width, narrower tuning curves would result in higher accuracy [28]. One simple algorithm for calculating image width is to first normalize the neural responses to the maximal response and then count the number of neurons that are active above a certain threshold [9].

Descending control plays an important role in the information processing that takes place in the ELL. In the ELL of Gymnotiform fish, efferent input is received from the nucleus of praeemintialis (PE), a midbrain structure. The input follows one of two pathways. Stellate cells from the PE project directly onto the ventral molecular layer of the ELL. Bratton and Bastian [29] suggested that the direct pathway from the PE to the ELL may enhance the sensitivity of ELL neurons to a local and novel stimulus. The second pathway consists of multipolar neurons projecting onto the eminentia granularis posterior (EGp) which in turn project onto the dorsal molecular layer of the

ELL [30]. It has been suggested that this descending input pathway serves as a gain control mechanisms [25]. Upon processing of information the ELL in turn projects onto the torus semicirularis, a structure in the midbrain. The torus semicircularis contains neurons that respond to amplitude and time (phase) modulations.

1.3 Aim of the Thesis

Electrolocation is the task of actively localizing a target object from sets of electric images. The rostro-caudal (2D) position of a target object relative to the animal's body surface can be determined from the pattern of activity over the 2D array of electroreceptors. Namely, the peak amplitude of the electric image coincides with the rostro-caudal location of the object. Evaluation of the lateral distance of the object to the fish surface is a far more difficult task. The electric image of an object depends on its electrical properties, size, and shape and on its distance from the fish. As such, for an object whose properties are unknown, no single electric image feature is sufficient for identifying the lateral distance (figure 1.7). Relying on multiple object features requires the use of multiple ELL maps with differing receptive fields for an accurate estimation. Several depth perception models have been proposed (see chapter 2). These models, based on empirical evidence, depend on multiple image parameters. Our first goal in this work is to provide a mathematical verification of these models (section 2.3). Next, we aim to develop a depth perception model which depends on a single electric image parameter (chapter 3). Such a mechanism is possible if the temporal characteristics of the electric image are taken into account. Finally, considering a static electric image, we would like to explore the minimum amount of information that would be required for the fish to unambiguously decode the location of an object (chapter 4). This goal requires a completely different approach to the problem of depth perception. We need to consider the information available at a single electroreceptor as opposed to the pattern of the generated electric image. Identification of the sensory processing algorithm used in depth perception would provide physiologists with important clues that should facilitate the search for neural correlates of this behavior.

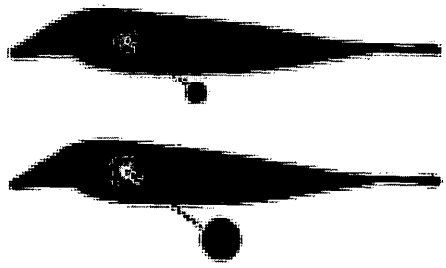

Figure 1.7: Size-distance ambiguity - A schematic of the two-dimensional electric image on the surface of the fish for objects of two different sizes and lateral distances. Although the widths of the images are different, the peak amplitudes are the same (measured in grayscale, with white being the largest). Thus, detecting object distance based only on amplitude leads to ambiguities, (from [28]).

2

Literature Reveiw

It is without doubt that weakly electric fish use their electric sense to locate objects [31]. Much work has been conducted in understanding how these fish perform this task. Although the rostro-caudal location of an object can be associated directly to the location of the peak electric image, the measure relating electric image features to the object distance has not been completely understood. Several depth perception algorithms have been proposed. These algorithms can be categorized into those which rely on static electric image features and those which incorporate the temporal aspects of the electric image. We have termed these algorithms static and spatiotemporal models, respectively. In this chapter we will begin with a review of past proposed algorithms. We note that of these algorithms those of Rasnow [32] and von der Emde [31] have become the accepted models within the community. Some questions remain as to which, if any, the fish actually use for object localization. We provide a mathematical proof that both methods can in fact be used for depth perception.

2.1 Static Models

2.1.1 Rasnow Model

Rasnow and his colleagues have used both direct measurements as well as mathematical simulations to model the electric image produced by a dielectric sphere [9, 32, 33]. Recognizing that each image feature (e.g. peak amplitude, width, phase shift) is dependent on multiple (unknown) object features (distance, size, impedance), creating

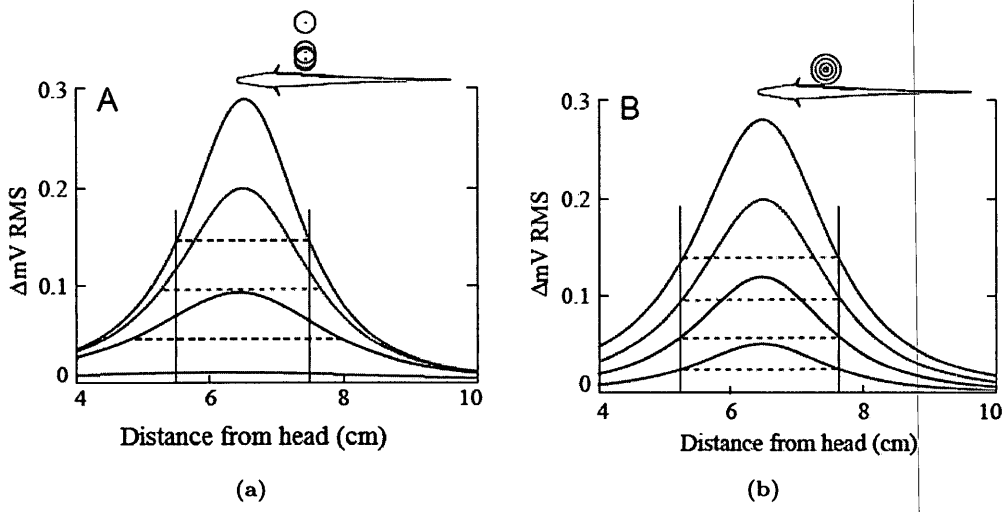

Figure 2.1: Raswnow model - (a) Electric images of conducting spheres in the midplane of *Apteronotus leptorhynchus*. Images from a 1 cm sphere at four object distances (inset), and (b) from four object sizes at the fixed distance of 1.4 cm. Dashed horizontal lines represent the relative width of the object image, with vertical lines to facilitate comparisons, (figures provided from [9]).

size-impedance-distance ambiguities, Rasnow proposed the use of multiple image parameters for decoding the object-fish distance. Rasnow suggested a method by which the fish calculate the relative width of the electric image, that is the width measured at half peak amplitude. He hypothesize that this measure is solely dependent on the object distance, and hence can unambiguously reveal depth information. Theoretical work has shown that this measure is independent of object size, (figure 2.1). However, von der Emde has pointed out that this measure can only be used to disambiguate the distance of an object whose impedance is already known [12], a fact that clearly does not hold true when the fish is presented with novel objects.

2.1.2 von der Emde Model

In a series of elegant behavioral experiments, von der Emde and his colleagues showed definitively that the weakly electric fish, *Gnathonemus petersii*, could use their electric sense for localization [12, 31, 34]. The experiments consisted of partitioning the fish tank into two compartments with two gates (gaps) built into the partition wall (see

figure 2.2). Objects were placed beyond each gate at different distances to the gate. In a forced-choice experiment the fish were trained to swim through the gate beyond which the object was furthest away.

It was shown that not only could the fish accurately determine the relative distance of two identical objects, but they could also correctly identify the relative distance when the objects differed in size and conductivity. Interestingly, von der Emde also found that when presented with a cube and a sphere of the same radius, the fish misjudged the distances and perceived the spheres to be further away, even when this was not the case.

Von der Emde proposes the use of a ratio of image features; namely that of maximal slope to peak amplitude, as a measure of object distance [12, 31, 34]. Empirical data obtained from *Gnathonemus petersii* indicate that the caudal image slopes of different electric images vary unsystematically with object distance, and so it cannot provide any reliable distance cues. To this end von der Emde suggests the fish use the rostral image slopes to determine the slope-to-amplitude ratio.

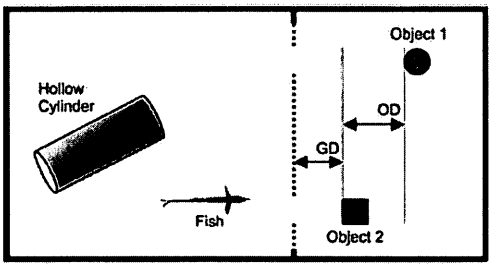

Figure 2.2: Von der Emde experimental set-up - Schematic of von der Emde's experimental tank set-up as seen from above. The thick dotted line marks the position of the dividing wall, containing the two gates (gaps). The distance between the gate and the closer object is denoted gate distance (GD). The distance between the two objects is the inter-object distance (OD).

2.2 Spatiotemporal Models

The importance of the temporal properties of the electric image in object localization was first alluded to by Rasnow [32]. Electric fish explore actively by moving their

bodies and tails around objects [35, 36]. It is well documented [37, 38, 39] that tail bending movements of electric fish are often involved with prey capture. Such probing movements change the magnitude of the electric image at the object and could provide further cues to object location.

2.2.1 Sim & Kim

Sim and Kim used mathematical modeling to study the effects of tail bending on the transdermal potential measured at a receptor [40]. They observed that changes in the lateral distance of an object significantly altered the temporal pattern of transdermal potential. Interestingly, object size and conductivity had no effect on the pattern. This led Sim and Kim to conclude that the temporal variation at a fixed electroreceptor during tail bending could allow localization of a target object.

Noting that fish may not be able to recognize the multitude of possible temporal patterns, Sim and Kim propose the use of the measure *slope ratio* to determine the lateral distance of an object. The slope ratio is defined as the ratio of the temporal changes in potential when the tail is bent from left to mid-line and from mid-line to the right with the same time interval. It is important to note that since the temporal pattern depends on the rostrocaudal position of a target object, the slope ratio curve also changes depending on the object's rostrocaudal position.

2.2.2 Englemann

Beside frontal approaching, exploratory behavior of weakly electric fish *Gnathonemus* include back and forth swimming, termed *va-et-vient* sampling. Hofmann *et al.* [41] use values from a mathematical model to study the electric image at one receptor during a va-et-vient object inspection. Mapped as a function of time, the modulations of the electric field at the receptor resemble a bell curve and are termed the temporal electric images (tEI), (see figure 2.3). Taking a similar approach as von der Emde, Hofmann *et al.* calculated the slope-to-amplitude ratio (tSAR) of the tEI. They found for a range of object size, the tSAR was size-invariant, and thus allowed for distance estimation.

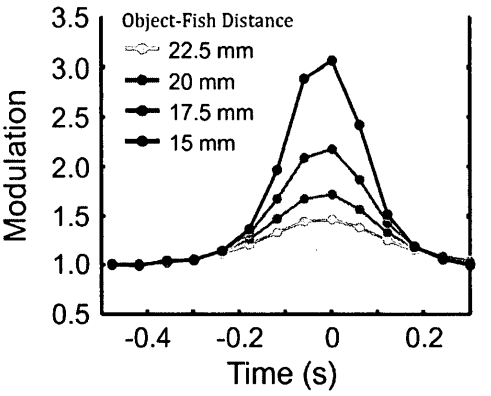

Figure 2.3: Temporal electric image - Electric image at a single receptor during va-et-vient object inspection for different object-fish distances.

2.2.3 Chen

The model developed by Rasnow was based on the assumption that the dielectric object is placed within a uniform electric field. Chen and colleagues expanded this viewpoint by developing a model of the electric field generation comprised of an array of point sources and sinks distributed along the midline of the fish [42]. Their model was in close agreement with the field measurements taken from several species of gymnotid fish [10]. Chen and colleagues used their model to estimate the spatiotemporal pattern of activation during active electrolocation when an object is moved passed a fish. The authors found that the measure proposed by Rasnow, namely the width at half peak amplitude was an accurate measure of object distance, and is size invariant with object distance.

2.2.4 Babineau

Babineau and colleagues used a model of the electric field generated by *Apternotus leptorhynchus* to study spatial acuity and small signal extraction [43]. The authors focus on a measure, *electro-acuity*, defined as the minimum spatial separation of two objects, such that two distinct peaks remain in the electric image on the fish's skin.

It is found that electro-acuity varies at different lateral distances, but is invariant with object conductivity and size. As such, it could provide a cue for localization. Further,

the authors found that to a reasonable approximation, electro-acuity is proportional to the normalized width of the image (width divided by amplitude) due to each of the objects. This is compatible with the relative width measure used for depth perception by Rasnow [32] .

Babineau and colleagues have simulated the va-et-vient scanning motion and show that under some conditions this behavior could assist in extracting small prey-like signals from large background ones. When the constituent objects of a complex scene are close enough to each other to result in a blurred (spatially uniform) image, a small spatially localized prey will affect the image by only a few percent. This suggests that fish using a static electric image would be unable to extract the prey signal from the large-background signal. However, during va-et-vient scanning, the blurred background component of the electric image does not change, whereas that due to the prey does. Consequently the prey signal is revealed during the scanning motion by looking at the transdermal potential at individual location on the fish's body.

2.3 Mathematical Verification of Rasnow & von der Emde Models

In this section, we would like to put the algorithms presented by Rasnow [32] and von der Emde *et al.* [31], herein referred to as the Rasnow and von der Emde Models, respectively, on a solid mathematical footing. First, we show that in contrast to von der Emde's claim [12], the method proposed by Rasnow can in fact disambiguate the location of a spherical object whose size and electrical properties are unknown. Second, we provide a mathematical proof that, for localization of a dielectric sphere, the ratio of maximum slope to peak amplitude is in fact solely dependent on the object distance as von der Emde *et al.*'s empirical data suggest. In both cases we find a simple equation relating the distance of a spherical object to the particular measure in question.

Electric Image

We begin by considering fields perpendicular to the fish surface. Such fields are of greatest significance, as they appear predominantly in the rostral region of the fish [44], where electroreceptors are most dense.

Next, to study the effects of a dielectric sphere on this uniform field, we orient a Cartesian reference frame such that the origin coincides with the sphere's center and the applicate (z-direction) lies parallel with the direction of the unperturbed field.

Over the region of interest, we approximate the fish surface to be planar. If the fish-object distance is d, the fish surface plane Π consists of points having the form (x, y, d). Assume the unperturbed field to be uniform with magnitude E, given by that of the EOD measured at the origin, prior to the introduction of the sphere there. The introduction of a dielectric sphere of radius a at the origin then induces a perturbation of

$$\delta\Phi(x, y, d) = \frac{\Gamma a^3 E d}{(x^2 + y^2 + d^2)^{3/2}} \tag{2.1}$$

at (x, y, d) on Π, where Γ is the electric contrast of the sphere defined in chapter 3. Measurements of this perturbation on the fish surface plane constitute the electric image of the dielectric sphere.

Rasnow Model

According to Rasnow [32] and Rasnow and Bower [33], it is sufficient for the fish to measure the relative width of the electric image for unambiguous distance information. Here we show that this measure is in fact sufficient for distance discrimination as it depends solely on the object's distance.

The perturbation (2.1) is maximized at the point $(0, 0, d)$ directly underneath the dielectric object, and decays in a Gaussian-like manner. The maximum perturbation is then given by

$$\delta\Phi_{max} = \frac{\Gamma a^3 E}{d^2}. \tag{2.2}$$

The potential on a curve C defined on the plane Π, by

$$C = \left\{(x, y, z) |\ x^2 + y^2 = d^2(\sqrt[3]{4} - 1), z = d\right\}$$

is half that of $\delta\phi_{max}$. It is clear that the curve C defines a circle on the plane Π, with center $(0, 0, d)$ and radius

$$r = d\sqrt{\sqrt[3]{4} - 1}, \tag{2.3}$$

which is solely dependent on the sphere's distance to the plane. Hence, we see that the distance of an object is linearly related to the radius of the electric image at half amplitude by

$$d = \frac{r}{\sqrt{\sqrt[3]{4} - 1}}, \tag{2.4}$$

where there is no dependence on the size a, or the electrical contrast Γ, of the sphere.

von der Emde Model

According to von der Emde *et al.* [31], von der Emde [12] and Schwarz and von der Emde [34] the ratio λ, of the electric image's maximum slope to maximum amplitude provides a measure of an object's distance. Here we show that this measure is solely dependent on the object's distance, and hence can be used to unambiguously localize an object. Further, we find the mathematical relationship between the object's distance d and λ.

It is easy to verify that on the horizontal plane Π the maximum amplitude of the perturbation (2.1) is attained at the point $(0, 0, d)$, and has value

$$\delta\Phi_{max} = \frac{\Gamma a^3 E}{d^2}. \tag{2.5}$$

On this same plane, the magnitude of the slope of the surface $\delta\Phi(x, y)$ is defined by

$$|\nabla\delta\Phi| = 3\Gamma a^3 E d \sqrt{\frac{x^2 + y^2}{(x^2 + y^2 + d^2)^5}}. \tag{2.6}$$

Using the symmetry of our problem we let $x^2 + y^2 = r^2$ to define the slope function

$$S(r, d) = |\nabla\delta\Phi| = \frac{3\Gamma a^3 E d r}{(r^2 + d^2)^{5/2}}. \tag{2.7}$$

Again, it can easily be verified that the slope is maximized on the circle $x^2 + y^2 = \frac{d^2}{4}$ and has value

$$S_{max} = \frac{48\Gamma a^3 E}{d^3\sqrt{5^5}}. \tag{2.8}$$

Hence, the slope to amplitude ratio λ is

$$\lambda = \frac{S_{max}}{\delta\Phi_{max}} = \frac{48}{d\sqrt{5^5}}. \tag{2.9}$$

Finally, we can see that object distance is linearly related to the inverse of the ratio λ by

$$d = \frac{48}{\sqrt{5^5}} \frac{1}{\lambda}. \tag{2.10}$$

2.4 Conclusion

All spatiotemporal models of depth preception, with the exception of Sim and Kim [40], are at least weakly compatible with either Rasnow's or von der Emde's static models. It remains unclear which, if either, of the two static algorithms the fish actually use for the task of depth perception. We hope that the work provided in this chapter will validate the method proposed by Rasnow [32] as a potential algorithm for depth perception as well as provide a mathematical complement to von der Emde's empirical work.

In the following chapter we propose an alternative model for depth perception based on measurements of a single image parameter. Such a model, based on both the spatial and temporal characteristics of the electric image would only require a single narrow tuned topological map to accurately estimate distance. It further provides an explanation for the probing behavior observed in weakly electric fish.

3

Single Parameter Spatiotemporal Model

Depth perception mechanisms suggested thus far are based on multi-parameter measurements [31, 32, 40, 41], and most take into account only the spatial profile of the electric image, disregarding its temporal characteristic. The EOD of weakly electric fish are amongst the most stable known biological oscillators [7], and electromotor behavior during distance discrimination [34] suggests that the image's temporal properties may play a far more significant role than previously thought.

In this chapter we develop a model for depth perception, based on both the spatial and temporal characteristics of the electric image. Our model is based on measurements of a single image parameter, namely the width of the electric image. In contrast to previously suggested algorithms, our model would only require a single narrow tuned topographic neuronal map to accurately estimate distance. More significantly, our model provides an explanation of the tail-bending (probing) behavior and va-et-vient sampling observed in weakly electric fish.

We begin with an outline of the model including both analytic as well as numerical results 3.1. We then use this model to study the effects of electromagnetic noise and assess the presence of stochastic resonance (3.2). Lastly we test our model for localization of non-spherical dielectrics (3.3).

3.1 Model

Motivation

The motivation behind developing a single parameter model is twofold. The physiological process of extracting distance information from one image parameter is far simpler than that required for multiple parameters. Other – multi-parameter based – algorithms such as those of Rasnow (image *width* calculated at half peak *amplitude*) and von der Emde (ratio of maximum *slope* to peak *amplitude*) would require at least two topographic maps with differing spatial resolution to accurately estimate distance [28]. Our single parameter based model can function with only a single narrow tuned map.

Electric fish explore novel objects differing in conductivity from water by swimming in a back-and-forth manner (va-et-vient sampling) [35, 45] or bending of the caudal one- or two-thirds of the body toward the object [46]. It has been hypothesized [9] that the tail-bending behavior, called "probing", as well as the va-et-vient sampling [41] , may allow the fish to disambiguate object features. The electric image is greatly affected by the location of the electric organ relative to the object. The va-et-vient sampling and probing behavior changes this position and hence changes the EOD amplitude at the object. We show that utilizing measurements of the electric image at multiple EOD amplitudes allow the fish to disambiguate the distance from other unknown object properties, and hence explain the probing behavior.

Model Outline

We consider fish with non-ideal electroreceptors. Such receptors are characterized by a threshold value T. Signals whose amplitude fall below this threshold remain undetected to such non-ideal receptors. In this way, we can regard the surface of the fish, in the presence of a given object, as being comprised of two distinct regions; detectable and non-detectable. Receptors within the detectable region are able to sense the perturbation caused by the presence of the object while the object remains invisible to receptors in the non-detectable region. It is clear that the size of the two regions are

functions of the EOD amplitude, the object-fish distance as well as other unknown object properties (i.e. size, shape and electric contrast). By itself, information about the size of the regions at any one instance in time is insufficient in inferring anything about the object-fish distance. However, comparison of the regions measured at two different EOD amplitudes allows the possibility of disambiguating the distance from the other object properties.

It is important to note that though we have chosen the receptor sensitivity threshold as the value at which the fish surface is partitioned; our model remains valid for any other threshold value. As such, if the signal is strong enough that the perturbation at *all* receptors is above threshold, a higher threshold value can be chosen with the aid of neuronal inhibition, such that regions where the perturbation falls above this new threshold value form a bounded region on the fish surface. In this way a value can always be chosen to ensure the size of the "detectable" region is limited to the surface of the fish.

3.1.1 Assumptions

Our model makes four key assumptions that need to be addressed. First, we have based our model on the localization of a dielectric sphere. We will show, this is an accurate representation of the problem faced by the fish, especially for more distant objects. Next, we assume that the field in which the object is placed is both uniform and perpendicular to the surface of the fish. Finally, we presume that the presence of the fish itself does not affect the electric image.

Object Geometry

Our model is based on the localization of a dielectric sphere. This assumption has been made by many authors in the past, [9, 32, 40, 42, 47, 48], and we believe it is an accurate representation of the problem faced by the fish.

Foremost, the geometry of electric fish's main prey, the *Daphnia Magna* is roughly spherical, see figure 3.1. Second, as the size of non-spherical objects is reduced or its distance increased the perturbation of the electric field due to the object, and hence

its electric image, converges to that produced by a spherical object. This property is reflected in the Laplace equation which links the electric potential to the charge distribution and is used to model the field perturbation by a dielectric object. In figure 3.2 we represent the electric image produced by a sphere 3.2a and a cube 3.2b. Both objects produce very similar electric image profiles with circular isopotential lines. As the distance of the cube is decreased the high-valued isopotential lines begin to deviate from their circular nature. However, the isopotential lines at the periphery of the electric image still maintain their circular pattern. For an algorithm based on the size of the electric image, only the weakest detectable isopotential line need be considered. As such even for near non-spherical objects, we may assume the profile of the electric image is circular in nature, similar to that which is produced for spherical objects.

Figure 3.1: ***Daphnia Magna*** - A female adult *daphnia magna.*

Field Uniformity

Far from the fish, the EOD induces an electric field resembling an elongated dipole [9, 10, 44], (see figure 3.3). The near field (< 1 body length), where electrolocation occurs [49, 50], is far more complicated [10]. Let us model the elongated field as that which is produced by an array of point charges [42]. The array of n electric poles is distributed uniformly along the rostro-caudal axis of the model fish. Starting at the head, the first m poles act as current source and the remaining $(n - m)$ as current sink. The electric potential Φ at a point $\mathbf{x}$ outside the fish is given by the sum of the

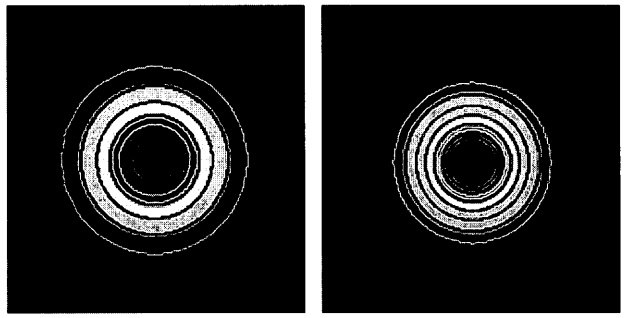

(a) (b)

Figure 3.2: Electric image comparison - (a) Contours representing the electric image for a sphere, (b) and a cube.

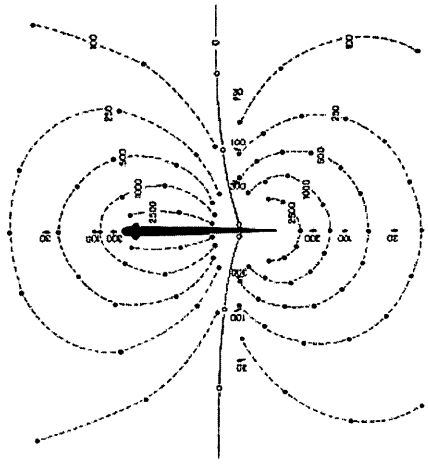

Figure 3.3: Fish dipole field - Elongated dipole field generated by an *Apteronotus albifrons*, (from [10]).

individual contributions to the potential from each pole. That is,

$$\Phi(\mathbf{x}) = \sum_{j=1}^{m} \frac{\frac{q}{m}}{4\pi\epsilon_0} \frac{1}{|\mathbf{x} - \mathbf{x}_j|} - \sum_{j=m+1}^{n} \frac{\frac{q}{n-m}}{4\pi\epsilon_0} \frac{1}{|\mathbf{x} - \mathbf{x}_j|}, \tag{3.1}$$

where $\mathbf{x}_j$ is the Cartesian position of the j^{th} pole, and q is the charge associated to each pole. The quantity q has been normalized such that the first m poles have a charge of q/m and the remaining poles a charge of $-q/(n-m)$, resulting in a total net charge of zero. The field is well described with a single negative pole at the tail [42].

Let us now derive the perturbation to this field by a dielectric sphere of radius a and relative permittivity ϵ_i centered at the origin. We begin by analysing the effect of the sphere on the field of a single point charge then generalize the idea to the multipole field above. Suppose the sphere-charge-receptor orientation is as in figure 3.4. The charge q is set on the z-axis a distance b from the center of the sphere which is located at the origin, $(b > a)$. The potential in such an arrangement is independent of the spherical coordinate ϕ, hence, $\Phi(r, \theta, \phi) = \Phi(r, \theta)$. The sphere is immersed in a media of relative permittivity ϵ_e. We begin with Gauss' Law $\nabla \cdot E = \rho/\epsilon_0$, which in the absence of charge leads to the Laplace equation, $\nabla^2\Phi = 0$. The solution of the Laplace equation in spherical coordinates is

$$\Phi(r, \theta) = \sum_{n=0}^{\infty} \left(A_n r^n + B_n \frac{1}{r^{n+1}} \right) [P_n(\cos\theta) + Q_n(\cos\theta)], \tag{3.2}$$

where A_n and B_n are constants, yet to be determined, and P_n and Q_n are the Legendre polynomials of the first and second kind, respectively, [51]. Noting that $\Phi(r, \theta) < \infty$ for all values of θ, we can set $Q_n = 0$, as this function diverges for $\theta = 0, \pi$. Hence, we look for solutions of the form

$$\begin{aligned} \Phi_i(r, \theta) &= \sum_{n=0}^{\infty} \left(A_n r^n + B_n \frac{1}{r^{n+1}} \right) P_n(\cos\theta) \quad \text{and} \\ \Phi_e(r, \theta) &= \sum_{n=0}^{\infty} \left(C_n r^n + D_n \frac{1}{r^{n+1}} \right) P_n(\cos\theta), \end{aligned} \tag{3.3}$$

where the subscripts i and e represent the potential interior and exterior to the sphere respectively. Our equations (3.3) need to satisfy the following boundary conditions.

BC.1 $\Phi_i(r, \theta) < \infty$ as $r \to 0$

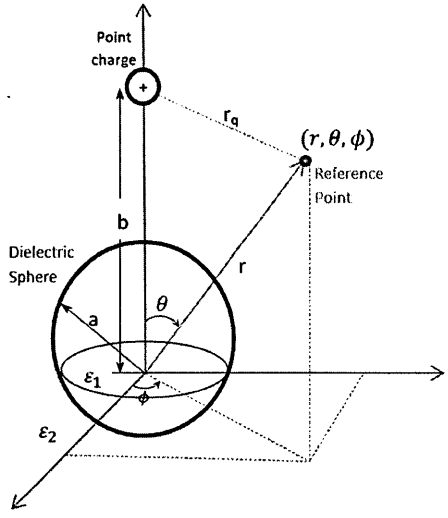

Figure 3.4: Point charge-sphere-receptor orientation - Orientation of the point charge, sphere and receptor in spherical coordinates. The symmetry of the problem is exploited by orienting the reference frame such that the origin coincides with the center of the sphere and the applicate $\vec{k}$, is directed along the line joining the sphere center and the point charge. In this frame the potential at a receptor located at (r, θ, ϕ) is independent of the azimuthal angle ϕ. The point charge is located at $(b, 0)$.

- if polarization of dielectric is uniform, bound charges only appear on the surface

BC.2 $\Phi_e(r,\theta) \to \frac{1}{4\pi\varepsilon_0}\frac{q}{r_q} \to 0$ as $r \to \infty$ where $r_q = \sqrt{b^2 + r^2 - 2br\cos\theta}$

- at great distances from the sphere, the effect of the sphere is negligible

BC.3 $\Phi_i(r,\theta) = \Phi_e(r,\theta)$ for $r = a$

- electric potential must be continuous across boundary
- discontinuity would imply an infinite electric field

BC.4 $(\mathbf{D}_e - \mathbf{D}_i) \cdot \mathbf{n} = \sigma = 0$ when $r = a$

- boundary condition for dielectric surfaces
- here $\mathbf{D}$ is the displacement field accounting for the effects of free charge within materials.
- normal component of displacement field is continuous across the boundary
- here σ is the *free* surface charge. We assume no free-charges on the surface of the sphere.

BC.5 $(\epsilon_0\epsilon_e\mathbf{E}_e - \epsilon_0\epsilon_i\mathbf{E}_i) \cdot \mathbf{n} = \sigma = 0$ when $r = a$

- derived from BC.4, where $\mathbf{D} = \epsilon_0\epsilon\mathbf{E} = \epsilon_0(1+\chi_e)\mathbf{E} = \epsilon_0\mathbf{E}+\epsilon_0\chi_e\mathbf{E} = \epsilon_0\mathbf{E}+\mathbf{P}$, and ϵ_0 is the vacuum permittivity
- here ϵ is the dielectric constant inside/ouside the sphere, $\chi_e = \frac{\epsilon-\epsilon_0}{\epsilon_0}$ is the dielectric susceptibility, and $\mathbf{P}$ is the electric polarization (or dipole moment per unit volume)

BC.6 $\Phi_e(r,\theta) \to \infty$ as $r \to b$ and $\theta \to 0$

BC.7 $\mathbf{E}_{it} = \mathbf{E}_{et}$

- assuming electrostatics (i.e. $\nabla \times \mathbf{E} = 0$)
- tangential component of the electric field is continuous across the boundary

The above boundary conditions may be used to explicitly find the coefficients A_n, B_n, C_n and D_n of equations (3.3).

- $\Phi_i(r,\theta) < \infty$ as $r \to 0$ [BC.1]

  $\Rightarrow B_n = 0 \quad \forall n$
  $\Rightarrow \Phi_i(r,\theta) = \sum_{n=0}^{\infty} (A_n r^n) P_n(\cos\theta)$

- $\Phi_e(r,\theta) \to \frac{1}{4\pi\epsilon_0} \frac{q}{\sqrt{b^2+r^2-2br\cos\theta}}$ as $r \to \infty$ [BC.2]

  Suppose we can express the potential outside the sphere as the sum of the unperturbed potential Φ_u - potential in the absence of the sphere - and the perturbation Φ_p, due to the presence of the sphere.

  $$\Phi_e = \Phi_u + \Phi_p \tag{3.4}$$

  Equation (3.4) must satisfy the following criteria:

  CT.1 $\nabla^2\Phi_e = 0$
  - As Φ_e is the solution to Laplace equation outside the sphere

  CT.2 $\Phi_u(r,\theta) = \frac{1}{4\pi\epsilon_0} \frac{q}{\sqrt{b^2+r^2-2br\cos\theta}}$
  - This is simply the point charge potential measured at a distance $\sqrt{b^2+r^2-2br\cos\theta}$.
  - We note Φ_u satisfies the Laplace equation (i.e. $\nabla^2\Phi_u = 0$)

  CT.3 Φ_p must satisfy the Laplace equation ($\nabla^2\Phi_p = 0$)
  - By CT.1 and CT.2

  CT.4 $\Phi_p(r,\theta) = \sum_{n=0}^{\infty} \left(C_n r^n + D_n \frac{1}{r^{n+1}}\right) P_n(\cos\theta)$
  - by CT.3

  CT.5 $\Phi_p(r,\theta) \to 0$ as $r \to \infty$
  - As a consequence of BC.2

  CT.6 $C_n = 0 \quad \forall n$
  - by CT.4 and CT.5

  $\Rightarrow \Phi_p(r,\theta) = \sum_{n=0}^{\infty} \left(D_n \frac{1}{r^{n+1}}\right) P_n(\cos\theta)$

Hence,

$$\Phi_e(r,\theta) = \frac{1}{4\pi\varepsilon_0}\frac{q}{\sqrt{b^2+r^2-2br\cos\theta}} + \sum_{n=0}^{\infty}\left(D_n\frac{1}{r^{n+1}}\right)P_n(\cos\theta). \tag{3.5}$$

Now, to write this equation in a more uniform way, consider the function

$$\frac{1}{1+\eta^2-2\eta x}. \tag{3.6}$$

If we expand this in a power series in x, we obtain a series that converges for $\eta < 1$. Furthermore, as the Legendre polynomials can be defined [52] as the coefficients in a Taylor series expansion

$$\frac{1}{\sqrt{1+\eta^2-2\eta x}} = \sum_{n=0}^{\infty}\eta^n P_n(x), \tag{3.7}$$

for $b > r$, we define $\eta = r/b$, and

$$\begin{aligned}\frac{q}{4\pi\varepsilon_0\sqrt{b^2+r^2-2br\cos\theta}} &= \frac{q}{4\pi\varepsilon_0 b\sqrt{1+(r/b)^2-2(r/b)\cos\theta}}\\ &= \frac{q}{4\pi\varepsilon_0 b\sqrt{1+\eta^2-2\eta\cos\theta}}\\ &= \frac{q}{4\pi\varepsilon_0 b}\sum_{n=0}^{\infty}\eta^n P_n(\cos\theta).\end{aligned} \tag{3.8}$$

For $b < r$, we define $\xi = b/r$, and

$$\begin{aligned}\frac{q}{4\pi\varepsilon_0\sqrt{b^2+r^2-2br\cos\theta}} &= \frac{q}{4\pi\varepsilon_0 r\sqrt{(b/r)^2+1-2(b/r)\cos\theta}}\\ &= \frac{q}{4\pi\varepsilon_0 r\sqrt{1+\xi^2-2\xi\cos\theta}}\\ &= \frac{q}{4\pi\varepsilon_0 r}\sum_{n=0}^{\infty}\xi^n P_n(\cos\theta).\end{aligned} \tag{3.9}$$

So,

$$\Phi_e(r,\theta) = \begin{cases}\frac{q}{4\pi\varepsilon_0}\sum_{n=0}^{\infty}\frac{r^n}{b^{n+1}}P_n(\cos\theta) + \sum_{n=0}^{\infty}\left(D_n\frac{1}{r^{n+1}}\right)P_n(\cos\theta) & \text{if } a<r<b,\\ \frac{q}{4\pi\varepsilon_0}\sum_{n=0}^{\infty}\frac{b^n}{r^{n+1}}P_n(\cos\theta) + \sum_{n=0}^{\infty}\left(D_n\frac{1}{r^{n+1}}\right)P_n(\cos\theta) & \text{if } b<r.\end{cases}$$

Upon simplifying we obtain,

$$\Phi_e(r,\theta) = \begin{cases}\sum_{n=0}^{\infty}\left(\frac{q}{4\pi\varepsilon_0}\frac{r^n}{b^{n+1}} + D_n\frac{1}{r^{n+1}}\right)P_n(\cos\theta) & \text{if } a<r<b,\\ \sum_{n=0}^{\infty}\left(\frac{q}{4\pi\varepsilon_0}\frac{b^n}{r^{n+1}} + D_n\frac{1}{r^{n+1}}\right)P_n(\cos\theta) & \text{if } b<r.\end{cases}$$

Note that the two equations coincide for the case $b = r$!

- $\Phi_i(r,\theta) = \Phi_e(r,\theta)$ for $r = a$. [BC.3]

Of course for the potential measured just outside of the sphere, we need only consider the case $a < r < b$. Hence, BC.3 states that

$$\sum_{n=0}^{\infty} (A_n a^n) P_n(\cos\theta) = \sum_{n=0}^{\infty} \left(\frac{q}{4\pi\varepsilon_0} \frac{a^n}{b^{n+1}} + D_n \frac{1}{a^{n+1}} \right) P_n(\cos\theta). \tag{3.10}$$

Equating the coefficients of the Legendre polynomials, we find for $n = 0, 1, 2, ...$

$$A_n = \frac{q}{4\pi\varepsilon_0} \frac{1}{b^{n+1}} + \frac{D_n}{a^{2n+1}}. \tag{3.11}$$

Hence,

$$\begin{aligned} \Phi_i(r,\theta) &= \sum_{n=0}^{\infty} (A_n r^n) P_n(\cos\theta), \\ &= \sum_{n=0}^{\infty} \left(\frac{q}{4\pi\varepsilon_0} \frac{1}{b^{n+1}} + \frac{D_n}{a^{2n+1}} \right) r^n P_n(\cos\theta). \end{aligned}$$

- $(\epsilon_0\epsilon_e \mathbf{E}_e - \epsilon_0\epsilon_i \mathbf{E}_i) \cdot \mathbf{n} = \sigma = 0$ when $r = a$. [BC.5]

Rearranging the terms and using the definition of electric potential

$$\begin{aligned} (\epsilon_0\epsilon_e \mathbf{E}_e - \epsilon_0\epsilon_i \mathbf{E}_i) \cdot \mathbf{n} &= 0, \\ \epsilon_e \mathbf{E}_e \cdot \mathbf{n} &= \epsilon_i \mathbf{E}_i \cdot \mathbf{n}, \\ \epsilon_e \nabla\Phi_e \cdot \mathbf{n} &= \epsilon_i \nabla\Phi_i \cdot \mathbf{n}, \\ \epsilon_e \left.\frac{\partial\Phi_e}{\partial n}\right|_{r=a} &= \epsilon_i \left.\frac{\partial\Phi_i}{\partial n}\right|_{r=a}, \\ \epsilon_e \left.\frac{\partial\Phi_e}{\partial r}\right|_{r=a} &= \epsilon_i \left.\frac{\partial\Phi_i}{\partial r}\right|_{r=a}. \end{aligned} \tag{3.12}$$

Again, for potential measured just outside of the sphere, we need only consider the

case $a < r < b$. Hence,

$$\epsilon_e \frac{\partial}{\partial r}\left(\sum_{n=0}^{\infty}\left(\frac{q}{4\pi\varepsilon_0}\frac{r^n}{b^{n+1}} + D_n\frac{1}{r^{n+1}}\right)P_n(\cos\theta)\right)\Bigg|_{r=a} =$$
$$\epsilon_i \frac{\partial}{\partial r}\left(\sum_{n=0}^{\infty}\left(\frac{q}{4\pi\varepsilon_0}\frac{1}{b^{n+1}} + \frac{D_n}{a^{2n+1}}\right)r^n P_n(\cos\theta)\right)\Bigg|_{r=a},$$
$$\epsilon_e\sum_{n=0}^{\infty}\left(n\frac{q}{4\pi\varepsilon_0}\frac{a^{n-1}}{b^{n+1}} - (n+1)D_n\frac{1}{a^{n+2}}\right)P_n(\cos\theta) =$$
$$\epsilon_i\sum_{n=0}^{\infty} n\left(\frac{q}{4\pi\varepsilon_0}\frac{1}{b^{n+1}} + \frac{D_n}{a^{2n+1}}\right)a^{n-1}P_n(\cos\theta).$$

Equating the coefficients of the Legendre polynomial, we find

$$D_n = n\frac{q}{4\pi\epsilon_0}\frac{a^{2n+1}}{b^{n+1}}\left(\frac{\epsilon_e-\epsilon_i}{n\epsilon_i+(n+1)\epsilon_e}\right) \text{ and}$$
$$A_n = \frac{q}{4\pi\epsilon_0}\frac{1}{b^{n+1}}\left(\frac{(2n+1)\epsilon_e}{n\epsilon_i+(n+1)\epsilon_e}\right).$$

We substitute these values into our equation for potential, and obtain

$$\Phi_i(r,\theta) = \frac{q}{4\pi\epsilon_0}\sum_{n=0}^{\infty}\frac{r^n}{b^{n+1}}\left(\frac{(2n+1)\epsilon_e}{n\epsilon_i+(n+1)\epsilon_e}\right)P_n(\cos\theta) \qquad r<a,$$
$$\Phi_e(r,\theta) = \begin{cases}\frac{q}{4\pi\epsilon_0}\sum_{n=0}^{\infty}\left(\frac{r^n}{b^{n+1}} + n\frac{a^{2n+1}}{b^{n+1}r^{n+1}}\left(\frac{\epsilon_e-\epsilon_i}{n\epsilon_i+(n+1)\epsilon_e}\right)\right)P_n(\cos\theta) & a<r<b\\ \frac{q}{4\pi\epsilon_0}\sum_{n=0}^{\infty}\left(\frac{b^n}{r^{n+1}} + n\frac{a^{2n+1}}{b^{n+1}r^{n+1}}\left(\frac{\epsilon_e-\epsilon_i}{n\epsilon_i+(n+1)\epsilon_e}\right)\right)P_n(\cos\theta) & b<r.\end{cases} \tag{3.13}$$

Equations (3.13) fully describe the potential of a point charge in the presence of a dielectric sphere at all points (r,θ,ϕ) in space. We identify, by equations (3.4), (3.8), (3.9) and CT.2 above, the *perturbation* $\delta\Phi$, to the electric potential by the sphere to be

$$\delta\Phi(r,\theta) = \frac{q}{4\pi\epsilon_0}\sum_{n=0}^{\infty}\left(n\frac{a^{2n+1}}{b^{n+1}r^{n+1}}\left(\frac{\epsilon_e-\epsilon_i}{n\epsilon_i+(n+1)\epsilon_e}\right)\right)P_n(\cos\theta). \tag{3.14}$$

Here, as before, P_n represent the Legendre polynomials, and θ is the polar angle which extends between the charge-axis (axis extending from the charge to the origin) and the ray extending from the origin to the reference point point (r,θ), (figure 3.4).

Writing out the first several terms of equation (3.14),

$$\begin{aligned}\delta\Phi(r,\theta) &= \frac{q}{4\pi\epsilon_0}\left(\frac{a^3}{b^2r^2}\left(\frac{\epsilon_e-\epsilon_i}{\epsilon_i+2\epsilon_e}\right)\right)\cos\theta \\ &\quad + \frac{q}{4\pi\epsilon_0}\sum_{n=2}^{\infty}\left(n\frac{a^{2n+1}}{b^{n+1}r^{n+1}}\left(\frac{\epsilon_e-\epsilon_i}{n\epsilon_i+(n+1)\epsilon_e}\right)\right)P_n(\cos\theta) \\ &= \left(\frac{\epsilon_e-\epsilon_i}{\epsilon_i+2\epsilon_e}\right)a^3\frac{q}{4\pi\epsilon_0}\frac{1}{b^2}\frac{\cos\theta}{r^2}+O\left(\frac{a^5}{r^3}\right), \qquad (3.15)\end{aligned}$$

it becomes clear that the perturbation of the point charge field due to the dielectric sphere is comprised of a dipole perturbation along with higher order terms. These terms become negligible for small ($a \ll 1$), distant objects.

Generalizing our analysis of the point charge field to an array of point charges is made simple with the aid of the superposition principle. Consider an array of N charges. For each charge q_j, we orient the reference frame such that the origin coincides with the center of the sphere and the applicate $\vec{k}$, is directed along the line joining the sphere center and q_j. The potential perturbation of charge q_j at a receptor due to the sphere can then be calculated by the method outlined above. Finally, by the superposition principle, we may add up the individual potential perturbations to acquire the perturbation of the array;

$$\delta\Phi(r,\theta) = \frac{1}{4\pi\epsilon_0}\sum_{n=0}^{\infty}\left[n\frac{a^{2n+1}}{r^{n+1}}\left(\frac{\epsilon_e-\epsilon_i}{n\epsilon_i+(n+1)\epsilon_e}\right)\sum_{j=1}^{N}\left(\frac{q_j}{b_j^{n+1}}\right)P_n(\cos\theta_j)\right], \qquad (3.16)$$

where (b_j,β_j) is the polar coordinate of charge j and $\theta_j = \theta-\beta_j$; see figure 3.5. Again, writing the first several terms of equation (3.16),

$$\begin{aligned}\delta\Phi(r,\theta) &= \left(\frac{\epsilon_e-\epsilon_i}{\epsilon_i+2\epsilon_e}\right)a^3\frac{1}{4\pi\epsilon_0}\sum_{j=1}^{N}\left(\frac{q_j}{b_j^2}\right)\frac{\cos\theta_j}{r^2} \\ &\quad + \frac{1}{4\pi\epsilon_0}\sum_{n=2}^{\infty}\left[n\frac{a^{2n+1}}{r^{n+1}}\left(\frac{\epsilon_e-\epsilon_i}{n\epsilon_i+(n+1)\epsilon_e}\right)\sum_{j=1}^{N}\left(\frac{q_j}{b_j^{n+1}}\right)P_n(\cos\theta_j)\right] \\ &= \left(\frac{\epsilon_e-\epsilon_i}{\epsilon_i+2\epsilon_e}\right)a^3\frac{1}{4\pi\epsilon_0}\sum_{j=1}^{N}\left(\frac{q_j}{b_j^2}\right)\frac{\cos\theta_j}{r^2}+O\left(\frac{a^5}{r^3}\right), \qquad (3.17)\end{aligned}$$

it becomes clear that the perturbation of the array potential is comprised of a sum of dipole potentials and higher order multi-pole perturbations which attenuate with

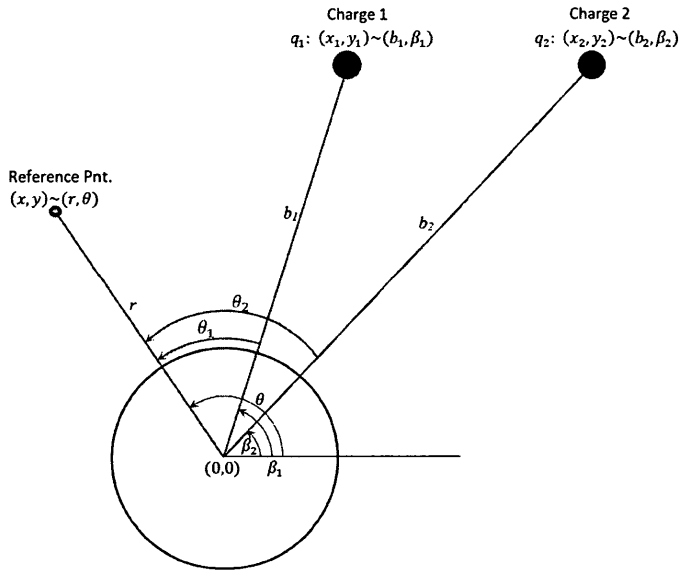

Figure 3.5: Charge array-sphere-receptor orientation - Orientation of the receptor, sphere and an array of two charges q_j. In a reference frame where the sphere center is located at the origin and the receptor at (r, θ), each charge is located at (b_j, β_j).

distance from the object more rapidly than the dipole perturbation. The attenuation of the higher order terms is exaggerated for small object $a \ll 1$, (equation (3.17)). Hence, we can conclude that the perturbation of a uniform field is a good representation of the perturbation to the actual field generated by the fish, especially for small objects.

Field Perpendicularity

Current flows between the head and tail ends of the electric organ, periodically alternating in direction with a frequency that is characteristic of the species [10]. In addition to firing periodically, different segments of the electric organ fire asynchronously, causing a propagation of the discharge. This results in different EOD waveforms along the length of the fish [9, 44]. For various locations along the fish's body, figure 3.6b depicts the paths the tips of the electric field vectors trace during one cycle of the EOD. Electric field vectors in the caudal part of the body change both magnitude and direction, whereas those in the rostral part only change magnitude and sign. In addition, the field vectors in the rostral region are perpendicular to the surface of the fish. Densities

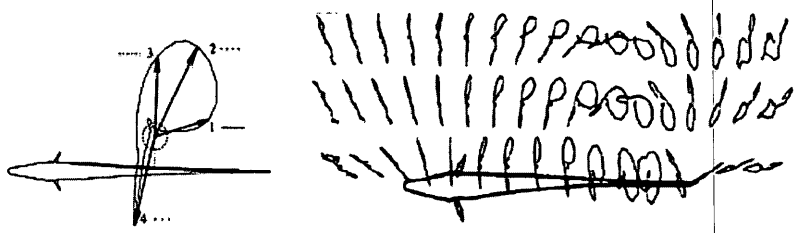

Figure 3.6: Vector representation of EOD-cycle - (a) Time domain representation of the EOD cycle, showing the direction of the electric field vector at a single point in the mid-plane. Four EOD phases are drawn as vectors, and for subsequent times, just the tip of the vector is traced. (b) The process is figure (a) is repeated for multiple points in the mid-plane showing the spatiotemporal nature of the generated field in a region around the fish. At each point, only the initial EOD phase is drawn as a vector, and for subsequent times, just the tip of the vector is traced. (From [44], with permission)

of electroreceptor organs on the head are on average approximately five times greater than those on the trunk of the fish [18]. This suggests the head acts as an electrosensory fovea, and orientation of fields in this region are far more significant than those in the trunk. This has lead us to presume that the field is oriented perpendicularly to the fish surface.

Fish Effect

Our final assumption is that the fish's body has no effect on the perturbation. That is, we assume the fish to be electrically invisible. This assumption relies on the fact that the fish skin does not produce a new ambiguity. In other words, the fish body does not introduce non-linearity into our model, where we may have multiple field magnitudes producing the same perturbation.

As a first approximation, let us take the fish interior to be isopotential with relative permittivity similar to that of the surrounding water. This assumption is based on the hypothesis that the internal cells are made up of mostly water. Examining the effect of the dielectric fish skin on the perturbation, we find the potential Φ at the point q_o

on the fish surface S to be

$$\Phi(q_o) = \frac{2}{\epsilon_e + \epsilon_{skin}}\Psi(q_o) + \frac{1}{2}\left(\frac{\epsilon_e - \epsilon_{skin}}{\epsilon_e + \epsilon_{skin}}\right)\iint \Phi(q)\frac{\partial}{\partial n_q}\frac{1}{|\bar{r}_q - \bar{r}_{q_o}|}dS, \tag{3.18}$$

(see Appendix B for derivation). If we consider the thinness of the skin (0.1 mm), we may represent S by a plane (figure 3.7). In this case

$$\frac{\partial}{\partial n_q}\frac{1}{|\bar{r}_q - \bar{r}_{q_o}|} = \nabla\left(\frac{1}{|\bar{r}_q - \bar{r}_{q_o}|}\right)\cdot\hat{n} = 0. \tag{3.19}$$

And so,

$$\Phi(q_o) = \frac{2}{\epsilon_e + \epsilon_{skin}}\Psi(q_o) \tag{3.20}$$

where, $\Psi(q_o)$ is the potential at the point q_o in the absence of the fish surface, ϵ_e and ϵ_{skin} are the relative permittivities of the water and fish skin, respectively. As equation (3.20) indicates, the potential in the presence of the fish is a scalar multiple of the potential in its absence. That is, the introduction of the fish has not resulted in the introduction of non-linearity into our model and can be disregarded.

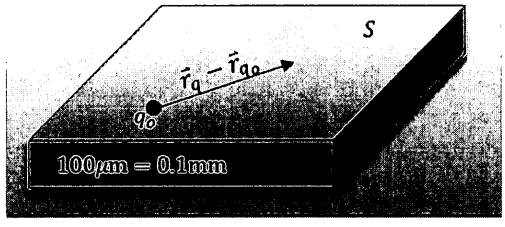

Figure 3.7: Fish skin model - A model representation of the dielectric fish skin.

3.1.2 Analytic Model

Consider a linear, homogeneous, isotropic sphere of radius a, centered at $\mathbf{x_{obj}}$, placed within a uniform electric field $\mathbf{E}$. The perturbation $\delta\Phi$, of the electric potential by the sphere measured at field point $\mathbf{x}$ is given by

$$\delta\Phi(\mathbf{x}) = \frac{\Gamma a^3 \mathbf{E}(\mathbf{x_{obj}})\cdot(\mathbf{x} - \mathbf{x_{obj}})}{|\mathbf{x} - \mathbf{x_{obj}}|^3}, \tag{3.21}$$

where $\mathbf{E}(\mathbf{x_{obj}})$ is the field vector at the location of the object prior to its placement there, and Γ is the electrical contrast, (see Appendix A for derivation). The electric

contrast is dependent on the temporal nature of the field:

$$\Gamma = \begin{cases} \frac{\epsilon_i - \epsilon_e}{\epsilon_i + 2\epsilon_e}, & \text{Static Field} \\ \frac{(\rho_e - \rho_i) + i\omega\rho_e\rho_i(\epsilon_i - \epsilon_e)}{(\rho_e + 2\rho_i) + i\omega\rho_e\rho_i(\epsilon_i + 2\epsilon_e)}, & \text{Oscillating Field [32]} \end{cases}$$

where ρ is the resistivity, ϵ the absolute permittivity and ω the angular frequency of the unperturbed field. The subscripts i and e identify the variables as being interior or exterior to the spherical object, respectively.

If we assume that the receptors of the fish are non-ideal with threshold value T, then a receptor located at $\mathbf{x}$ is able to detect the perturbation caused by an object if

$$|\delta\Phi(\mathbf{x})| \geq T. \tag{3.22}$$

Equation (3.22) defines a "detectable" region on the fish surface. Receptors that fall within this region can sense the presence of the dielectric sphere. It is clear from equation (3.21) and the detectability criteria (3.22) that the size of the detectable region is contingent on the EOD amplitude, the object-fish distance, as well as other object properties (i.e. size, shape and electric contrast).

By defining the Cartesian reference frame such that the origin coincides with the sphere's center, and such that the applicate vector $\vec{k}$ (see figure 4.1 for definition) is parallel to $\mathbf{E}$, the detectability criteria (3.22) simplifies to

$$\left| \Gamma a^3 E \frac{z}{(x^2 + y^2 + z^2)^{3/2}} \right| \geq T, \tag{3.23}$$

where $E = \|\mathbf{E}\|$. By rearranging the terms, we can define a *detection disk* on the fish surface within which electroreceptors detect the perturbation caused by a dielectric object;

$$x^2 + y^2 \leq \left(\frac{z}{\tau}\right)^{3/2} - z^2, \tag{3.24}$$

where we have defined $\tau = T/\Gamma a^3 E$ for convenience.

At any instance in time, information about the size of the disk is, on its own, insufficient to infer anything about the object-fish distance. This is due to the fact that the value of the weighted threshold τ is a function of other unknown object properties, namely, object size, electric contrast, field magnitude at the object and even perhaps

sensitivity threshold value. Furthermore, for a fixed disk radius, τ is a non-injective function of distance z (figure 3.9).

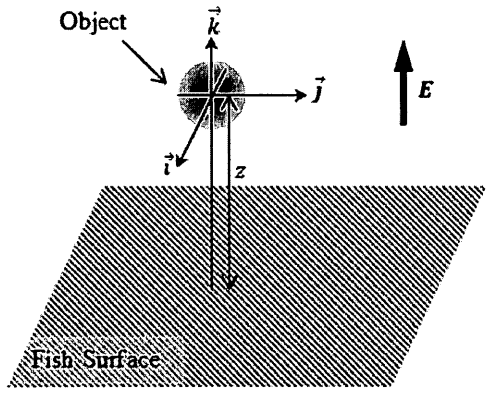

Figure 3.8: Orientation of Cartesian reference frame - Orientation of the Cartesian reference frame in relation to the object and electric field. The origin is chosen to coincide with the location of the center of the object and the applicate $\vec{k}$, is set to be parallel with the unperturbed electric field.

We begin by considering the electric image produced for two different magnitudes of the electric field. If the two fields are measured within a sufficiently small time interval then we can expect the object-fish distance to remain unchanged. Denote the generated field at time t_j by E_j. The magnitude of the field E_j, attenuates to $f(z, E_j)$ at the location of the object. Hence, at time instance t_j, the radius of each detection disk is

$$r_j^2 = \left(\frac{z \left| \Gamma a^3 f(z, E_j) \right|}{T} \right)^{2/3} - z^2. \tag{3.25}$$

Comparison of the two electric images allows us to derive a relationship between the object-fish distance z, and detection disk radii, r_j;

$$\frac{r_1^2 + z^2}{f(z, E_1)^{2/3}} = \frac{r_2^2 + z^2}{f(z, E_2)^{2/3}}. \tag{3.26}$$

The only unknown quantity in equation (3.26) is the fish-object distance z, and so it can theoretically be evaluated.

The electric field generated by the electric organ (EO) attenuates with distance. There

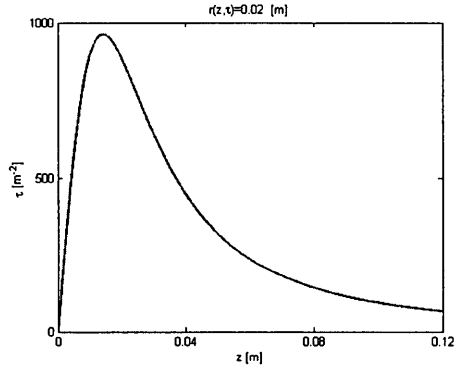

Figure 3.9: Fixed radius ambiguity - For a fixed radius $\left(\frac{z}{\tau}\right)^{3/2} - z^2 = c$, each 2-tuple (z, τ) on the curve satisfies equation (3.24). Hence, knowing the value of the radius at one instance is insufficient to determining the object-fish distance.

is evidence to indicate that the electric potential and field do not attenuate with distance from the fish at a constant rate [44]. Close to the fish, the field strength falls approximately as the inverse of the distance [42]. At large distances, the falloff approaches the inverse of the fourth power of the distance. At distances relevant for electrolocation the scaling varies between -1 and -3. Regardless of the particular scaling, the attenuation is in proportion to the fish's electric field [42]. In other words, the function f is a separable function of E and z. That is, $f(z, E) = \alpha E f_z(z)$. Consider the general case where the field attenuates with the $n-$th power of the distance $\left(f(z, E) = \frac{\alpha E}{z^n}\right)$. Then the fish-object distance is unambiguously defined by

$$z = \sqrt{\frac{r_1^2 E_2^{2/3} - r_2^2 E_1^{2/3}}{E_1^{2/3} - E_2^{2/3}}}. \tag{3.27}$$

3.1.3 Numerical Implementation

Equation (3.27) analytically relates the object-fish distance to the radius of the electric image and the magnitude of the generated EOD. It can be used to categorically disambiguate the distance of an object from its other unknown properties. To be implemented, equation (3.27) must be discretized by the fish. That is, as receptors are not present at all locations on the fish surface, the radius of the detection disk must be estimated numerically.

Any single electric image parameter is simultaneously influenced by an object's material, size and distance to the fish. As such there are three degrees of ambiguity to consider in distance detection. Further, as the electroreceptors are located at discrete locations on the surface of the fish, we test the ability of our model (3.27) to correctly localize a dielectric sphere for varying values of each of object size, distance and dielectric constant, under a discretization process.

Method

We begin by discretizing a horizontal plane Π, a distance $d = 7$ cm away from the center of a dielectric sphere of size $a = 2$ cm and dielectric constant $\epsilon_i = 2.25$ (polyethylene), into sub-squares of some predetermined size (see below). The perturbation to the otherwise uniform electric field by the introduction of the sphere is recorded at the center of each sub-square on the plane. If such a perturbation is above a threshold $T = 10^{-4}$ mV/cm, then we consider that sub-square to be within the region of detection. The dielectric media, within which the sphere is introduced, is assumed to have a dielectric constant of value $\epsilon_e = 80.1$ (i.e. that of water at 20°C). The electric image is recorded for EOD strengths of 0.9 and 0.55 mV/cm, measured at the fish, and is assumed to attenuate according to

$$f(z, E) = \frac{\alpha E}{z^n}. \tag{3.28}$$

We assume that the sub-squares forming the region of detection form a perfect disk. The radius of this disk is calculated by $r = \sqrt{A/\pi}$, where A is the sum of the areas of the "active" sub-squares.

Clearly, the smaller we choose our sub-squares the better an estimate of the electric image's radius we attain. We are, however, bounded by the number of receptors that must be contained within each sub-square. Below we have chosen to discretize Π into sub-squares of width 0.06 cm. For receptor densities ranging from 9-15 per mm^2 [18], this would ensure that there would be approximately 3.24-5.4 receptor organs within each sub-square. Requiring multiple receptors within the same sub-square would ensure against false activation of a sub-square due to internal receptor noise. Such noise would arise from the random fluctuations in membrane potential and transmitter release.

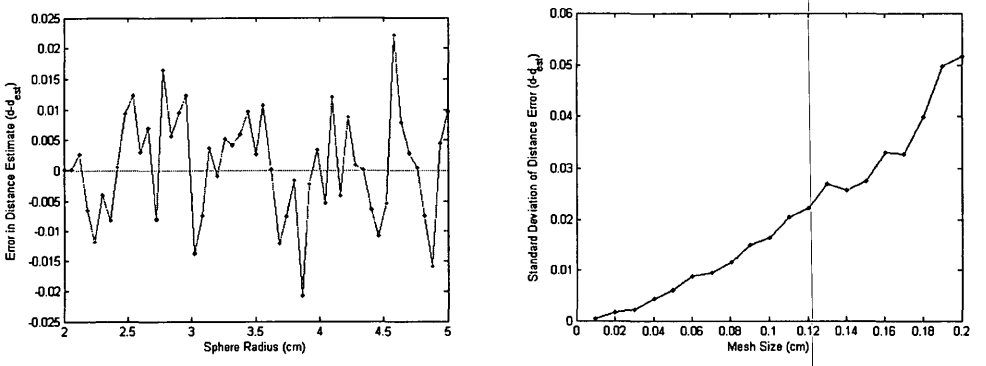

(a) (b)

Figure 3.10: Model results - sphere size - (a) Error in estimate of distance for spheres of varying sizes calculated at a mesh size of 0.06 cm. The non-zero error is due to the discretization procedure we implement when calculating the detection disk radius, (see text). (b) Standard deviation of the error in distance estimate as a function of mesh size. The standard deviation of (a) represents a single point at 0.06 cm on this graph. The parameter values are: $d = 7$ cm, $T = 10^{-4}$ mV/cm, $\epsilon_e = 80.1$, $\epsilon_i = 2.25$, $E(t_1) = 0.9$ mV/cm and $E(t_2) = 0.55$ mV/cm.

Sphere Size

Figure 3.10a shows the error in our estimate of distance for spheres of varying size. The error clearly fluctuates about zero, with a mean value of 6.56×10^{-4} cm. These results indicate that the size of the sphere does not influence our model's estimate of distance. The non-zero error in our estimate is due to the discretization procedure we implement when calculating the detection disk radius. A plot of the standard deviation of the error as a function of the mesh size (fig.3.10b) clearly demonstrates this.

Sphere Dielectric Constant

Figure 3.11a shows the error in our estimate for spheres of different material (relative permittivity). Again, as in the case of the different sized spheres, we see fluctuations about zero, caused by the discretization procedure, (fig. 3.11b). The small value of the mean (2.74×10^{-5} cm), and that of the largest deviation (1.188×10^{-2} cm at $\epsilon_i = 2.4$), indicates that our model's estimate is not influenced by the objects material.

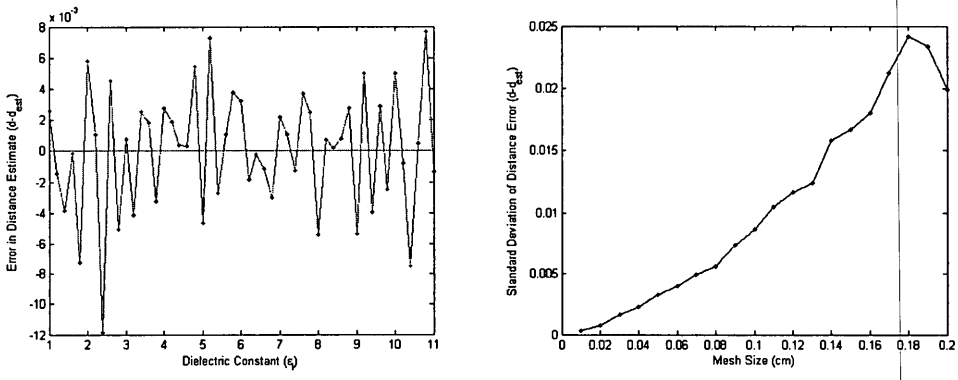

(a) (b)

Figure 3.11: Model results - sphere relative permittivity - (a) Error in estimate of distance for spheres varying relative permittivity, calculated at a mesh size of 0.06 cm. The non-zero error is due to the discretization procedure we implement when calculating the detection disk radius, (see text).(b) Standard deviation of the error in distance estimate as a function of mesh size. The standard deviation of (a) represents a single point at 0.06 cm on this graph. The parameter values are: $a = 2$ cm, $d = 7$ cm, $T = 10^{-4}$ mV/cm, $\epsilon_e = 80.1$, $E(t_1) = 0.9$ mV/cm and $E(t_2) = 0.55$ mV/cm.

For ideal receptors (those with $T = 0$ mV/cm), an object is undetectable when its relative permittivity matches that of the water exactly, that is when $\epsilon_i = \epsilon_e$. The range of relative permittivity of non-detectable objects increases greatly for non-ideal receptors. Figure 3.12a depicts the radius of the electric image of a sphere as a function of its dielectric constant ϵ_i. The sphere has a radius of $a = 2$ cm and is immersed in a medium of dielectric constant $\epsilon_e = 80.1$. We can see that objects with relative permittivities ranging anywhere in between 36-153 remain undetectable; as the radius of the electric image is zero for these values of ϵ_i. Increasing the field strength and sensitivity reduces this range, see figures 3.12c and 3.12d, respectively.

Another factor affecting the range of materials detectable to the fish is distance. Figure 3.12b depicts the radius of the electric image of a sphere at $d = 5$ cm. Here, the relative permittivity of non-detectable materials range in value from 70-91; an 82% reduction in the range compared to objects at $d = 7$ cm. This reliance of material detectability on distance helps in decluttering the electric image.

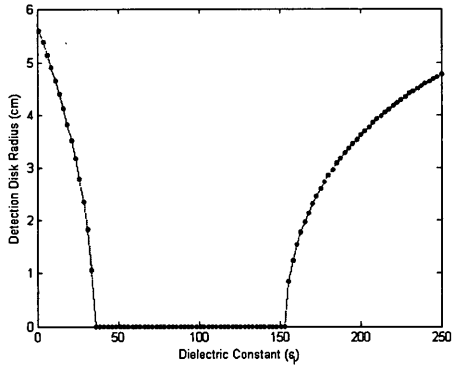

(a) Default parameter values: $d = 7$ cm, $E = 0.9$ mV/cm, $T = 10^{-4}$ mV/cm

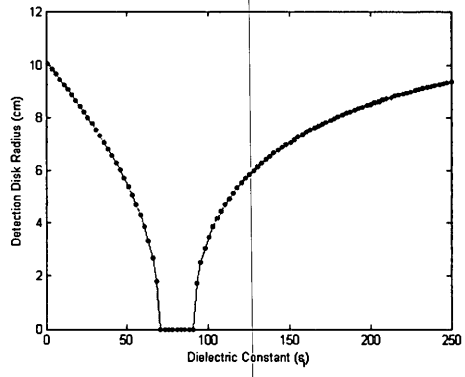

(b) Reduced distance, $d = 5$ cm

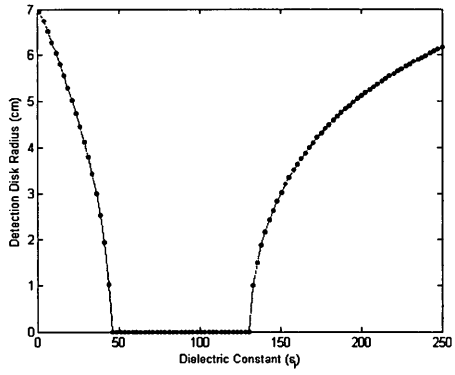

(c) Increased field strength, $E = 1.1$ mV/cm

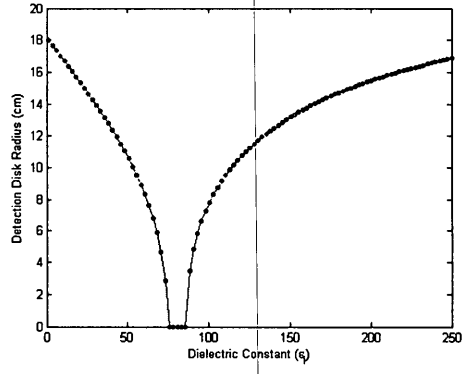

(d) Increased Sensitivity, $T = 10^{-5}$ mV/cm

Figure 3.12: Radius of the electric image of a 2 cm sphere as a function of the sphere's dielectric constant ϵ_i. The sphere is placed in a dielectric media of relative permittivity $\epsilon_e = 80.1$. (a) radius for default parameter values: $d = 7$ cm, $T = 10^{-4}$ mV/cm and $E = 0.9$ mV/cm. (b): radius at reduced distance $d = 5$ cm. (c) radius at increased electric field strength $E = 1.1$ mV/cm. (d) radius for increased sensitivity $T = 10^{-5}$ mV/cm

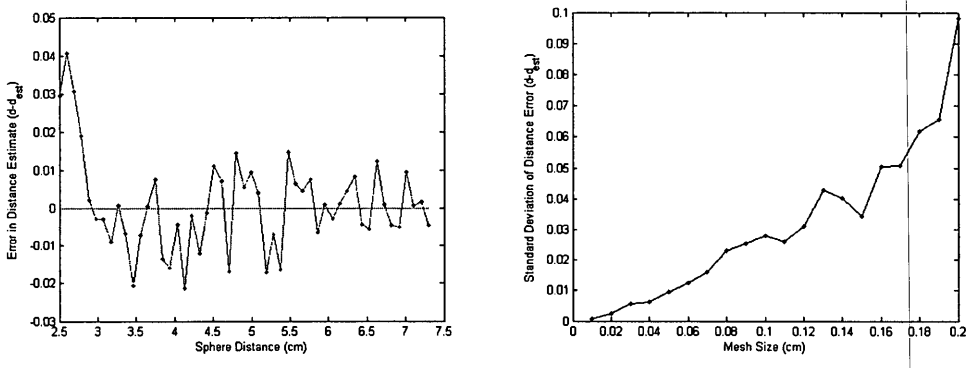

(a) (b)

Figure 3.13: Model results - sphere distance - (a) Error in estimate of distance for spheres varying distances, calculated at a mesh size of 0.06 cm. The non-zero error is due to the discretization procedure we implement when calculating the detection disk radius, (see text).(b) Standard deviation of the error in distance estimate as a function of mesh size. The standard deviation of (a) represents a single point at 0.06 cm on this graph. The parameter values are: $a = 2$ cm, $T = 10^{-4}$ mV/cm, $\epsilon_e = 80.1$, $\epsilon_i = 2.25$, $E(t_1) = 0.9$ mV/cm and $E(t_2) = 0.55$ mV/cm.

Sphere Distance

We finally consider our model's ability to localize objects at varying distances (fig. 3.13a). Once again we observe non-zero error values caused by the discretization process (fig. 3.13b). The small mean value of the error (9.458×10^{-4} mV) confirms our model's ability to detect objects at varying distances.

The relatively large error values (0.01-0.04 mV) recorded for near distances (2.5-2.8 cm) are virtually eliminated by reducing the mesh size (results not shown).

We note that for the electric field strengths used ($E(t_1) = 0.9$ mV/cm, $E(t_2) = 0.55$ mV/cm) the 2 cm sphere is not detected for distances beyond 7.3 cm. To sense more distant objects greater electric fields or higher sensitivity must be used.

Electric Field Strength

Localization as described by our model requires analysis of the electric image at two different magnitudes of the EOD. In theory, localization could occur for any two electric images not produced by electric fields of identical magnitude. In practice however, for an accurate approximation, the field magnitudes must be chosen to differ by a certain degree. Figure 3.14a illustrates the dependence of the absolute error on the difference in field magnitudes. It is clear that the closer in magnitude the two field strengths E_1 and E_2 are, the larger the error in the estimate.

The amount by which the fields need to differ depends on the density of the receptors, which is much higher in the rostral region. Receptor density is akin to spatial resolution; the higher the density, the finer the mesh containing a certain number of receptors that can be made. Figure 3.14b depicts the absolute error as a function of the difference in field magnitude for mesh sizes 0.04, 0.06 and 0.1 cm. Notice, the larger the mesh size, the greater the difference the field magnitudes $(E_1 - E_2)$ must be to achieve the same level of error. For example, if we choose an error upper bound of 0.04 cm, then with a 0.04 cm mesh size, the difference between E_1 and E_2 can be anywhere within the interval $[-0.022, 0.0285]$. On the other hand for the same error bound, using a 0.1 cm mesh size, the range of $(E_1 - E_2)$ must increase to be within the interval $[-0.090, 0.142]$.

Choosing E_1 to be the maximum amplitude that can be achieved at the object; the denser the receptors, the larger the value of E_2 that can be chosen. As such, we can conclude that the more dense the receptors, the greater, both the distance and variation of materials (ϵ_I) that can be sensed.

3.2 Noise

The electrosensory systems of weakly electric fish are well known for their ability to detect weak electromagnetic signals, on the order of μV/cm in some species [42]. This extreme sensitivity has been attributed to a multitude of receptor organ characteristics such as continuous partial activation of Ca conductance, ribbon synapses, efficiency of transmitter release and the large convergence of receptor cells to afferent fibers [53]. High sensitivity, however, is only useful if accompanied by mechanisms to limit noise.

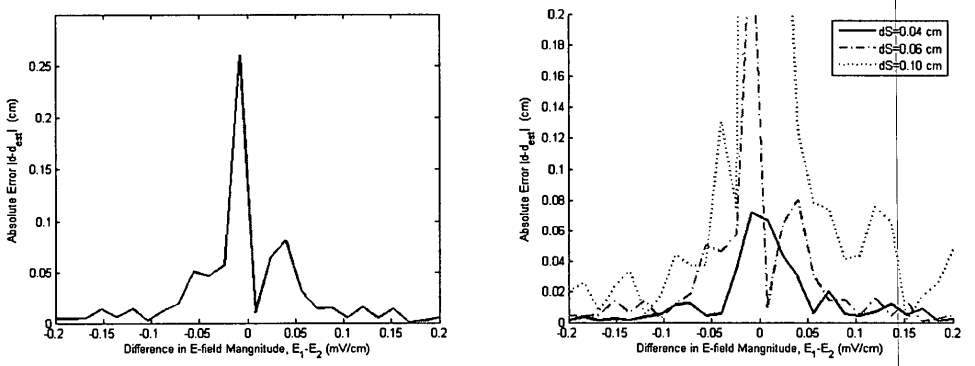

(a) (b)

Figure 3.14: Model results - effect of field difference ($E_1 - E_2$) on error - (a) Magnitude of error in the distance estimate ($|d - d_{est}|$), as a function of difference in field magnitudes ($E_1 - E_2$), generating the two electric images. (b) Same as (a), evaluated for three different mesh sizes, dS.

The noise in the fish's electrosensory system is due to internal as well as external sources. Internal noise such as that arising from random fluctuations in membrane potential and transmitter release can be canceled out by the convergence of multiple receptor cells onto an afferent nerve fiber as well as multiple synaptic connections between an individual cell and the fiber. On the other hand, as environmental noise affects the signal itself, receptor convergence does nothing to filter out this type of noise.

To this effect, we devise an algorithm based on our model (3.27) for the detection of objects in the presence of external environmental noise. This novel algorithm is based on repeated recordings of the radius of detection for two amplitudes of the EOD. For each particular EOD amplitude, the variation in the recorded radii is due to the noise in the signal. Calculating the sample mean of the recorded radii allows us to formulate an equation solely based on the object-fish distance.

We begin by assuming that the noise ξ is present at the location of the object center. That is;

$$E_{obj} = f(z, E_{fish}) + \xi,$$

where the noise ξ is taken to come from a *zero*-mean distribution (one important source of noise, a *daphnia* swarm, was found to produce band-limited Gaussian noise [54]).

Under this assumption our detectability disk is defined by all ordered pairs (x, y) satisfying

$$\left(\frac{z\,|\Gamma a^3(f(z,E)+\xi)|}{T}\right)^{2/3} \geq x^2+y^2+z^2. \tag{3.29}$$

On the fish surface, the boundary of this region is characterized by the stochastic radius

$$R^2 = \left(\frac{z\,|\Gamma a^3(f(z,E)+\xi)|}{T}\right)^{2/3} - z^2. \tag{3.30}$$

Supposing that the environmental noise $\xi \sim N(0,\sigma^2)$, where the standard deviation σ determines a measure of the maximum noise levels, the probability density function of R^2 is

$$\begin{aligned} f_{R^2}(r^2) &= \frac{1}{\sigma\sqrt{2\pi}}\frac{3T\sqrt{r^2+z^2}}{2z|\Gamma a^3|}\left[\exp\left\{\frac{-1}{2\sigma^2}\left[\frac{T(r^2+z^2)^{3/2}}{z|\Gamma a^3|}-f\right]^2\right\}\right. \\ &\qquad \left. +\exp\left\{\frac{-1}{2\sigma^2}\left[\frac{T(r^2+z^2)^{3/2}}{z|\Gamma a^3|}+f\right]^2\right\}\right], \end{aligned} \tag{3.31}$$

where we have denoted $f(z,E) \equiv f$ for clarity.

There are two ways by which our model can incorporate external noise. Each involves repeated recordings of the radius of detection for two particular values of EOD amplitude, E_1 and E_2. For each recording, the EOD has the same magnitude (either E_1 or E_2) and the only variation in the radius is due to the noise in the signal. Let us denote by R_{jk} the $k\,th$ recorded radius associated with E_j, that is

$$R_{jk}^2 = \left(\frac{z|\Gamma a^3(f(z,E_j)+\xi_k)|}{T}\right)^{2/3} - z^2 \qquad \text{for } j=1,2. \tag{3.32}$$

Our first approach is to use the sample mean of the recorded radii to evaluate distance. In other words

$$\begin{aligned} \hat{z} &= \sqrt{\frac{\bar{R}_1^2 E_2^{2/3} - \bar{R}_2^2 E_1^{2/3}}{E_1^{2/3}-E_2^{2/3}}}, \\ \text{where}\quad \bar{R}_j^2 &= \frac{1}{n}\sum_k R_{jk}^2. \end{aligned} \tag{3.33}$$

We have denoted our estimate of the distance by $\hat{z}$.

The second possible approach is to evaluate - based on our model - a sample estimate for distance z_k, for *each* recording. A final, more precise, estimate of distance $\hat{z}$, is then derived by taking the mean of the sample distances. Symbolically,

$$\begin{aligned} \hat{z} &= \frac{1}{n}\sum_k z_k, \\ \text{where} \quad z_k &= \sqrt{\frac{R_{1k}^2 E_2^{2/3} - R_{2k}^2 E_1^{2/3}}{E_1^{2/3} - E_2^{2/3}}}. \end{aligned} \tag{3.34}$$

In both cases above, we have assumed that the field is proportional to a separable function of E and z.

Electric image width is encoded by a neuronal population in the early stages of the electrosensory pathway. Our first approach requires only repeated recordings of the electric image profile, before downstream electrosensory networks extract information about object location. On the other hand, the second approach would require the use of downstream electrosensory networks for each recording. With no clear advantage in accuracy or speed, we disregard the second possibility and adopt the first as "the" approach used by the fish in extracting distance information in the presence of external noise.

Our algorithm implicitly requires the object location to remain relatively stationary while repeated recordings are obtained. The high EOD frequency of wave-type fish (15-1800 Hz; [55]) and increased EOD emission (80 Hz; [34]) of pulse-type fish indicate that multiple recordings can be made in a very short time interval, within which the object can be expected to remain relatively stationary.

3.2.1 Numerical Implementation

Investigation of our model's performance in the presence of external noise ξ begins with the assumption that $\xi \sim N(0, \sigma^2)$. As previously mentioned, the standard deviation σ, provides a measure of the level of maximum noise. Taking the maximum noise to be on the same order as the signal itself, (i.e. on the order of 1 mV/cm), we allow σ to be as

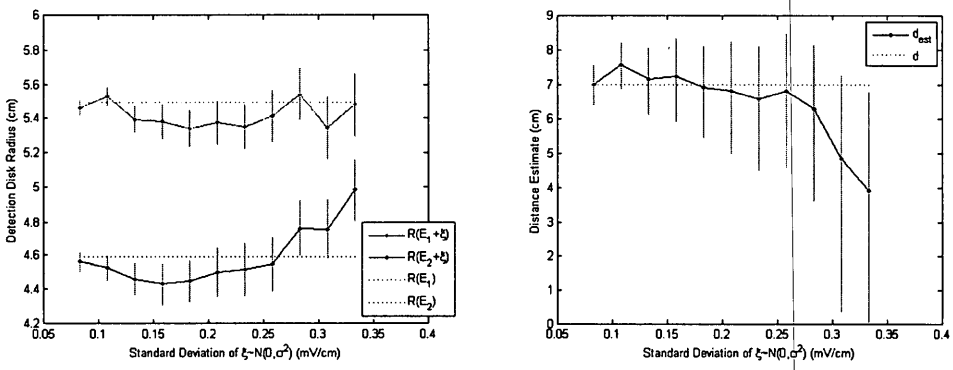

(a) (b)

Figure 3.15: Model performance in presence of $N(0, \sigma^2)$ noise - (a) Mean radius of 400 sampled electric images generated by EOD amplitudes $E_1 = (0.9 + \xi)$ mV/cm (blue) and $E_2 = (0.75 + \xi)$ mV/cm (black), where $\xi \sim N(0, \sigma^2)$. The noiseless radii for magnitudes E_1 and E_2 are depicted by the blue and black dashed lines, respectively. The horizontal axis (σ) gives a measure of noise strength. Red horizontal bars represent a 95% confidence interval. (b) For each σ the two radii in figure (a) are used along with equation (3.33) to generate an estimate $\hat{z}$ of the object distance. The two 95% CI in figure (a) are used to generate a 90% (Bonferroni) confidence interval for the estimate distance, shown as red horizontal bars. Actual object distance was $d = 7$ cm, (dotted line).

large as 1/3 mV/cm, ensuring that 99.7% of the time $\xi \in [-1 \text{ mV/cm}, 1 \text{ mV/cm}]$. One particular source of external electromagnetic noise, a *Daphnia* swarm, produces noise on the order 10^{-2} mV/cm, [54], deeming our noise levels more than adequate.

Figure 3.15a displays the detection disk radius in the presence of $N(0, \sigma^2)$ noise. The means of 400 sampled radii at each of field strengths $E_1 = 0.9$ mV/cm (solid blue) and $E_2 = 0.75$ mV/cm (solid black) are displayed along with a 95% confidence interval (red) for each σ value. The dotted blue and black curves designate the corresponding radii in the absence of electromagnetic noise.

For each value of σ, we have used equation (3.33) along with the means of the 400 sampled radii at the two field strengths to calculate an estimate of the object distance $\hat{z}$, (solid black line in figure 3.15b). The 95% confidence interval range of the two radii have been used to calculate a 90% (Bonferroni) confidence interval for $\hat{z}$. We can see

that for all but the strongest noise levels the actual distance is well within the confidence interval of our estimate.

In the absence of noise, using equal parameter values, our estimate of distance is $z = 6.9957$ cm. This estimate is one order of magnitude more accurate than the most accurate estimate in the presence of noise ($\hat{z} = 6.9792$ cm at $\sigma = 1/12$). This result suggests that environmental noise, at any level, has a negative effect on distance estimation.

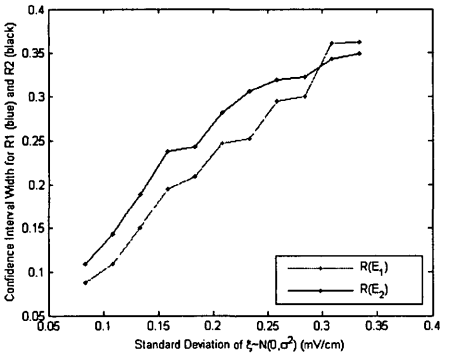

Figure 3.16: CI width - Width of the 95% confidence intervals for the two radii R_1 (blue) and R_2 (black) of figure 3.15a.

Figure 3.16 depicts the width of the 95% confidence intervals of the radii $R(E_1)$ (blue) and $R(E_2)$ (black) presented in figure 3.15a. For $\sigma \in [1/12, 0.2833]$ the confidence interval of $R(E_2)$ is consistantly wider than that for $R(E_1)$. Intuitively this is clear, as the noise is a larger percentage of the signal $E_2 + \xi$ than of $E_1 + \xi$. For fish to electrolocate effectively in noisy environments it is advantages to utilize larger EOD magnitudes. Large values of σ cause the noise to mask the EOD signal.

3.2.2 Stochastic Resonance

Stochastic resonance (SR) is a mechanism by which a system embedded in a noisy environment can enhance its sensitivity to weak time-dependent signals. It has been suggested [56] that by the theory of stochastic resonance, signal detection can be improved in some fish species.

To study the role that SR plays in signal detection, we begin by recalling the detectability disk in the presence of noise:

$$\left(z\frac{\left|\Gamma a^3\left(f(z,E_0)+\xi\right)\right|}{T}\right)-z^2\leq x^2+y^2. \tag{3.35}$$

In practice it may be reasonable to require the image radius to have some minimum value. But here, strictly speaking, a signal is detectable if the radius of the disk is positive. That is

$$\left(z\frac{\left|\Gamma a^3\left(f(z,E_0)+\xi\right)\right|}{T}\right)-z^2>0. \tag{3.36}$$

Upon manipulation, we arrive at a minimum bound required for a signal to be detectable.

$$|f(z,E_0)+\xi|>\frac{Tz}{|\Gamma a^3|}. \tag{3.37}$$

Stochastic resonance occurs if the signal-to-noise ratio of a *non-linear* system increases for moderate values of noise intensity. The intensity-response function of electroreceptors is roughly linear [21, 57], suggesting that a small increase in the intensity of the input would solicit a small increase in the response of the electroreceptors. The presence of stochastic resonance is not supported in systems lacking a threshold response. However, our depth perception mechanism, based on the threshold dependent region of detection, and our results above, clearly demonstrate the criteria necessary for the existence of stochastic resonance.

Our findings indicate that although the addition of external noise aids in the detection; it plays a counterproductive role in the localization of objects. These results are in line with Russell et al.'s findings in that the addition of noise caused the paddlefish *Polyodon spathula* to broaden the spatial range for the detection of plankton *Daphnia*, however, the capture rate of *Daphnia* did not increase with the addition of noise compared to controls [56].

3.3 Localization of Cube

Behavioral experiments have shown that weakly electric fish perceive the distance of a cube to be less than that of a sphere when placed at the same distance to the fish

[12, 31, 34]. In this section we test our depth perception model against these experimental results.

We consider a dielectric cube of side length $2a$ and dielectric constant ϵ_i, immersed in a media (water) of dielectric constant ϵ_e. Assuming a uniform electric field prior to the introduction of the dielectric cube, the perturbation to the potential measured at the field point P_e after the introduction of the cube is described by

$$\delta\Phi(P_e) = \frac{\epsilon_e - \epsilon_i}{4\pi\epsilon_e} \iint_S \Phi(q) \frac{\partial}{\partial n} \frac{1}{|\bar{r}_q - \bar{r}_{P_e}|} \, \mathrm{d}s, \tag{3.38}$$

where $\bar{r}_q - \bar{r}_{P_e}$ is the directed distance from the field point P_e to the point q on the cube surface, S, (see Appendix B for derivation). As the integral in equation (3.38) is evaluated for q ranging over the entire surface S, it is clear that the potential at any point exterior to S is dependent on the surface potential distribution. To this end we also require the expression

$$\Phi(q_0) = \frac{2\epsilon_e}{\epsilon_e + \epsilon_i} \Psi(q_0) + \frac{\epsilon_e - \epsilon_i}{2\pi(\epsilon_e + \epsilon_i)} \iint_S \Phi(q) \frac{\partial}{\partial n_q} \frac{1}{|\bar{r}_q - \bar{r}_{q_0}|} \, \mathrm{d}s_q. \tag{3.39}$$

which describes the potential at the point q_0 on the surface of the cube, (see Appendix B for derivation). Equations (3.38) and (3.39) need to be approximated numerically.

Numerical Methodology

To simplify the algebra we orient our reference frame such that the center of the cube coincides with the origin and the electric field lies parallel with the applicate, $\vec{k}$. Each face of the cube is partitioned into N^2 sub-squares, and the symmetries

$$\Phi(x, y, z) = \Phi(\pm x, y, z) = \Phi(x, \pm y, z) = -\Phi(x, y, -z) = \Phi(y, x, z) \tag{3.40}$$

are used to approximate the surface integral in equation (3.39), [58];

$$\iint_S \Phi(q)\frac{\partial}{\partial n_q}\frac{1}{|\bar{r}_q-\bar{r}_{q_0}|}\,\mathrm{d}s_q \approx 4\frac{a^2}{N^2}\sum_{\xi,\eta,\zeta=\pm 1}\Bigg\{ \tag{3.41}$$

$$\sum_{0<y_q<a}\sum_{0<z_q<a}\Phi(a,y_q,z_q)\Bigg[\frac{-\zeta(a-\xi x_{q_0})}{\{(a-\xi x_{q_0})^2+(y_q-\eta y_{q_0})^2+(z_q-\zeta z_{q_0})^2\}^{3/2}}$$

$$+\frac{-\zeta(a-\eta y_{q_0})}{\{(y_q-\xi x_{q_0})^2+(a-\eta y_{q_0})^2+(z_q-\zeta z_{q_0})^2\}^{3/2}}\Bigg]$$

$$+\sum_{0<x_q<a}\sum_{0<y_q<a}\Phi(x_q,y_q,a)\frac{-\zeta(a-\zeta z_{q_0})}{\{(x_q-\xi x_{q_0})^2+(y_q-\eta y_{q_0})^2+(a-\zeta z_{q_0})^2\}^{3/2}}\Bigg\},$$

where above we have denoted the Cartesian coordinates of points q and q_0 on the surface by (x_q, y_q, z_q) and $(x_{q_0}, y_{q_0}, z_{q_0})$ respectively. Next, a horizontal plane, representing the fish's skin surface, is defined. The surface is discretized in such a way that each sub-square has area 0.36 mm^2. As such, each sub-square is expected to contain approximately 3.24-5.4 electroreceptors organs [18]. The potential perturbation for each sub-square is calculated using equations (3.38) and (3.39). Those potentials whose amplitude fall below the threshold T are discarded. The remaining sub-squares combine to form the electric image of the cube, which we assume to be circular. Subsequently, the radius of this electric image is calculated using $r = \sqrt{A/\pi}$, where A is the sum of the areas of the remaining "active" sub-squares. Finally, the obtained radius is used in equation (3.27) to estimate the distance of the cube.

Figure 3.17 shows the error in the perceived distance of both a sphere (red) and a cube (blue). In particular, the error associated with the sphere fluctuates around zero, while the error in the perceived distance of the cube is linearly correlated with the distance of the cube. Using linear regression, the correlation is found to follow

$$\text{error} = z - \hat{z} = 0.1033z - 0.6552. \tag{3.42}$$

This analysis indicates that when the center of the cube is around 6.343 cm to the fish surface, the fish is capable of detecting the cube's actual location. However, when the distance deviates from this value, the fish is prone to make a mistake. When the cube's distance is larger than 6.343 cm the fish perceives the cube to be closer and

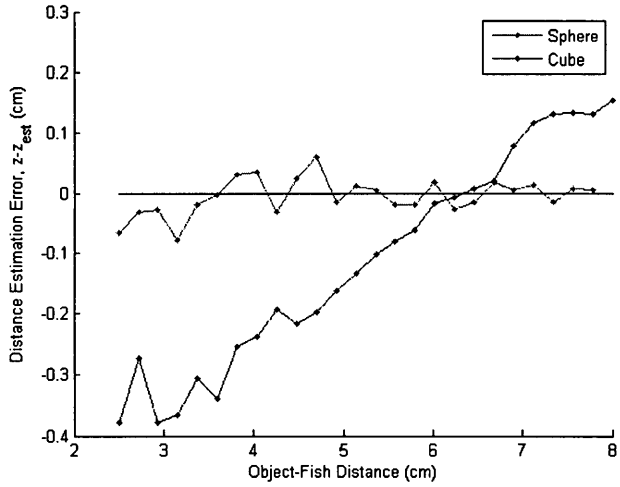

Figure 3.17: Cube localization error - Error in the percieved distance $(z - \hat{z})$ of a cube (blue) and sphere (red) at different object-fish distances. We have kept all parameter values the same with $\epsilon_i = 2.25$, $\epsilon_e = 80.1$, $T = 10^{-4}$ mV/cm, $E_1 = 0.9$ mV/cm and $E_2 = 0.75$ mV/cm. The radius of the sphere and the half-width of the cube were set to 2 cm. At $z = 8$ cm the electric image associated to the sphere for field strength E_2 has zero radius and so is not included in the diagram.

when it is less than 6.343 cm the cube is perceived to be further than its actual location.

These results can be used to test the validity of our model. In comparing the distance of two dielectrics; a cube and sphere of the same size, located the same distance to the fish, the fish should perceive the cube to be further than the sphere up until a particular object-fish distance (6.343 cm using our parameters). When the object-fish distance is increased beyond this value the opposite should be observed, where the sphere is perceived to be further than the cube.

3.4 Conclusion

Our results show that active electrolocation, based on single parameter measurements, can be achieved if the temporal properties of the electric image are taken into account. Such a mechanism would require only a single, narrowly tuned topographic neuronal map to accurately estimate distance. Our algorithm's performance in localizing an object is independent of the object's size, material and distance.

Our model is based on non-ideal electroreceptors. As with any physical system, weakly electric fish electroreceptors are not perfect. Non-ideal receptors partition the fish surface into two distinct regions; detectable and non-detectable. Comparing the size of the detectability region for two different magnitudes of the EOD allows us to formulate an equation, in which the only unknown is the object-fish distance. It is worth noting that although we have chosen the receptor threshold as the value at which the fish surface is partitioned, our model would also work with any other value. As such, we can always choose the threshold at a level to ensure that the size of the "detectable" region is limited to the surface of the fish.

There are three major assumptions that are made by our model. The first is that the field is uniform prior to the introduction of the object. Alhough the near field, where electrolocation takes place, is highly complicated, in the vicinity of small objects, we can assume the field to be uniform. Furthermore, it can be shown that in addition to a dipole moment, a non-uniform field induces higher order multi-pole perturbations which attenuate with distance from the object more rapidly than the dipole

perturbation. A second assumption in the model is that the perturbations at the skin are not affected by the presence of the fish. We have shown that a resistive fish skin will scale the potential perturbation but will not introduce any nonlinearity into the system. Depending on the relative permittivity of the skin, this perturbation may need to be taken into account, however, the mechanism described in this chapter, and the results shown, remain valid.

Finally, we have assumed that objects to be localized are spherical. Earlier we noted that the fish's main prey, the *Daphnia Magna* is roughly spherical. Also, the perturbation of the electric field due to small or distant non-spherical objects converges to that of a spherical object. This property is reflected in the Laplace equation which links the electric potential to the charge distribution and is used to model the field perturbation by a dielectric object. Figure 3.2b demonstrates how at far enough distances the contours of the electric image of a cube resemble those of a sphere. A spherical representation of distant objects is a good approximation.

Objects, whose relative permittivity is close to that of the surrounding media, remain invisible to non-ideal receptors, characterizing an *invisible permittivity spectrum*. The range of permittivities that comprise this spectrum depend on the object's distance, the strength of the electric field and the receptor's sensitivity threshold. An increase in the object's distance tends to increase the range of this spectrum, thereby in effect, de-cluttering the electric image. Increases in both field strength and receptor sensitivity have the opposite effect; decreasing the spectrum range.

We have chosen to model the field such that it is oriented perpendicular to the fish surface. Such fields appear predominantly in the rostral region, where receptors are more dense. Our model has shown that receptor density is positively correlated with the distance at which objects can be localized and negatively correlated with the invisible permittivity spectrum. In other words, the more dense the receptors, the greater the distance that can be determined and the more varied the relative permittivity of material that can be localized.

We have devised an algorithm, based on repeated recordings of the electric image radius, for localization of objects in the presence of environmental electromagnetic noise. Our algorithm relies primarily on neuronal population codes in the early stages of the electrosensory pathway. Downstream electrosensory networks are employed only to extract the final information about the object location. We have shown that noise at any level has a negative effect, and that greater EOD magnitudes facilitate electrolocation in noisy environments. Our model provides the threshold dependent physiological basis on which stochastic resonance can be employed. Our results are in line with Russell et al.'s (1999) findings in that the addition of noise can facilitate the detection of subthreshold signals, but does not aid in their localization.

The validity of our spatiotemporal model can be corroborated by our work in predicting the distance of a cube. Our model predicts that a fish presented with a dielectric cube and a sphere of equal lateral distance would perceive the cube to be closer if both objects are near and further if the two objects are far. A behavioral experiment in line with von der Emde's experiment [31] could be conducted to test these results.

4

Receptor Arrays: An Inverse Problem Approach to Depth Perception

Past studies of depth perception have focused on extracting location information from sets of electric image features [9, 12, 31, 32, 33, 34, 40, 41], (chapter 3). In this chapter, we take a completely different approach to the problem of depth perception by considering the information that is available at a single receptor. By treating the problem as an inverse problem, we show that distance information can completely be encoded within the amplitude of the electric image measured at four or fewer receptor locations on the fish surface. We present a mechanism, by way of choosing an array of receptors, by which this information can be unambiguously extracted. Our choice of array is independent of the object size, its electric contrast, the EOD's variation in time and its magnitude. We propose that the fish's probing movements, observed during electrolocation tasks could serve to identify such suitable receptors and/or verify the assessment made from one such array. Our approach provides a lower bound on the information that is necessary for the fish to unambiguously decode the location of an object.

Our choice of receptors is one which could unambiguously extract the relevant information. Given the high electroreceptor density (9-15 organs/mm^2 on the head and 0.6-3.4 organs/mm^2 on the trunk [18]) over the fish skin surface, the existence of other arrays having similar properties is highly probable. The distribution of electroreceptors

on the surface of the body provides a spatial array of receptors intrinsically capable of representing stimulus location [53]. The receptors contact primary afferent fibers that terminate on neuronal maps in the electrosensory lateral line lobe (ELL). The neurons comprising these maps have preferred locations for which they respond maximally, with their activity decreasing for other locations. Hence, the neural responses of the ELL maps are described by bell-shaped tuning curves. Amplitude of the electric image is more accurately encoded by neurons encompassing wider tuning curves [28]. Activity of each neuron in each of the ELL maps reflects the aggregate response of several electroreceptor organs in a small region on the surface. Partitioning the fish surface into small regions, the high density of receptors ensures that each region is represented by neuronal activity within the ELL maps.

We begin this chapter with an overview of the model, defining regions of receptor ambiguity and array ambiguity. We apply our methodology to analytically extract distance information for objects placed in fields perpendicular, parallel and generally oriented to the fish surface. In every case, it is shown that amplitude information from at most four locations is necessary to localize an object. Next, we study the effects of electromagnetic noise. It is found that external noise does not mask location information, but rather information regarding the size and electric contrast of objects. Lastly, we consider the case where the receptors are non-ideal.

4.1 Model

Motivation

To date, several depth perception mechanisms have been proposed. Each has focused on extracting location information from sets of electric image features. Whereas earlier studies have relied on extracting location information from sets of electric image parameters [9, 12, 31, 32, 33, 34, 40, 41], we have thus far concentrated on a single image parameter measured at two points in time (chapter 3). Now that we have been able to show that localization can be achieved using a single image parameter, we ask what the minimum amount of information required to achieve this task would be.

Model Outline

To answer this question we look at the information (amplitude of EOD perturbation) at a *single* receptor. If we know the perturbation is due to a spherical dielectric with unknown size and relative permittivity, where could the object be located? Identifying all such locations we define the receptor's ambiguity region. As can be imagined, a receptor's ambiguity region is large; consisting of an infinite number of points.

To narrow down the location possibilities, we consider the ambiguity regions of multiple receptors. For an array of receptors, the set of locations common to each member receptor's ambiguity region constitute the array's ambiguity region. Expectedly, the ambiguity region of an array of receptors is far smaller than that of a single receptor. Further, the actual location of the object is guaranteed to be in the set of *any* array as it is in the ambiguity region of all receptors.

Our task then is the identification of an array whose ambiguity region consists of only one point; the actual object location. Such an array needs to be independent of the object size and relative permittivity. The minimum number of receptors that form such an array provide the lower bound on the information that is necessary for object localization.

4.1.1 Assumptions

Our model makes three key assumptions that need to be addressed. First, we have based our model on the localization of a dielectric sphere which we assume is placed within a uniform electric field. Also, we have assumed that the presence of the fish itself does not affect the electric image. These assumptions are similar to those made and justified in chapter 3. We will briefly state some of the key points here, but direct the reader to chapter 3 for the full rationalization.

Object Geometry

Foremost, the geometry of electric fish's main prey, the *Daphnia Magna* is roughly spherical. Second, as the size of a non-spherical object is reduced or its distance increased the perturbation of the electric field due to the object, and hence its electric

image, converges to that produced by a spherical object. This property is reflected in the Laplace equation, which is used to accurately simulate the electric image of any dielectric object from a boundary value problem.

Field Uniformity

The perturbation of a uniform field by a dielectric sphere is in the form of a dipole potential. The actual fish electric organ discharge (EOD) resembles an elongated dipole. However, a non-uniform field induces higher order multi-pole perturbations as well as the dipole perturbation. As multi-poles attenuate with distance more rapidly than the dipole perturbation, the non-uniformity of the field is of little significance, especially for small objects..

Fish Effect

Though the resistivity of the fish skin will change the magnitude of the perturbation, it does not introduce non-linearity, where we may have multiple field magnitudes producing the same perturbation. As such it does not affect our findings in this chapter, and we may assume the fish has no effect on the field perturbation.

4.1.2 Ambiguity

Consider the case where the electric field, $\mathbf{E}(\cdot)$, over the whole domain, is given by that at the location of the object's center, $\mathbf{x_o}$, prior to its placement there. The potential perturbation, $\delta\Phi$, measured at $\mathbf{x}$ due to the introduction of a linear, homogeneous, isotropic sphere of radius a, is

$$\delta\Phi(\mathbf{x}, \mathbf{x_o}) = \frac{\Gamma a^3 \mathbf{E}(\mathbf{x_o}) \cdot (\mathbf{x} - \mathbf{x_o})}{|\mathbf{x} - \mathbf{x_o}|^3}, \tag{4.1}$$

where Γ is the electrical contrast. The electric contrast is dependent on the temporal nature of the field:

$$\Gamma = \begin{cases} \frac{\epsilon_i - \epsilon_e}{\epsilon_i + 2\epsilon_e} & \text{Static Field} \\ \frac{(\rho_e - \rho_i) + i\omega\rho_e\rho_i(\epsilon_i - \epsilon_e)}{(\rho_e + 2\rho_i) + i\omega\rho_e\rho_i(\epsilon_i + 2\epsilon_e)} & \text{Oscillating Field [32]} \end{cases}$$

where ρ is the resistivity, ϵ the absolute permittivity and ω the angular frequency of the unperturbed field. The subscripts i and e identify the variables as being interior or exterior to the spherical object, respectively.

Aside from distance, other unknown object properties appearing in equation (4.1) are the electric contrast Γ, object size a, and field magnitude measured at the object's center $\mathbf{E}(\mathbf{x_o})$. For clarity let us combine these unknown properties under the single entity τ. That is, we let $\tau = \Gamma a^3$. Then the perturbation can be represented by

$$\delta\Phi(\mathbf{x}, \mathbf{x_o}, \tau) = \frac{\tau \mathbf{E}(\mathbf{x_o}) \cdot (\mathbf{x} - \mathbf{x_o})}{|\mathbf{x} - \mathbf{x_o}|^3} \tag{4.2}$$

Receptor Ambiguity

A point $\mathbf{x_A}$ in space is said to be a *point of ambiguity* for a receptor located at $\mathbf{x}$, if the perturbation of the electric field measured at the receptor, by a sphere having property $c\tau$ centered at $\mathbf{x_A}$ is identical to one having property τ centered at $\mathbf{x_o}$, where the multiplication factor $c \in \mathbb{R}$. Symbolically, the point $\mathbf{x_A}$ is a point of ambiguity *of a receptor* located at $\mathbf{x}$ if

$$\delta\Phi(\mathbf{x}, \mathbf{x_o}, \tau) = \delta\Phi(\mathbf{x}, \mathbf{x_A}, c\tau). \tag{4.3}$$

By orienting the Cartesian reference frame such that the origin coincides with the sphere's center $\mathbf{x_o}$, and such that the applicate vector, $\vec{k}$, lies parallel with $\mathbf{E}$, (see figure 4.1) the ambiguity criteria (4.3) is simplified to

$$\frac{z}{(x^2 + y^2 + z^2)^{3/2}} = c\frac{z - w}{((x-u)^2 + (y-v)^2 + (z-w)^2)^{3/2}}, \tag{4.4}$$

where we have let $\mathbf{x} = (x, y, z)$ and $\mathbf{x_A} = (u, v, w)$ be the Cartesian coordinates of the receptor and point of ambiguity, respectively.

Having defined the condition necessary for ambiguity, we would now like to identify all points which satisfy this condition. That is, we would like to find the *ambiguity region* of a receptor $\mathbf{x}$. Let us denote

$$\kappa_c = \frac{c^2 \left(x^2 + y^2 + z^2\right)^3}{z^2}, \tag{4.5}$$

and

$$R_{wc}^2 = \sqrt[3]{\kappa_c (z-w)^2} - (z-w)^2. \tag{4.6}$$

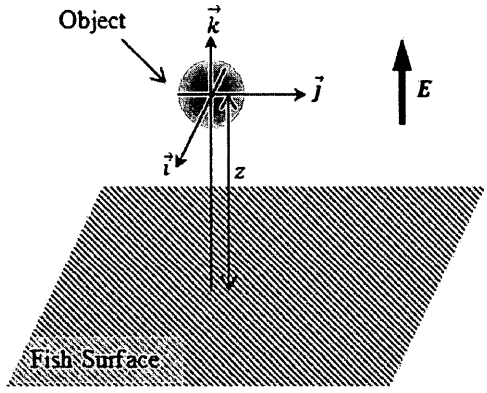

Figure 4.1: Reference frame setup - Orientation of the Cartesian reference frame in relation to the object and electric field. The origin is chosen to coincide with the center of the sphere and the applicate is set to align with the unperturbed electric field. Finding the perturbation of a uniform field caused by a dielectric sphere involves solving the Laplace equation. In this setting the dimension of the Laplace equation is reduced by one degree when using spherical coordinates.

The domain of ambiguity $\mathfrak{D}$, of receptor $\mathbf{x}$, is defined as the set of all points satisfying equation (4.4). Symbolically,

$$\mathfrak{D} = \left\{(u,v,w) \in \mathbb{R}^3 : (x-u)^2 + (y-v)^2 = R_{wc}^2, \quad \text{and} \quad w \in \mathfrak{D}_{wc}\right\}, \tag{4.7}$$

where $\mathfrak{D}_{wc}$ is the domain of the z-component of the ambiguity space.

Equation (4.4) imposes certain relations between w and z which depend on the value of the multiplication factor c, (see table 4.1). Taking these relations into account, we

	$c > 0$	$c < 0$
$z < 0$	$w > z$	$w < z$
$z > 0$	$w < z$	$w > z$
$z = 0$	$w = z$	$w = z$

Table 4.1: Relations imposed on w and z due to equation (4.4). Note that strictly speaking z cannot be zero as this would mean the object-center-fish distance is zero and hence a portion of the object is imbedded within the fish body. For mathematical completeness we ignore this fact.

define the domain $\mathfrak{D}_{wc}$, of w by:

$$\mathfrak{D}_{wc} = \begin{cases} \left[z - \sqrt[4]{\kappa_c}, z\right), & \text{if } cz > 0, \\ \{0\}, & \text{if } z = 0, \\ \left(z, z + \sqrt[4]{\kappa_c}\right], & \text{if } cz < 0. \end{cases}$$

Closer analysis of the domain $\mathfrak{D}$ reveals that for any multiplication factor $c \in \mathbb{R}$, and particular value $w' \in \mathfrak{D}_{wc}$, the ambiguity region of a receptor located at (x, y, z) consists of a circle in the w'-plane centered at (x, y) with radius $R_{w'c}$, (see figure 4.2).

The radius R_{wc} is zero on $\partial\mathfrak{D}_{wc}$, namely, when $w = z, z \pm \sqrt[4]{\kappa_c}$, and follows a continuous arc for other interior values. Hence, for any fixed $c \in \mathbb{R}$, the ambiguity region consists of an ovoidal surface which we term the *ambiguity surface.*

In theory, although the receptor itself is not on the ambiguity surface, the distance from the receptor to a point on the surface could be made infinitesimally small by choosing the point appropriately (see figure 4.3a). In principle, however, the distance from the receptor to any point on the ambiguity surface must be larger than the radius of the sphere associated to that particular surface. Without loss of generality we accept the larger theoretical surface, as the surface of ambiguity (for, if these larger surfaces of different receptors fail to co-intersect then so do the smaller actual surfaces, see below).

As c is varied, successive ambiguity surfaces envelope one another, (figure 4.3b), combining to form a solid *ambiguity region.*

Array Ambiguity

Sharing of information from multiple electroreceptors allows fish to make more precise inferences about the location of objects.

Given an array of N receptors, a point, $\mathbf{x_A}$, in space is said to be a point of ambiguity *of the array*, if $\mathbf{x_A}$ is a point of ambiguity of each receptor within the array. That is, for a given multiplication factor $c \in \mathbb{R}$, $\mathbf{x_A}$ is a point of intersection of all N ambiguity surfaces. We emphasize that c must be the same for all receptors, i.e. the

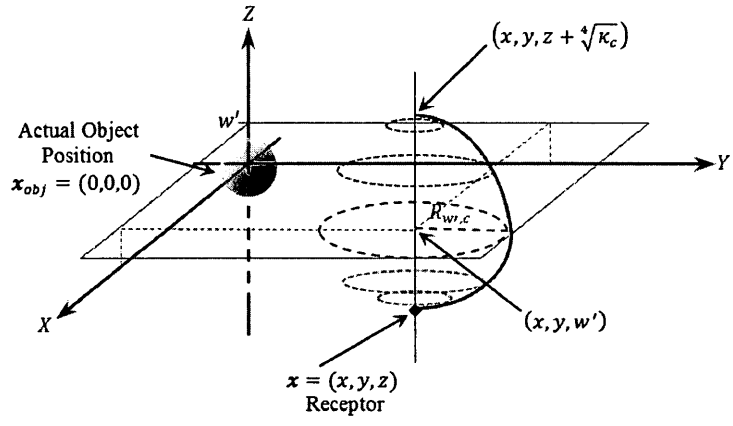

Figure 4.2: Ambiguity region schematic - Ambiguity surface features; fixed multiplication factor c. For receptor $\mathbf{x} = (x, y, z)$ and fixed $w' \in \mathfrak{D}_w$ the surface consists of a circle of radius $R_{w',c}$ centered at (x, y) on the w'-plane. Several such circles are shown for different $w \in \mathfrak{D}_w$. Bold red line shows radius of ambiguity $R_{w,c}$ for fixed c and $w \in \mathfrak{D}_w$.

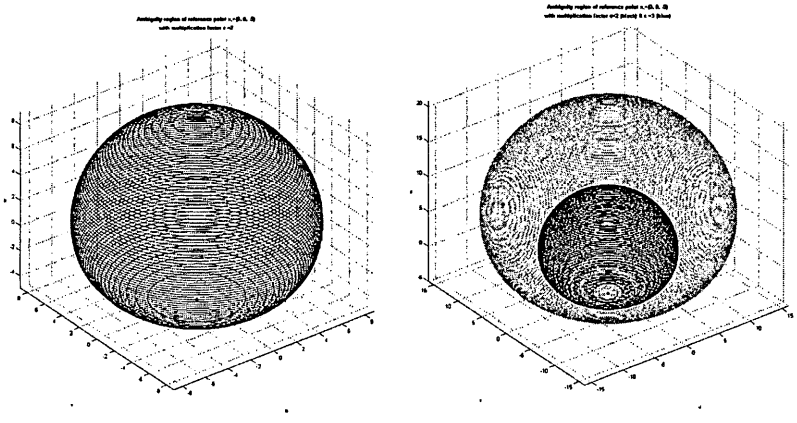

(a) (b)

Figure 4.3: Receptor ambiguous surface - (a) Ambiguity surface of receptor $\mathbf{x} = (0, 0, -5)$ for fixed multiplication factor $c = 2$. Black filled circle indicates the position of the receptor. This point is not a point on the surface.(b) Two ambiguity surfaces of receptor $\mathbf{x} = (0, 0, -5)$ for multiplication factor $c = 2$ (black) and $c = 3$ (blue). As c is varied continuously in $\mathbb{R}^+$ the ambiguity surfaces envelope one another, combining to form a solid ambiguity region.

fish requires consistency between receptors.

It is trivial to show that when $c = 1$ the origin is a point of ambiguity for any receptor array. This is simply due to the fact that the point $(u, v, w) = (0, 0, 0)$ is a solution of equation (4.4) for $c = 1$. An array that has a single point, i.e. the origin, in its ambiguity region is fully capable of disambiguating location information. We aim to show that for any electric field, such an array can always be found.

4.1.3 Results

We consider electric fields of varying direction, measured at the position of the sphere's center, prior to its placement there. It is shown that for any multiplication factor $c \in \mathbb{R}^+$, $(c \neq 1)$ and electric field $\mathbf{E}$, an array of receptors whose ambiguity regions do not co-intersect can always be found. The case of $c \in \mathbb{R}^-$ follows identically and is not included. Furthermore, we show that for $c = 1$, the ambiguity surface of all receptors must include the actual position of the object. The presence of such arrays provides a lower bound on the information necessary to localize an object and suggests a mechanism by which the fish could in theory distinguish the location of objects.

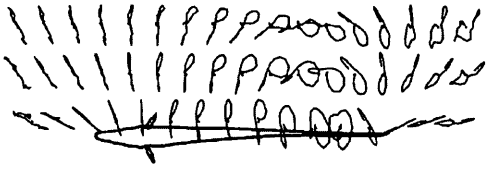

Figure 4.4: EOD cycle - Time domain representation of the EOD cycle, showing the direction of the electric field vector at several points in the mid-plane. At each point, the initial EOD phase is drawn as a vector, and for subsequent times, just the tip of each vector is traced. (From [44], with permission)

Perpendicular Field

Suppose the electric field $\mathbf{E}$, measured at the sphere's center, prior to its placement there, to be perpendicular to the surface of the fish. Such perpendicular fields are of most significance, as they appear in the rostral region of the fish (fig. 4.4), where electroreceptor organs are most dense. With the reference frame oriented such that the

sphere's center coincides with the origin, and such that the applicate vector, $\vec{k}$, lies in parallel with **E**, the z-coordinate of all receptors on the skin surface is identical.

In total we consider an array of four receptors $\mathcal{R}_j$, $(j = 1, ..., 4)$. The first receptor $\mathcal{R}_1$ is chosen to be at the point closest to the sphere. Such a receptor can be identified as one where the amplitude of the perturbation is measured to be greatest. That is, the line joining the sphere's center with $\mathcal{R}_1$ has direction vector parallel to the fish surface normal (see figure 4.5). The following two receptors $\mathcal{R}_{j=2,3}$ are chosen such that the line joining them also passes through $\mathcal{R}_1$. In other words, $\mathcal{R}_1$, $\mathcal{R}_2$, and $\mathcal{R}_3$ are collinear. As the x- and y-directions in our reference frame are chosen arbitrarily, for simplicity, we may choose the ordinate (y-coordinate) of our reference framce to lie in the same direction as the direction vector of the line joining the three receptors. Chosen in this manner, the receptors have Cartesian coordinates

$$\mathcal{R}_1 = (0, 0, z) \quad \text{and} \quad \mathcal{R}_{j=2,3} = (0, y_j, z).$$

As all points on the fish surface have the same z-coordinate, without loss of generality we may assume $z < 0$. Denoting receptor j's domain of ambigity by $\mathfrak{D}_j$, we have

$$\mathfrak{D}_1 = \left\{ (u, v, w) \in \mathbb{R}^3 : u^2 + v^2 = z^2 \sqrt[3]{\frac{c^2(z-w)^2}{z^2}} - (z-w)^2, \right. \tag{4.8}$$
$$\left. \text{and } w \in \left(z, z + |z|\sqrt{c}\right] \right\} \quad \text{and}$$
$$\mathfrak{D}_{j=2,3} = \left\{ (u, v, w) \in \mathbb{R}^3 : u^2 + (y_j - v)^2 = (y_j^2 + z^2) \sqrt[3]{\frac{c^2(z-w)^2}{z^2}} - (z-w)^2, \right.$$
$$\left. \text{and } w \in \left(z, z + \sqrt[4]{\frac{c^2(y_j^2 + z^2)^3}{z^2}} \right] \right\}.$$

Noting that,

$$\mathfrak{D}_1 \cap \mathfrak{D}_{j=2,3} = \Bigg\{ (u_j, v_j, w_j) \in \mathbb{R}^3 : \\ u_j = \pm \sqrt{z^2 \left(\frac{c(z-w_j)}{z}\right)^{2/3} - (z-w_j)^2 - \frac{y_j^2}{4}\left[1 - \left(\frac{c(z-w_j)}{z}\right)^{2/3}\right]^2}, \\ v_j = \frac{y_j}{2}\left[1 - \left(\frac{c(z-w_j)}{z}\right)^{2/3}\right] \text{ and } w_j \in \left(z, z + |z|\sqrt{c}\,\right] \Bigg\}, \tag{4.9}$$

a point $(u, v, w) \in \mathfrak{D}_1 \cap \mathfrak{D}_2 \cap \mathfrak{D}_3$ when $(u, v, w) = (u_2, v_2, w_2) = (u_3, v_3, w_3)$. That is, if either

$$\begin{aligned} y_2 = y_3 \quad &\Longrightarrow \quad \mathcal{R}_2 = \mathcal{R}_3 \text{ (trivial) or} \\ \sqrt[3]{\frac{c^2(z-w_j)^2}{z^2}} = 1 \quad &\Longrightarrow \quad w_2 = w_3 = z + \frac{|z|}{c}. \end{aligned} \tag{4.10}$$

We have discarded the solution $w_j = z - \frac{|z|}{c}$, as $\left(z - \frac{|z|}{c}\right) < z$ and hence not in the domain $(z, z + |z|\sqrt{c}\,]$. Furthermore, $\left(z + \frac{|z|}{c}\right) \in (z, z + |z|\sqrt{c}\,]$ only for values of $c \geq 1$. For the non-trivial case,

$$\mathfrak{D}_1 \cap \mathfrak{D}_2 \cap \mathfrak{D}_3 = \left\{ \left(\pm \frac{|z|}{c}\sqrt{c^2 - 1}, 0, z + \frac{|z|}{c} \right) \right\} \text{ with } c \geq 1. \tag{4.11}$$

Finally, we would like to choose the fourth receptor $\mathcal{R}_4 = (x, y, z)$ such that

$$\bigcap_j \mathfrak{D}_j = \begin{cases} \{\emptyset\} & \text{if } c > 1 \\ \{\mathbf{0}\} & \text{if } c = 1 \end{cases} \tag{4.12}$$

Points in $\mathfrak{D}_1 \cap \mathfrak{D}_4$ have the form

$$\mathfrak{D}_1 \cap \mathfrak{D}_4 = \Bigg\{ (u_4, v_4, w_4) \in \mathbb{R}^3 : \\ u_4 = \frac{x}{2}\left[1 - \left(\frac{c(z-w_4)}{z}\right)^{2/3}\right] \\ \pm \frac{y}{2}\sqrt{\frac{4}{x^2+y^2}\left[z^2\left(\frac{c(z-w_4)}{z}\right)^{2/3} - (z-w_4)^2\right] - \left[1 - \left(\frac{c(z-w_4)}{z}\right)^{2/3}\right]^2}, \\ v_4 = \frac{y}{2}\left[1 - \left(\frac{c(z-w_4)}{z}\right)^{2/3}\right] \\ \pm \frac{x}{2}\sqrt{\frac{4}{x^2+y^2}\left[z^2\left(\frac{c(z-w_4)}{z}\right)^{2/3} - (z-w_4)^2\right] - \left[1 - \left(\frac{c(z-w_4)}{z}\right)^{2/3}\right]^2} \\ \text{and} \\ w_4 \in \left(z, z + |z|\sqrt{c}\,\right] \Bigg\}. \tag{4.13}$$

For $c > 1$ the points $\left(\pm\frac{|z|}{c}\sqrt{c^2-1}, 0, z + \frac{|z|}{c}\right) \in \mathfrak{D}_1 \cap \mathfrak{D}_4$ only if $x = 0$. That is, only if the receptor $\mathcal{R}_4$ is collinear with the other three receptors. And, for $c = 1$, $\left(\pm\frac{|z|}{c}\sqrt{c^2-1}, 0, z + \frac{|z|}{c}\right) = (0,0,0) \in \mathfrak{D}_1 \cap \mathfrak{D}_4$. Hence, by choosing $\mathcal{R}_4$ anywhere away from the line joining the three other receptors, we can ensure $\cap\mathfrak{D}_j$ satisfies criteria (4.12). In conclusion, an array of four receptors chosen in this manner can fully disambiguate the location of a dielectric object.

General Field

We now consider an electric field $\mathbf{E}$ whose orientation relative to the surface of the fish is given in some general direction. We take the same approach as in the case of perpendicular fields. That is, we find three receptors and their commmon points of ambiguity, then show that (with the exception of the origin for $c = 1$) there is at least one other receptor whose ambiguity region does not contain those points.

Suppose in a reference frame where the applicate is in the direction of the field and the origin is at the center of the sphere (figure 4.8), the unit normal vector to the fish

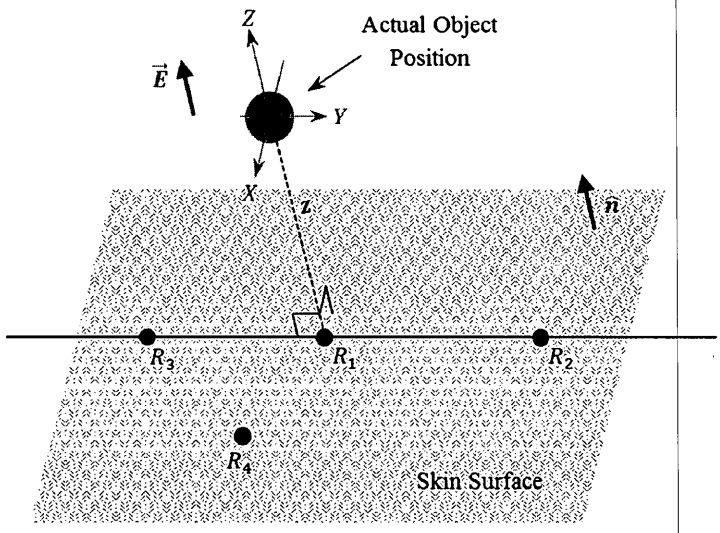

Figure 4.5: Array arrangement in perpendicular field - Unambiguous array in perpendicular field. When the field is perpendicular to the fish surface, the Cartesian coordinate system (X, Y, Z), is chosen such that the origin is at the sphere's center and the Z-direction is in the direction of the field. The X- and Y-directions are chosen arbitrarily. Four receptors having coordinate $(0, 0, z)$, $(0, y_{2,3}, z)$ and (x, y, z) constitute an unambiguous array; where $y_2 \neq y_3$, $x \neq 0$ and z is the distance from the center of the sphere to the fish surface.

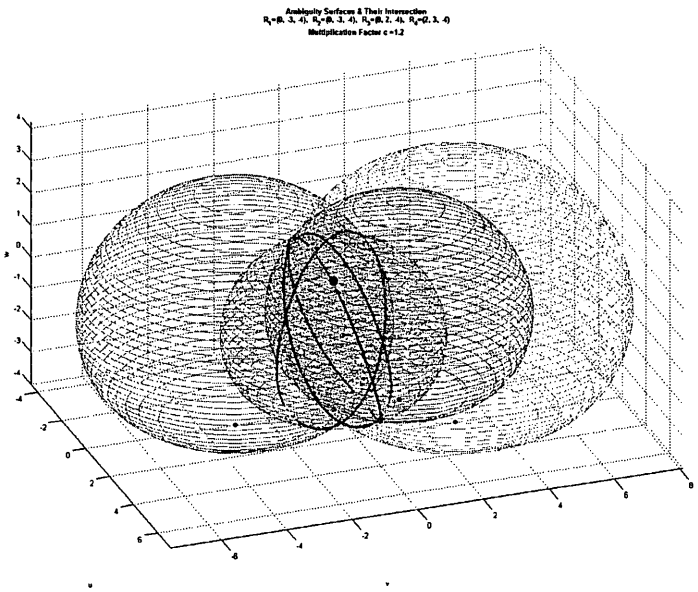

Figure 4.6: Multi-receptor ambiguity surfaces and intersection - Ambiguity surfaces of receptors in perpendicular field and their intersection. Four receptors (small filled circles) and their corresponding ambiguity surfaces evaluated for multiplication factor $c = 1.2$. Bold red line indicates intersection of ambiguity surfaces of $\mathcal{R}_{2,3,4}$ with that of $\mathcal{R}_1$. Large filled circle in center indicates actual position of sphere.

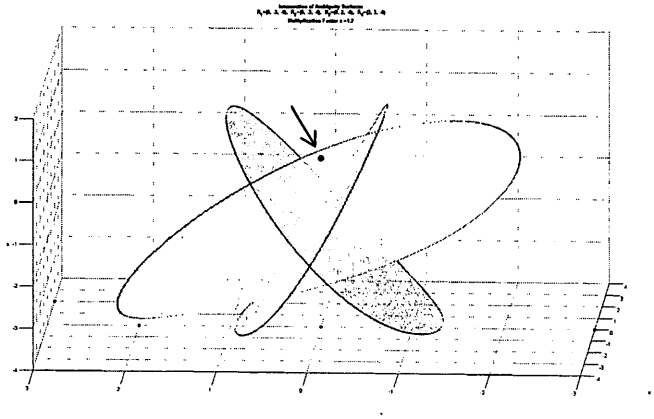

Figure 4.7: Intersection highlight - Highlight of the intersections depicted in figure 4.6. Bold red line indicates intersection of ambiguity surfaces of $\mathcal{R}_{2,3,4}$ with that of $\mathcal{R}_1$. Small filled circles indicate the position of the receptors and large filled circle (arrow) in center the position of the sphere. Areas within each disk are filled to elucidate orientation.

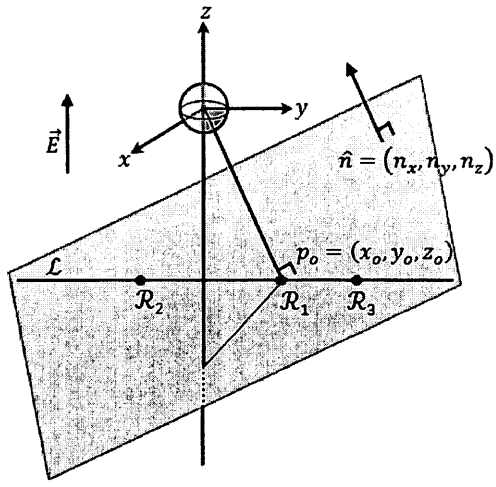

Figure 4.8: General field set-up - Object-fish orientation in a generally directed field. In a reference frame where the applicate is in the direction of the field and the origin is at the center of the sphere, the unit normal vector to the fish surface is given by $\hat{n}$.

surface has coordinates $\hat{n} = (n_x, n_y, n_z)$. If $p = (p_x, p_y, p_z)$ is any point on the fish surface, then the surface is defined by the equation

$$xn_x + yn_y + zn_z - (p_x n_x + p_y n_y + p_z n_z) = 0. \tag{4.14}$$

Let $p_o = (x_o, y_o, z_o)$ be the point on the fish surface closest to the object. That is, the surface-perpendicular line passing through the origin intersects the fish surface plane at p_o. Then p_o has coordinates

$$\begin{aligned} x_o &= (p_x n_x + p_y n_y + p_z n_z) n_x, \\ y_o &= (p_x n_x + p_y n_y + p_z n_z) n_y \text{ and} \\ z_o &= (p_x n_x + p_y n_y + p_z n_z) n_z. \end{aligned} \tag{4.15}$$

We choose the first receptor $\mathcal{R}_1$ at p_o. Then defining the line $\mathcal{L}$ by

$$\mathcal{L} : (x, y, z) = (x_o, y_o, z_o) + t(n_y, -n_x, 0), \tag{4.16}$$

the second and third receptor can be chosen anywhere on $\mathcal{L}$. Receptors chosen in this manner have Cartesian coordinates

$$\mathcal{R}_1 = (x_o, y_o, z_o) \quad \text{and} \quad \mathcal{R}_{j=2,3} = (x_o + t_j n_y, y_o - t_j n_x, z_o). \tag{4.17}$$

Notice that the receptors have identical z-coordinates. This condition, though not necessary, allows us to *explicitly* define the array's ambiguity regions. Without loss of generality we again assume $z_o < 0$. Then for each receptor defined above, the domain of ambiguity is

$$\begin{aligned}\mathfrak{D}_1 = \Bigg\{ &(u_1, v_1, w_1) \in \mathbb{R}^3 : (x_o - u_1)^2 + (y_o - v_1)^2 = R_{w_1 c}^2 \\ &\qquad \text{and } w_1 \in \left(z_o, z_o + \sqrt[4]{\kappa_c^{(1)}} \right] \Bigg\} \quad \text{and} \\ \mathfrak{D}_{j=2,3} = \Bigg\{ &(u_j, v_j, w_j) \in \mathbb{R}^3 : (x_o + t_j n_y - u_j)^2 + (y_o - t_j n_x - v_j)^2 = R_{w_j c}^2 \\ &\qquad \text{and } w_j \in \left(z_o, z_o + \sqrt[4]{\kappa_c^{(j)}} \right] \Bigg\},\end{aligned} \tag{4.18}$$

where $\kappa_c^{(j)}$ and $R_{w_j c}^2$ are defined as in equations (4.5) and (4.6) for each receptor, $j = 1, 2, 3$.

We begin by considering $\mathfrak{D}_1 \cap \mathfrak{D}_{j=2,3}$. For clarity, we denote

$$\begin{aligned} A &= (z_o - w_j)^2 \quad \text{and} \\ B &= \sqrt[3]{\frac{c^2 (z_o - w_j)^2}{z_o^2}}. \end{aligned} \tag{4.19}$$

Beginning with the z-component, note that by equation (4.15) since

$$y_o n_x - x_o n_y = (p_x n_x + p_y n_y + p_z n_z)(n_x n_y - n_x n_y) = 0, \tag{4.20}$$

it must be that

$$\begin{aligned} \sqrt[4]{\kappa_c^{(j=2,3)}} &= \sqrt[4]{\frac{c^2 \left(x_o^2 + y_o^2 + z_o^2 + t_j^2 (n_x^2 + n_y^2) + 2 t_j (x_o n_y - y_o n_x) \right)^3}{z_o^2}} \\ &= \sqrt[4]{\frac{c^2 \left(x_o^2 + y_o^2 + z_o^2 + t_j^2 (n_x^2 + n_y^2) \right)^3}{z_o^2}} \\ &> \sqrt[4]{\frac{c^2 \left(x_o^2 + y_o^2 + z_o^2 \right)^3}{z_o^2}} = \sqrt[4]{\kappa_c^{(1)}}. \end{aligned} \tag{4.21}$$

Hence if $w_j \in \mathfrak{D}_1 \cap \mathfrak{D}_{j=2,3}$, then $w_j \in \left(z_o, z_o + \sqrt[4]{\frac{c^2(x_o^2+y_o^2+z_o^2)^3}{z_o^2}} \right]$. Next, solving for the x- and y-components, we find

$$\begin{aligned}
\mathfrak{D}_1 \cap \mathfrak{D}_{j=2,3} = \Bigg\{ & (u_j, v_j, w_j) \in \mathbb{R}^3 : \\
& u_j = \frac{t_j n_y}{2}(1-B) + \frac{n_x(x_o n_x + y_o n_y)}{n_x^2 + n_y^2} \\
& \qquad \pm \frac{n_x}{2}\sqrt{\frac{4}{n_x^2+n_y^2}\left[B\left(x_o^2+y_o^2+z_o^2\right) - A\right] - t_j^2(B-1)^2}, \\
& v_j = \frac{n_y}{n_x}u_j + \frac{t_j}{2n_x}(n_x^2+n_y^2)(B-1) \quad \text{and} \\
& w_j \in \left(z_o, z_o + \sqrt[4]{\frac{c^2\left(x_o^2+y_o^2+z_o^2\right)^3}{z_o^2}} \right] \Bigg\}.
\end{aligned} \tag{4.22}$$

We now turn our attention to the ambiguity region of the array consisting of all three receptors. In other words, $\mathfrak{D}_1 \cap \mathfrak{D}_2 \cap \mathfrak{D}_3$. Using the argument that if the point $(u, v, w) \in \mathfrak{D}_1 \cap \mathfrak{D}_2 \cap \mathfrak{D}_3$ then it must be in both $\mathfrak{D}_1 \cap \mathfrak{D}_2$ and $\mathfrak{D}_1 \cap \mathfrak{D}_3$. We set $u_2 = u_3$ and $v_2 = v_3$ to arrive at,

$$\begin{aligned}
(n_x^2 + n_y^2)(B-1)(t_3 - t_2) &= 2n_y(u_2 - u_3), \\
&= 0.
\end{aligned} \tag{4.23}$$

This equation has two solutions;

$$\begin{aligned}
t_2 = t_3 \quad &\Longrightarrow \quad \mathcal{R}_2 = \mathcal{R}_3 \quad \text{and} \\
B = \sqrt[3]{\frac{c^2(z_o - w_j)^2}{z_o^2}} = 1 \quad &\Longrightarrow \quad w_2 = w_3 = z_o \pm \frac{|z_o|}{c}.
\end{aligned} \tag{4.24}$$

The first solution is trivial and is not considered. Let us assume $B = 1$. Then

$$\begin{aligned}\mathfrak{D}_1 \cap \mathfrak{D}_2 \cap \mathfrak{D}_3 = \Bigg\{ & (u,v,w) \in \mathbb{R}^3 : \\ & u = \frac{n_x\left(x_o n_x + y_o n_y\right)}{n_x^2 + n_y^2} \pm n_x \sqrt{\frac{1}{n_x^2+n_y^2}\left[x_o^2 + y_o^2 + z_o^2\left(1 - \frac{1}{c^2}\right)\right]} \\ & v = \frac{n_y\left(x_o n_x + y_o n_y\right)}{n_x^2 + n_y^2} \pm n_y \sqrt{\frac{1}{n_x^2+n_y^2}\left[x_o^2 + y_o^2 + z_o^2\left(1 - \frac{1}{c^2}\right)\right]} \\ & w = z_o \pm \frac{|z_o|}{c} \Bigg\}\end{aligned} \tag{4.25}$$

Notice that the array's ambiguity points do not depend on the location of $\mathcal{R}_2$ and $\mathcal{R}_3$ on $\mathcal{L}$. In other words, the points in the set (4.25) are independent of t_2 and t_3.

The set $\mathfrak{D}_1 \cap \mathfrak{D}_2 \cap \mathfrak{D}_3$ consists of eight points. We now find the set of all receptor locations on the fish surface whose ambiguity regions *contain* at least one of these eight points. If this set of receptors does not consist of the entire fish surface, then we can conclude that there are receptors $\mathcal{R}_4$ whose ambiguity regions do not contain *any* of the points in (4.25), and hence, $\cap_j \mathfrak{D}_j$ satisfies equation (4.12).

For each ambiguity point (u_j, v_j, w_j), $(j = 1, ..., 8)$ in (4.25), the points (x, y, z) satisfying

$$\begin{aligned}(x - u_j)^2 + (y - v_j)^2 &= (x^2 + y^2 + z^2)B - A \quad \text{and} \\ z &= \frac{(p_x n_x + p_y n_y + p_z n_z) - (x n_x + y n_y)}{n_z},\end{aligned} \tag{4.26}$$

define the set of points on the fish surface whose ambiguity region contains (u_j, v_j, w_j). Here A and B are defined as in equation (4.19).

We note that equations (4.26) define curves on the fish surface plane (4.14). These curves do not form a dense subset of the plane. Hence points on the fish plane can be found which do not belong to these curves. Any such point can be chosen for the location of our fourth receptor, $\mathcal{R}_4$. An example is demonstrated in figure 4.9.

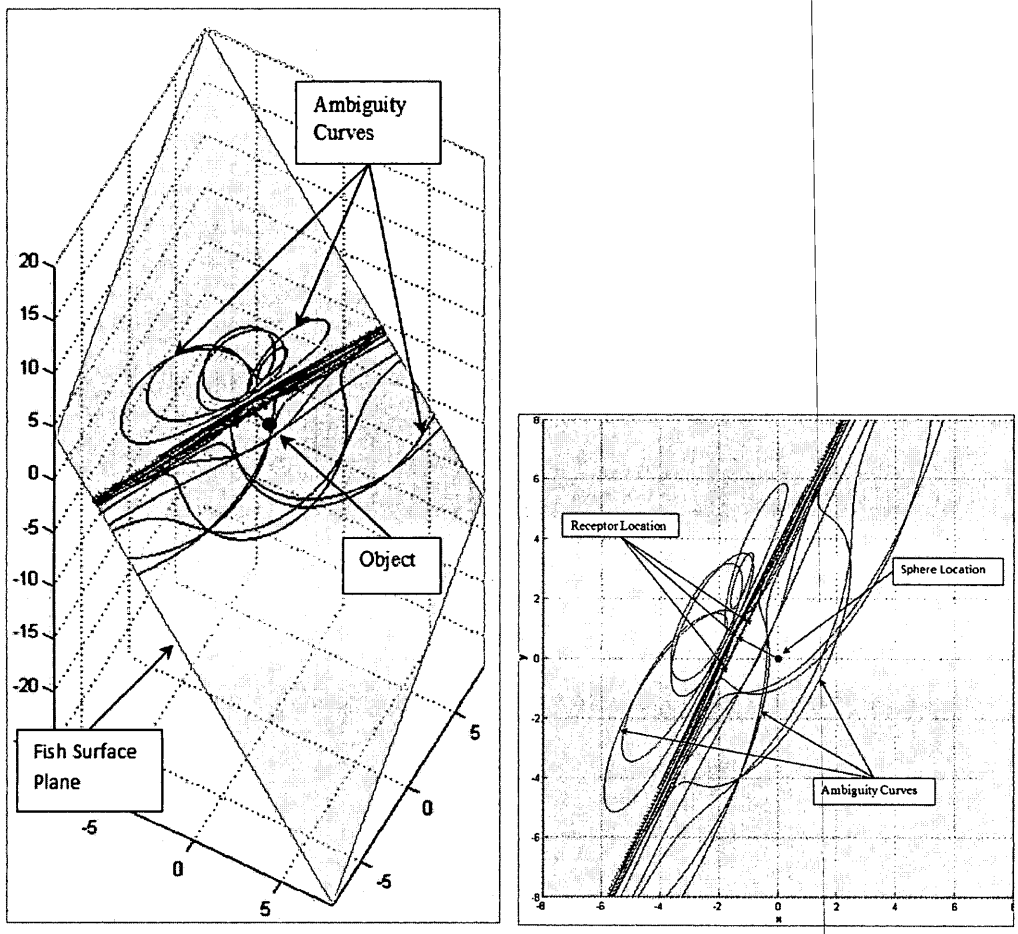

Figure 4.9: Ambiguity curves - general electric field - (a) Ambiguity curves (blue) of three collinear receptors (black stars) in a general electric field. The receptors are aligned on a line of constant height (red). The location of the center of the sphere is represented by the black circle. Ambiguity curves described by equations (4.26) do not form a dense subset of the fish plane. Choosing a fourth receptor anywhere on the plane and not on the ambiguity curves will allow the four receptors to disambiguate the location of the sphere.(b) Another view of the fish surface plane.

Parallel Field

Finally, we consider the case where the electric field **E** at the object's center, prior to its placement there, to be parallel to the surface of the fish. Such fields are of least significance, as they only appear in the caudal portion of the fish where electroreceptors are least dense (figure 4.4).

Consider three collinear receptors, $\mathcal{R}_j$, $(j = 1, 2, 3)$ aligned in parallel to the electric field **E**. Suppose the line segment joining $\mathcal{R}_1$ and the origin is perpendicular to the field, (see figure 4.10). In the defined coordinate system, such receptors have coordinates $(x, y, 0), (x, y, z_2)$ and (x, y, z_3) respectively. For each receptor $\mathcal{R}_j$, defined

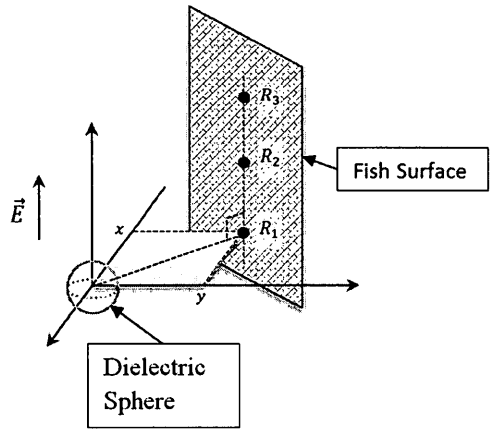

Figure 4.10: Parallel field schematic - Three collinear receptors $\mathcal{R}_{1,2,3}$, where one receptor $\mathcal{R}_1$, is located on the XY-plane. The line segment joining the receptors is parallel to the electric field, **E**. Receptors positioned in this manner, where $\mathcal{R}_2$ and $\mathcal{R}_3$ are both on the same side of $\mathcal{R}_1$, do not have any common points of ambiguity.

above, the domain of ambiguity is

$$\begin{aligned} \mathfrak{D}_1 &= \{(u_1, v_1, w_1) \in \mathbb{R}^3 : u_1 \neq x,\ v_1 \neq y \text{ and } w_1 = 0\} \\ \mathfrak{D}_{j=2,3} &= \left\{(u_j, v_j, w_j) \in \mathbb{R}^3 : (x - u_j)^2 + (y - v_j)^2 = R_{w_j c}^2 \text{ and } w_j \in \mathfrak{D}_{w_j c}\right\}. \end{aligned} \tag{4.27}$$

Notice, that the domain of ambiguity of $\mathcal{R}_1$ is simply the entire horizontal XY-plane excluding the position of the receptor. A point (u, v, w) in space is an ambiguous point of the array $\{\mathcal{R}_j\}$ only if $(u, v, w) \in \cap \mathfrak{D}_j\ \forall j$.

Noting,

$$\mathfrak{D}_1 \cap \mathfrak{D}_{j=2,3} = \left\{(u,v,w) \in \mathbb{R}^3 : w = 0 \text{ and } (x-u)^2 + (y-v)^2 = c^{2/3}(x^2+y^2) + z_j^2(c^{2/3}-1)\right\},$$

it is clear that,

$$\begin{aligned} \bigcap \mathfrak{D}_j \;=\; & \{(u,v,w) \in \mathbb{R}^3 : w = 0, \text{ and} \\ & (x-u)^2 + (y-v)^2 = c^{2/3}(x^2+y^2) + z_2^2(c^{2/3}-1) \text{ and} \\ & (x-u)^2 + (y-v)^2 = c^{2/3}(x^2+y^2) + z_3^2(c^{2/3}-1)\Big\}. \end{aligned} \tag{4.28}$$

Equation (4.28) simply states that any point of ambiguity (u,v,w), if it exist, must be located at the intersection of two circles on the XY-plane centered at (x,y).

Clearly, two such circles either overlap completely ($R_{w_2c} = R_{w_3c}$) or not at all ($R_{w_2c} \neq R_{w_3c}$). The former is satisfied only if $z_2 = \pm z_3$. In other words, when either, the receptors coincide ($\mathcal{R}_2 = \mathcal{R}_3$; trivial), or when they are on opposite sides, an equal distant apart from $\mathcal{R}_1$, as in figure 4.11.

In short an array of at least three collinear electroreceptors aligned in parallel with the uniform electric field could allow the fish to unambiguously locate a dielectric sphere. It is required that one receptor be positioned on the XY-plane and not bisect the line segment connecting the other two receptors (see figure 4.10 or 4.12).

4.2 Noise

We now turn our attention to the effects of electromagnetic noise arising from external environmental sources. We explore whether an array can be devised to unambiguously locate a dielectric object in the presence of such noise. We limit our study of the effects of noise to the most pertinent of cases, that is, to perpendicular fields.

The addition of noise ξ to the self-generated electric field can effect both the magnitude and the direction of the field at the object center. To simplify the problem we only consider noise in the z-component. That is, we suppose that the addition of noise to the self-generated field results in the field $\mathbf{E} = [0, 0, E_o + \xi]$ at the object center; where the Cartesian reference frame has been defined so that the applicate vector lies

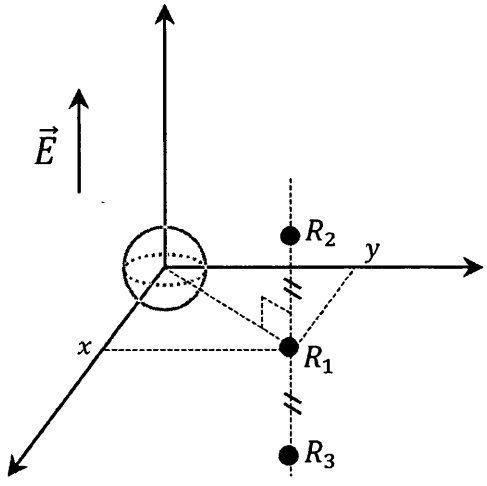

Figure 4.11: Ambiguous array - parallel field - If the receptor positioned on the XY-plane bisects the line segment joining the other two receptors, then the ambiguity region of the array consists of a circle of radius $r = \sqrt{c^2(x^2+y^2) + z_3^2(c^2-1)}$ on the XY-plane, centered at $(x, y, 0)$.

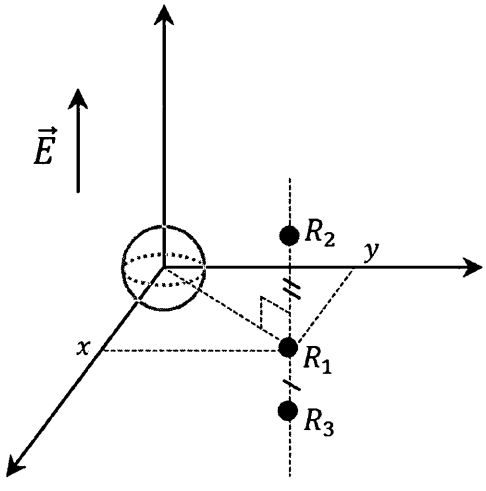

Figure 4.12: Unambiguous array - parallel field - If the receptor positioned on the XY-plane does not bisect the line segment joining the other two receptors, then the three receptors do not share a common ambiguity region. The ambiguity region of the array is the empty set.

in parallel with the field and the origin coincides with the object center. A dielectric object placed in such a field would result in the perturbation

$$\delta\Phi_\xi(\mathbf{x}) = \frac{\tau\,(E_o+\xi)\,z}{(x^2+y^2+z^2)^{3/2}}, \tag{4.29}$$

measured at $\mathbf{x} = (x, y, z)$. Points of ambiguity are those where a dielectric object of property $c\tau$, placed there, would produce the same perturbation at $\mathbf{x}$. Mathematically, the set of points $(u, v, w) \in \mathbb{R}^3$ satisfying

$$\frac{\tau\,(E_o+\xi)\,z}{(x^2+y^2+z^2)^{3/2}} = \frac{c\tau E_o\,(z-w)}{((x-u)^2+(y-v)^2+(z-w)^2)^{3/2}} \tag{4.30}$$

define the region of ambiguity for the receptor $\mathbf{x}$.

To identify an array of receptors capable of disambiguating object distance, we take a similar approach as the case in the absence of noise. Let us consider three collinear receptors $\mathcal{R}_j$, where the first receptor is chosen at the point closest to the object, namely $(0, 0, z)$. As the $x-$ and $y-$directions in our reference frame can be chosen arbitrarily, we set them such that for $\mathcal{R}_{j=2,3} = (0, y_j, z)$. The domain of ambiguity $\mathfrak{D}$ for each receptor $\mathcal{R}$, is now defined by

$$\mathfrak{D}_1 = \left\{ (u,v,w) \in \mathbb{R}^3 : u^2+v^2 = z^2 \sqrt[3]{\frac{\tilde{E}c^2(z-w)^2}{z^2}} - (z-w)^2, \right. \tag{4.31}$$
$$\left. \text{and } w \in \mathfrak{D}_{wc}^{(1)} \right\} \quad \text{and}$$
$$\mathfrak{D}_{j=2,3} = \left\{ (u,v,w) \in \mathbb{R}^3 : u^2+(y_j-v)^2 = (y_j^2+z^2) \sqrt[3]{\frac{\tilde{E}c^2(z-w)^2}{z^2}} - (z-w)^2, \right.$$
$$\left. \text{and } w \in \mathfrak{D}_{wc}^{(j)} \right\},$$

where $\tilde{E} = \left(\frac{E_o}{Eo+\xi}\right)^2$ and

$$\mathfrak{D}_{wc}^{(j)} = \begin{cases} (z, z+\sqrt[4]{\tilde{E}\kappa_c^{(j)}}], & \text{if } cz < 0, \\ [z-\sqrt[4]{\tilde{E}\kappa_c^{(j)}}, z), & \text{if } cz > 0. \end{cases} \tag{4.32}$$

Equation (4.32) was derived by assuming $E_o > 0$ and $|\xi| < E_o$ and taking equation (4.30) into consideration. The term κ_c in equation (4.32) is that given by equation

(4.5). It is worth mentioning that when considering the intersection of the ambiguity domains, $\mathfrak{D}_{wc}^{(1)} \subset \mathfrak{D}_{wc}^{(j)}$, as $\kappa_c^{(1)} < \kappa_c^{(j)}$.

For clarity let $\sqrt[3]{\frac{\tilde{E}c^2(z-w)^2}{z^2}} = A$. Then for $j = 2, 3$, the set $\mathfrak{D}_1 \cap \mathfrak{D}_j$ is defined by

$$\begin{aligned}\mathfrak{D}_1 \cap \mathfrak{D}_j = \Bigg\{ & (u_j, v_j, w_j) \in \mathbb{R}^3 : \\ & u_j = \pm\sqrt{z^2 A - (z - w_j)^2 - \frac{y_j^2}{4}(1 - A)^2}, \\ & v_j = \frac{y_j}{2}(1 - A) \text{ and} \\ & w_j \in \begin{cases} (z, z + |z|\sqrt[4]{\tilde{E}c^2}] & \text{if } cz < 0, \\ [z - |z|\sqrt[4]{\tilde{E}c^2}, z) & \text{if } cz > 0 \end{cases} \Bigg\}.\end{aligned} \tag{4.33}$$

It is easy to see that a point $(u, v, w) \in \mathfrak{D}_1 \cap \mathfrak{D}_2 \cap \mathfrak{D}_3$ if and only if

$$\begin{aligned} y_2 = y_3 \quad &\Longrightarrow \quad \mathcal{R}_2 = \mathcal{R}_3 \text{ (trivial) or} \\ A = \sqrt[3]{\frac{\tilde{E}c^2(z - w_j)^2}{z^2}} = 1 \quad &\Longrightarrow \quad w_2 = w_3 = z + \frac{|z|}{\sqrt{\tilde{E}c^2}}. \end{aligned} \tag{4.34}$$

Assuming the latter,

$$\mathfrak{D}_1 \cap \mathfrak{D}_2 \cap \mathfrak{D}_3 = \left\{ \left(|z|\sqrt{1 + \frac{1}{\tilde{E}c^2}}, 0, z \pm \frac{|z|}{\sqrt{\tilde{E}c^2}} \right) \right\}. \tag{4.35}$$

Now, let $\mathcal{R}_4$ be any receptor not collinear with the other three receptors. If the position of $\mathcal{R}_4$ on the fish surface is defined by (x, y, z), then

$$\begin{aligned}\mathfrak{D}_1 \cap \mathfrak{D}_4 = \Bigg\{ & (u, v, w) \in \mathbb{R}^3 : \\ & u = \frac{1}{2}\left[x(1 - A) \pm y\sqrt{\frac{4}{x^2 + y^2}\left(z^2 A - (z - w)^2\right) - (1 - A)^2} \right], \\ & v = \frac{1}{2}\left[y(1 - A) \pm |x|\sqrt{\frac{4}{x^2 + y^2}\left(z^2 A - (z - w)^2\right) - (1 - A)^2} \right] \text{ and} \\ & w = \mathfrak{D}_{wc}^{(1)} \Bigg\}.\end{aligned} \tag{4.36}$$

To explore the intersection of all four set $\cap\mathfrak{D}_j$, we begin with the applicate component w, which according to equation (4.35) is given by $w = z \pm \frac{|z|}{\sqrt{\tilde{E}c^2}}$. This leads us to the

following two simplifying terms,

$$(z-w)^2 = \frac{z^2}{\tilde{E}c^2} \qquad \text{and} \qquad A = \sqrt[3]{\frac{\tilde{E}c^2(z-w)^2}{z^2}} = 1. \tag{4.37}$$

Upon substitution into equation (4.36) for u, we find

$$\begin{aligned} u &= \frac{1}{2}\left[x(1-A) \pm y\sqrt{\frac{4}{x^2+y^2}\left(z^2A - (z-w)^2\right) - (1-A)^2}\right], \\ &= \frac{1}{2}\left[\pm y\sqrt{\frac{4}{x^2+y^2}\left(z^2 - \frac{z^2}{\tilde{E}c^2}\right)}\right], \\ &= \pm y|z|\sqrt{\frac{1}{x^2+y^2}\left(1 - \frac{1}{\tilde{E}c^2}\right)}. \end{aligned} \tag{4.38}$$

Then by equation (4.35) we must have

$$\begin{aligned} |z|\sqrt{1+\frac{1}{\tilde{E}c^2}} &= \pm y|z|\sqrt{\frac{1}{x^2+y^2}\left(1-\frac{1}{\tilde{E}c^2}\right)}, \\ &= \pm\left(|z|\sqrt{1+\frac{1}{\tilde{E}c^2}}\right)\left(\frac{y}{\sqrt{x^2+y^2}}\right), \\ 1 &= \pm\frac{y}{\sqrt{x^2+y^2}}. \end{aligned} \tag{4.39}$$

This equation can only hold if $x = 0$ or equivelantly if $\mathcal{R}_4$ is collinear with the other three receptors; the condition we excluded. This analysis shows that even in the presence of moderate noise levels ($|\xi| < E_o$), an array of receptors can be found by which the location of an object can be realized.

In the following theorem we show that the origin is the only point common to *all* ambiguity surfaces and that the addition of noise masks the true value of multiplication factor c.

Theorem:

Suppose the noisy field $E + \xi$ is perpendicular to the surface of the fish. For any arbitrary array of receptors, the only point in space, guaranteed to be in the ambiguity region of the array is the origin.

Proof:

For fields perpendicular to the fish surface, receptors can be characterized by their x and $y-$coordinates. Hence, if (u, v, w) is a point common to all ambiguity surfaces, then it must satisfy equation (4.30), and be independent of both x and y.
Let $u = g(z)$, $v = h(z)$ and $K = \left(\frac{cE_o}{Eo+\xi}\right)^{2/3}$.
Then from equation (4.30),

$$\begin{aligned} u &= x \pm \sqrt{K(x^2+y^2+z^2)\left(\frac{z-w}{z}\right)^{2/3} - (y-v)^2 - (z-w)^2}, \\ &= x \pm f(x,y,z), \\ &= g(z). \end{aligned} \tag{4.40}$$

That is, $\pm f(x,y,z) = x - g(z)$. Now, differentiating with respect to y,

$$\begin{aligned} \pm\frac{\partial f}{\partial y} &= \pm\frac{v - y + yK\left(\frac{z-w}{z}\right)^{2/3}}{\sqrt{K(x^2+y^2+z^2)\left(\frac{z-w}{z}\right)^{2/3} - (y-v)^2 - (z-w)^2}}, \\ &= 0. \end{aligned} \tag{4.41}$$

Equation (4.41) implies

$$v = y\left[1 - K\left(\frac{z-w}{z}\right)^{2/3}\right]. \tag{4.42}$$

Again, since $v = h(z)$ it must be that

$$\begin{aligned} &\left[1 - K\left(\frac{z-w}{z}\right)^{2/3}\right] = 0 \\ \Longrightarrow\ & v = 0, \quad K\left(\frac{z-w}{z}\right)^{2/3} = 1 \quad \text{and} \quad (z-w)^2 = \frac{z^2}{K^3} \\ \Longrightarrow\ & u = g(z) = x \pm \sqrt{x^2 + z^2 - \frac{z^2}{K^3}}, \\ \Longrightarrow\ & g^2(z) - 2xg(z) = z^2 - \frac{z^2}{K^3} \\ \Longrightarrow\ & g(z) = u = 0, \quad \text{(as } x \text{ only appears on one side of the equation)} \\ \Longrightarrow\ & z^2 - \frac{z^2}{K^3} = 0 \\ \Longrightarrow\ & K^3 = 1 \\ \Longrightarrow\ & (z-w)^2 = z^2 \\ \Longrightarrow\ & w(w-2z) = 0 \\ \Longrightarrow\ & w = 0 \quad \text{or} \quad w = 2z. \end{aligned} \tag{4.43}$$

Hence, $(u, v, w) = (0, 0, 0)$ or $(0, 0, 2z)$. The point $(0, 0, 2z)$ can be discarded as it is located interior to the fish (see figure 4.13). Consequently, for a fixed multiplication factor c, the only point common to all ambiguity surfaces is the actual position of the object. This completes the proof of our theorem above.

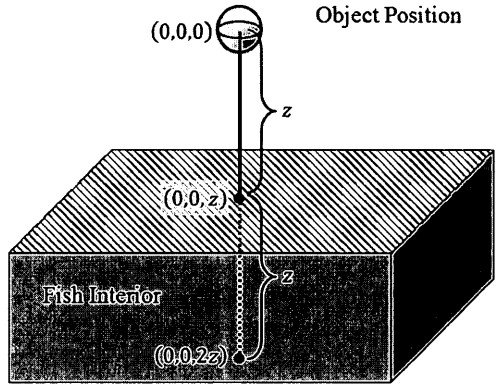

Figure 4.13: Noisy field ambiguous array - Schematic diagram indicating the location of the two points, $(0, 0, 0)$ and $(0, 0, 2z)$, common to all ambiguity surfaces. As indicated the point $(0, 0, 2z)$ is located to the interior of the fish and hence can be discarded.

Although the introduction of electromagnetic noise has had no effect in masking the location of the object, it has veiled the value of $\tau = \Gamma a^3$. The requirement that $K^3 = 1$ incorrectly designates the value of c to $1 + \frac{\xi}{E_o}$. Clearly, the larger the noise term ξ, the larger the error term, ξ/E_o in the multiplication factor. For a zero-mean distributed noise, the true value of c can be approximated by taking multiple recordings and calculating the sample mean.

4.3 Non-Ideal Receptors

In this section we consider non-ideal electroreceptors. Such receptors are characterized by a threshold value T. Signals whose amplitude fall below this threshold remain undetected to such non-ideal receptors. Hence, if the difference in perturbation from two different locations is less than the threshold T, then a receptor is incapable of differentiating between two locations as the source of the perturbation. In other words, if a dielectric sphere is located at $\mathbf{x_o}$, then for a fixed multiplication factor c, the point

$\mathbf{x_A}$ is a point of ambiguity if

$$|\delta\Phi(\mathbf{x}, \mathbf{x_o}, \tau) - \delta\Phi(\mathbf{x}, \mathbf{x_A}, c\tau)| \leq T. \tag{4.44}$$

Under certain conditions, which we will expand on shortly, equation (4.44) provides an upper and lower bound for the ambiguity region of a receptor. Equation (4.44) expanded gives:

$$\left| \frac{\tau E_o z}{(x^2+y^2+z^2)^{3/2}} - \frac{c\tau E_o (z-w)}{((x-u)^2+(y-w)^2+(z-w)^2)^{3/2}} \right| < T, \tag{4.45}$$

$$\alpha < \frac{c(z-w)}{((x-u)^2+(y-w)^2+(z-w)^2)^{3/2}} < \beta,$$

where

$$\alpha = \frac{z}{(x^2+y^2+z^2)^{3/2}} - \frac{T}{|\tau E_o|} \quad \text{and} \quad \beta = \frac{z}{(x^2+y^2+z^2)^{3/2}} + \frac{T}{|\tau E_o|}.$$

It is worth mentioning that irrespective of threshold value T, the actual object location $(0,0,0)$ falls within the bounded region of equation (4.45) for multiplication factor $c = 1$. It is easy to show that when $\alpha > 0 \Longrightarrow \beta > 0$ and when $\beta < 0 \Longrightarrow \alpha < 0$. In such cases, for any fixed c, the ambiguity region of the receptor is bounded by two surfaces:

$$\begin{aligned} R_\beta \leq (x-u)^2 + (y-v)^2 \leq R_\alpha, \quad & \text{if } \alpha, \beta > 0 \quad \text{or} \\ R_\alpha \leq (x-u)^2 + (y-v)^2 \leq R_\beta, \quad & \text{if } \alpha, \beta < 0, \end{aligned} \tag{4.46}$$

where we have defined,

$$\begin{aligned} R_\alpha &= \left(\frac{c(z-w)}{\alpha}\right)^{2/3} - (z-w)^2, \quad \text{and} \\ R_\beta &= \left(\frac{c(z-w)}{\beta}\right)^{2/3} - (z-w)^2, \end{aligned} \tag{4.47}$$

and the range of w for which these radii are positve is given in table 4.2.

In addition to these bounded ambiguity regions, we may also come across the undesirable situation where $\alpha < 0 < \beta$. In such a case, the ambiguity region would be defined by the unbounded set

$$\left\{ (u,v,w) \in \mathbb{R}^3 : (x-u)^2 + (y-v)^2 \geq \left(\frac{c(z-w)}{\alpha}\right)^{2/3} - (z-w)^2, \text{ and } \right.$$
$$\left. (x-u)^2 + (y-v)^2 \geq \left(\frac{c(z-w)}{\beta}\right)^{2/3} - (z-w)^2 \right\}$$

	$c > 0$	$c < 0$
$\beta < 0$	$w_R \in \left(z, z + \sqrt{\frac{c}{\lvert\beta\rvert}}\right]$ $w_r \in \left(z, z + \sqrt{\frac{c}{\lvert\alpha\rvert}}\right]$	$w_R \in \left[z - \sqrt{\frac{c}{\beta}}, z\right)$ $w_r \in \left[z - \sqrt{\frac{c}{\alpha}}, z\right)$
$\alpha > 0$	$w_R \in \left[z - \sqrt{\frac{c}{\alpha}}, z\right)$ $w_r \in \left[z - \sqrt{\frac{c}{\beta}}, z\right)$	$w_R \in \left(z, z + \sqrt{\frac{\lvert c\rvert}{\alpha}}\right)$ $w_r \in \left(z, z + \sqrt{\frac{\lvert c\rvert}{\beta}}\right)$

Table 4.2: Domain of w for the upper w_R and lower w_r bounding surfaces of the ambiguity region. These upper and lower bounding surfaces are described by equation 4.46.

Let us explore the condition under which this unfavourable situation arises. For $z > 0$ we can see that $\beta > 0$ for all values of x and y. However, $\alpha < 0$ only if $x^2 + y^2 > \left(\frac{z|\tau E_o|}{T}\right)^{2/3} - z^2$. Similarly, for $z < 0$, $\alpha < 0$ for all x and y, but $\beta > 0$ only if $x^2 + y^2 > \left(\frac{z|\tau E_o|}{T}\right)^{2/3} - z^2$. Hence, unbounded ambiguity regions can only arise if

$$x^2 + y^2 > \left(\frac{z|\tau E_o|}{T}\right)^{2/3} - z^2. \tag{4.48}$$

However, rearranging the terms we see that this equation is satisfied only if

$$\begin{aligned} T &> \frac{z\tau E_o}{(x^2 + y^2 + z^2)^{3/2}}, \\ &= \delta\Phi(\mathbf{x}, \mathbf{x_o}, \tau). \end{aligned} \tag{4.49}$$

That is, only if the perturbation signal is undetectable. Such a case is trivial and we may conclude that if a signal is detectable to a non-ideal receptor, then the ambiguity region of the receptor is bounded. The criteria required for a non-ideal receptor (x, y, z) to detect the presence of a dielectric object is given by

$$x^2 + y^2 \leq \left(\frac{z|\tau E_o|}{T}\right)^{2/3} - z^2. \tag{4.50}$$

We numerically explore the effect of non-ideal receptors on the information required for localization

Consider a receptor (x, y, z) chosen to satisfy (4.50). Without loss of generality let

us suppose $c > 0$ and $\alpha, \beta < 0$. Then for each $w' \in \left(z, z + \sqrt{c/|\beta|}\right]$, (see table 4.2) the ambiguity region is an annulus centered at (x, y, w') on the w'-plane, where the inner and outer radii are defined by equation (4.47), (see figure 4.14a).

To greatly reduce the numerical complexity involved in calculating the intersection of multiple *circular* ambiguity regions, at each level height w' we bound each annulus within a square annulus of half-side width

$$s_\alpha = \frac{R_\alpha}{\sqrt{2}} \qquad \text{and} \qquad s_\beta = R_\beta, \tag{4.51}$$

centered at (x, y, w'), where s_α and s_β are the half-side widths of the inner and outer bounding squares, respectively (see figure 4.14b). In this way, the intersection of the multiple circular-annuli are bounded within the intersection of the square-annuli.

It is important to note that our simplification results in the introduction of error. The area of the circular annular bound region is simply given by $\pi(R_\beta^2 - R_\alpha^2)$, where as that of the bounding square annulus is $4R_\beta^2 - 2R_\alpha^2$. Hence, at any level height the ratio of the area of our bounded estimate to the true area is $\frac{2}{\pi} + \frac{2R_\beta^2}{\pi(R_\beta^2 - R_\alpha^2)}$. Though the calculation of the intersection of multiple ambiguity regions can be greatly simplified by the limiting square annulus approximation, we must bear in mind that the computed area of intersection is only an upper bound on the true area of intersection, (see figure 4.15).

Figure 4.16 depicts the volume of ambiguity for five non-ideal receptors, presented with a dielectric sphere of radius 2 cm at a distancd of 7 cm. The sphere has relative permittivity 2.25 (polyethylene) and is immersed in a media of relative permittivity 80.1 (water at 20°C). The magnitude of the electric field at the object center is measured to be 0.95 mV/cm, and the receptors are assumed to have a sensitivity threshold of 10^{-4} mV/cm. This volume is calculated by the square-annulus approximation described above, and provides an upper bound on the actual volume of intersection. The first four receptors (black circles) are chosen at random within a small disk of radius 3 cm. For each point within the disk (4.50), we define the region of ambiguity and calculate its intersection with that of the array of four receptors. In other words, our array of five receptors is comprised of the four fixed receptors (black circles) and a

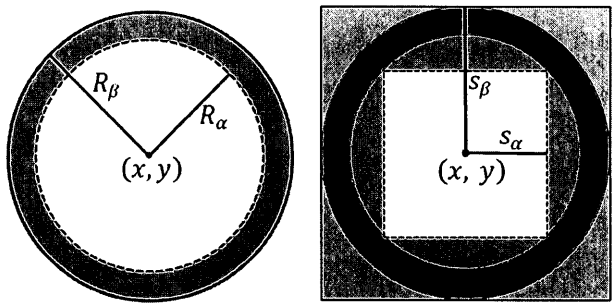

Figure 4.14: Ambiguity region bound - (a) The ambiguity region of receptor (x, y, z) at some fixed height $w' \in \mathfrak{D}_{wc}$ is in the form of an annulus centered at (x, y, w') with inner and outer radii defined by equation (4.47). (b) The two squares centered at (x, y, w') and of half width s_β and s_α (given by equation (4.51)) provide an upper and lower bound to the region of ambiguity of figure 4.14a.

final receptor defined at each point within the disk (4.50). In this way we can assign a number, representing the volume of intersection, to each point on the disk (4.50). The volume of ambiguity is minimum at the point $(x, y) = (0, -1.260)$ with a value of 6.814×10^{-5} cm^3. The addition of receptors to this array will decrease its volume of ambiguity and increase its ability to positively localize the object. As this volume is an upper bound on the true ambiguity volume, we can conclude that non-ideal receptors may also localize objects using the methodology described in this chapter.

4.4 Conclusion

In the past many studies have focused on extracting location information from sets of electric image features (e.g. position, amplitude, spread). In this chapter we have approached the problem of object localization from a different perspective. By treating the localization problem as an inverse problem, we have been able to find a lower bound on the amount of information that would be necessary for fish to unambiguously localize an object.

Our algorithm is based on three major assumptions. The first is that the field is

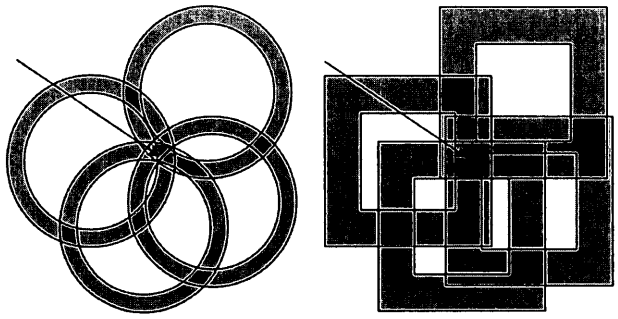

Figure 4.15: Level height ambiguity region intersection - (a) Intersection of four ambiguity regions at a particular level height $w' \in \mathfrak{D}_{wc}$. The arrow points to the common region of intersection.(b) Intersection of square annuli bounding each annulus of figure 4.15a. The arrow again points to the common region of intersection. Note the difference in size between the two regions of common intersection.

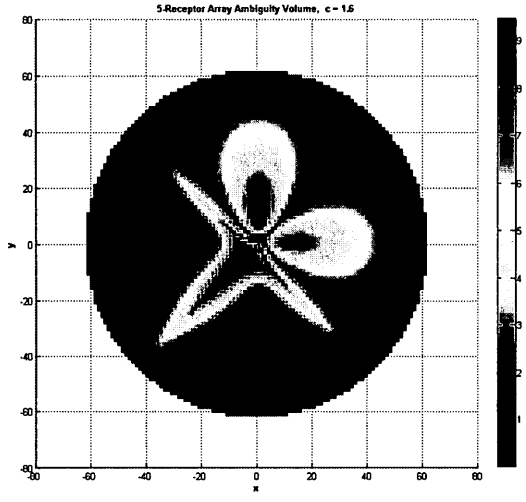

Figure 4.16: Non-ideal array ambiguity volume - Ambiguity volume of an array consisting of four fixed receptors (black circles) and a final fifth receptor at each location on the xy-plane, (see text for details). The color bar to the right indicates the volume in cm^3. Parameter values: sphere radius $a = 2$ cm, sphere distance $z = 7$ cm, sphere relative permittivity $\epsilon = 2.25$ (polyethylene), media relative permittivity $\epsilon_e = 80.1$ (water at 20° C), electric field magnitude at sphere $E_o = 0.95$ mV/cm, receptor sensitivity $T = 10^{-4}$ mV/cm, multiplication factor $c = 1.6$. The four fixed receptors are located at $(2.743, -0.190), (-0.088, 2.493), (1.802, 1.402)$ and $(-2.149, 1.923)$

uniform prior to the introduction of the object. Although the near field where electrolocation takes place is highly complicated, in the vicinity of very small objects, we can assume the field to be uniform. Furthermore, it can be shown that in addition to a dipole moment, a non-uniform field induces higher order multi-pole perturbations which attenuate with distance from the object more rapidly than the dipole perturbation. A second assumption in the model is that the perturbations at the skin are not affected by the presence of the fish. We have shown that a resistive fish skin will scale the potential perturbation but will not introduce any nonlinearity into the system. Depending on the relative permittivity of the skin, this perturbation may need to be taken into account, however, the mechanism described in this chapter and the results shown remain valid.

As has been noted, the geometry of electric fish's main prey, the *Daphnia Magna* is roughly spherical. Further, as the size of a non-spherical object is reduced or its distance increased the perturbation of the electric field due to the object, and hence its electric image, converges to that produced by a spherical object. For example, at far enough distances the contours of the electric image of a cube are close to perfect circles; identical to those of a sphere (chapter 3). This property is reflected in the Laplace equation, which is used to accurately simulate the electric image of any dielectric object from a boundary value problem. A spherical representation of distant objects is a good approximation.

We have shown that independent of field direction, the lower bound on the information required to successfully localize an object consist of amplitude information at three or four locations on the skin surface. We have shown that this information is not masked by the presence of environmental electromagnetic noise. Rather, external noise conceals the true value of $\tau = \Gamma a^3$. It must be noted that even though our method can be used to determine the distance of an object, it cannot be used to infer any information about its size and electrical properties.

We have devised a method, with the aid of square annuli to numerically calculate an upper bound on the volume of ambiguity of non-ideal receptors. Our numerical results show that non-ideal receptors are also capable of detecting object distances using

the method described here. Information from more non-ideal receptors may be required for accurate localization in comparison to ideal (zero-threshold) receptors.

If the fish localize objects by comparing information received from multiple receptors and treating the problem as an inverse problem as described here, then the fish's probing movements, observed during electrolocation tasks [34] could serve to identify such suitable receptors and or/verify the assessment made from one such array. A localization algorithm based on this method is independent of the field magnitude, time variation and the object's size and electric contrast.

5

Conclusion

Weakly electric fish use electrolocation - the detection of electric fields - to sense their environment. The task of electrolocation involves the decoding of the third dimension – depth – from a two-dimensional electric image. In this thesis we have presented three important advances in the area of depth-perception. In chapter 2, we have provided a mathematical foundation for two of the most accepted depth perception models currently in use. Chapter 3 outlines a novel model for electrolocation based on a single parameter. Finally, in chapter 4 we approach the problem of depth perception from the perspective of information constraints, asking; what is the minimum amount of information necessary for location disambiguation?

Depth perception models presented by Rasnow [32] and von der Emde [31] have become the accepted models within the community. Emde's model is based on empirical data and to our knowledge, as of the time of writing this thesis, no mathematical proof of it exists. Rasnow's model was discredited by von der Emde [12], maintaining that such a model would only work if the electrical properties of the target object are previously known to the fish; an impossibility. In this work we have provided a mathematical proof of both models showing that von der Emde's experimentally based model is mathematically valid. Further, contrary to von der Emde's claim [12], we have also shown that Rasnow's model can also be used to localize objects whose electrical properties are unknown to the fish.

Depth perception mechanisms suggested thus far are based on multi-parameter mea-

surements [31, 32, 40, 41] and most take into account only the spatial profile of the electric image, disregarding its temporal characteristic. Mechanisms based on multi-parameter measurements require multiple topographic neuronal maps with different tuning curves to accurately estimate distance. In contrast a mechanism based on a single image parameter would only need a single topographic neuronal map, thereby being intrinsically simpler in its implementation. In this thesis we have developed a novel mechanism for depth perception based on a single image parameter. Our model takes into account the temporal properties of the electric image and provides an explanation of the tail-bending behavior observed in electrolocating fish. Based on non-ideal electroreceptors, our model's performance in localizing an object is independent of the object's size, material and distance.

We have shown that objects, whose relative permittivity is close to that of the surrounding media, remain invisible to non-ideal receptors, characterizing an *invisible permittivity spectrum*. The range of permittivities which comprise this spectrum depend on the object's distance, the strength of the electric field and the receptor's sensitivity threshold. An increase in the object's distance tends to increase the range of this spectrum, thereby in effect, de-cluttering the electric image. Increases in both field strength and receptor sensitivity have the opposite effect; decreasing the spectrum range.

Electroreceptor density varies on the surface of the fish, with higher densities being found on the head region and lower densities on the trunk and tail regions. We have found that receptor density is positively correlated with the distance at which objects can be localized and negatively correlated with the invisible permittivity spectrum. This indicates that the more dense the receptors, the greater the distance and the more varied the relative permittivity of material that can be localized.

We have devised an algorithm, based on repeated recordings of the electric image radius, for localization of objects in the presence of environmental electromagnetic noise. Our algorithm relies primarily on neuronal population codes in the early stages of the electrosensory pathway. Downstream electrosensory networks are employed only to extract the final information about the object location. We have shown that noise at any level has a negative effect and that greater EOD magnitudes facilitate electrolocation

in noisy environments. Our model provides the threshold dependent physiological basis on which stochastic resonance can be employed. Our results are in line with Russell et al.'s [56] findings in that the addition of noise can facilitate the detection of sub-threshold signals, but does not aid in their localization.

Past studies of depth perception have focused on extracting location information from sets of electric image features [9, 12, 31, 32, 33, 34, 40, 41]. In chapter 4, we have taken a completely different approach to the problem of depth perception by considering the information that is available at a single receptor. Treating the problem as an inverse problem, we have shown that distance information can completely be encoded within the amplitude of the electric image measured at at most four receptor locations on the fish surface. This provides a lower bound on the amount of information that would be necessary for fish to unambiguously localize an object. We present a mechanism, by way of choosing an array of receptors, by which this information can be unambiguously extracted. Our choice of array is independent of the object size, its electric contrast, the EOD's variation in time and its magnitude. We have proposed that the fish's probing movements, observed during electrolocation tasks could serve to identify such suitable receptors and/or verify the assessment made from one such array. Our approach provides a lower bound on the information that is necessary for the fish to unambiguously decode the location of an object.

The choice of the receptor array presented in chapter 4 may at first glance appear unnatural. For example, it may appear difficult to justify the presence of a receptor located at the point closest to the object. However, consider partitioning the fish surface into small sub-squares of some area such that each partition contains one or more receptors. Then, the choice of receptors, as described in chapter 4 would be analogous to a choice of sub-squares and the information/signal at each sub-square can be thought of as the aggregate information available to all receptors within the sub-square. Hence identification of a receptor closest to the object would correspond to identification of the sub-square where the amplitude f the perturbation is measured to be greatest.

Throughout this thesis three major assumptions have been made. The first is that prior to the introduction of the dielectric object the electric field is spatially uniform.

Although the near field where electrolocation takes place is highly complicated, in the vicinity of very small objects we can assume the field to be uniform. Furthermore, it has been shown that in addition to a dipole moment, a non-uniform field induces higher order multi-pole perturbations which attenuate with distance from the object more rapidly than the dipole perturbation. A second assumption is that the perturbations at the skin are not affected by the presence of the fish. We have shown that a resistive fish skin will scale the potential perturbation but will not introduce any nonlinearity into the system. Depending on the relative permittivity of the skin, this perturbation may need to be taken into account, however, the work described in this thesis and the results shown remain valid.

Finally, we have assumed that objects to be localized are spherical. Foremost, the geometry of electric fish's main prey, the *Daphnia Magna* is roughly spherical. Second, as the size of a non-spherical object is reduced or its distance increased the perturbation of the electric field due to the object, and hence its electric image, converges to that produced by a spherical object. This property is reflected in the Laplace equation, which is used to accurately simulate the electric image of any dielectric object from a boundary value problem.

Our work in the area of electrolocation has contributed to the field of knowledge in three distinct ways. We have provided mathematical proofs of electrolocation models first devised by Rasnow and von der Emde, showing that both models could provide electrolocation cues to the fish. To our knowledge few studies have investigated the role of the temporal component of the electric image in the electrolocation process. In this work we have developed a model for distance detection based on both the spatial as well as the temporal characteristics of the electric image. Our spatiotemporal model can accurately be processed in the higher brain regions with only a single narrowly tuned topographic neuronal map. Further, our model may explain the probing movements (tail-bending) and back and forth swimming (*va-et-vient* sampling) behavior observed in electrolocating fish, in that these behaviors change the magnitude of the electric field at the object and hence the electric image. Lastly, we have explored the minimum amount of information that would be required for the electrolocation

process. We have looked at the problem of electrolocation from a completely new perspective, by considering the information available at individual receptors. We have presented a mechanism by way of choosing an array of receptors, by which information about the location of an object can unambiguously be extracted. Probing movements and *va-et-vient* sampling behavior observed during electrolocation tasks could serve to identify such suitable receptors and/or verify the assessment made from one such array.

The validity of the spatiotemporal model presented in chapter 3 can be verified by our work in predicting the distance of a cube. Our model predicts that a fish presented with a dielectric cube and a sphere of equal lateral distance would perceive the cube to be closer if both objects are near and further if the two objects are far. A behavioral experiment in line with von der Emde's experiment [31] could be conducted to test these results.

Our work in this area has far reaching applications. The greatest potential is in engineering and biomimetic applications for instances where visual information is absent. Some examples include naval mine detection and robotic electrolocation. A further interesting application is in the area of bubble detection such as that in hemodialysis machinery, infusions or two-phase flows [59].

Appendix A

Potential Perturbation by Dielectric Sphere

Consider a linear, homogeneous, isotropic sphere of radius a, centered at $\mathbf{x}_{obj}$, placed within a spatially uniform, temporally oscillating electric field $\mathbf{E}$. The perturbation to the potential measured at $\mathbf{x}$ is described by,

$$\partial\Phi(\mathbf{x}) = \frac{\Gamma a^3 \mathbf{E}(\mathbf{x}_{obj})(\mathbf{x}-\mathbf{x}_{obj})}{|\mathbf{x}-\mathbf{x}_{obj}|^3}, \qquad \text{where}$$

$$\Gamma = \frac{(\rho_e-\rho_i)+i\omega\rho_e\rho_i(\epsilon_i-\epsilon_e)}{(\rho_e+2\rho_i)+i\omega\rho_e\rho_i(\epsilon_i+2\epsilon_e)}$$

and ρ is the resistivity, ϵ the absolute permittivity and ω the angular frequency of the unperturbed field. The subscripts i and e identify the variables as being interior or exterior to the spherical object, respectively. This result was briefly described in [32]. Here, we would like to extend this result for the case of static fields.

We begin with Gauss's Law, $\nabla \cdot \mathbf{E} = \rho/\epsilon_o$, which in the absence of charge leads to the Laplace equation, $\nabla\Phi^2 = 0$.

We define the reference frame such that the origin coincides with the sphere's center and the applicate vector lies parallel with $\mathbf{E}$. In spherical coordinates, the potential in such an arrangement is independent of the azimuthal angle ϕ, hence, $\Phi(r,\theta,\phi) = \Phi(r,\theta)$. The solution of the Laplace equation in spherical coordinates is

$$\Phi(r,\theta) = \sum_{n=0}^{\infty}\left(A_n r^n + B_n\frac{1}{r^{n+1}}\right)P_n(\cos\theta), \tag{A.1}$$

where A_n and B_n are constants, yet to be determined, and P_n is the Legendre function of the first kind. To solve for the constants, we study the potential both at the surface boundary of the sphere and the exterior media as well as at infinitely far distances to the sphere.

Boundary Conditions

B.C. 1. $\Phi(r,\theta) \to -E_o r\cos(\theta)$ as $r \to \infty$

Proof:

Noting that the field is in the direction of the applicate, we can expect the perturbation due to the dielectric sphere to be negligable far from the sphere. Hence, far from the sphere,

$$\begin{aligned} E &= E_o\vec{k}, && \text{Cartesian coordinates} \\ &= E_o\left(\cos(\theta)\hat{e}_r - \sin(\theta)\hat{e}_\theta\right), && \text{spherical coordinates.} \end{aligned}$$

Also, by the following relation between the electric field and potential,

$$\begin{aligned} E &= -\nabla\Phi, \\ &= -\left[\frac{\partial\Phi}{\partial r}\hat{e}_r + \frac{1}{r}\frac{\partial\Phi}{\partial\theta}\hat{e}_\theta\right], \end{aligned}$$

it must be that,

$$\begin{aligned} \frac{\partial\Phi}{\partial r} &= -E_o\cos(\theta) && \Longrightarrow && \Phi(r,\theta) = -E_o r\cos(\theta) + f(\theta), \\ \frac{1}{r}\frac{\partial\Phi}{\partial\theta} &= E_o\sin(\theta) && \Longrightarrow && \Phi(r,\theta) = -E_o r\cos(\theta) + g(r). \end{aligned}$$

Hence,

$$\Phi(r,\theta) = -E_o r\cos(\theta).$$

■

B.C. 2. $\Phi(r,\theta) < \infty$ as $r \to 0$

Proof:

The only charges in the system are those that produce the external electric field

and those induced on the surface of the sphere due to polarization of the dielectric. Hence, no volume distribution of induced charges exist.

■

B.C. 3. $(\mathbf{D}_e - \mathbf{D}_i) \cdot \hat{\mathbf{n}} = 0$

Proof:

Consider a Gaussian pillbox straddling the boundary between the two different dielectrics (figure A.1). Denote by $\mathbf{D}$ the electric displacement vector within each dielectric media and by σ the free charge on the surface boundry. Subscripts i and e represent the measure interior and exterior of the sphere, respectively. Letting $\hat{\mathbf{n}}$ denote the surface normal, we may use Gauss' Law over the surface

$$\oint \mathbf{D} \cdot \hat{\mathbf{n}}\, ds = Q.$$

Considering the three distinct sides of the pillbox,

$$\oint_{btm} \mathbf{D}_i \cdot d\mathbf{S}_{btm} + \oint_{top} \mathbf{D}_e \cdot d\mathbf{S}_{top} + \oint_{side} \mathbf{D} \cdot d\mathbf{S}_{side} = Q.$$

If we reduce the height of the pillbox, the contribution of the flux through the sides become negligable. Hence,

$$\oint_{btm} \mathbf{D}_i \cdot d\mathbf{S}_{btm} + \oint_{top} \mathbf{D}_e \cdot d\mathbf{S}_{top} = Q.$$

We now reduce the diamter of the pillbox so that any variation of σ and $\mathbf{D}$ over the surface can be ignored and thus can be considered constant at the site of the pillbox. Since $\mathbf{D}$ is constant over the surface S and the area of the top and bottom surfaces are equal,

$$-\mathbf{D}_i \cdot \hat{\mathbf{n}}\, S + \mathbf{D}_e \cdot \hat{\mathbf{n}}\, S = \sigma S,$$
$$-\mathbf{D}_i \cdot \hat{\mathbf{n}} + \mathbf{D}_e \cdot \hat{\mathbf{n}} = \sigma.$$

In the absence of free surface charges, the normal component of $\mathbf{D}$ is continuous accross the boundary,

$$(\mathbf{D}_i - \mathbf{D}_e) \cdot \hat{\mathbf{n}} = 0.$$

■

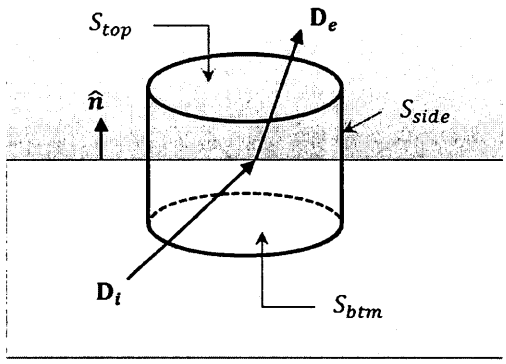

Figure A.1: Gaussian pillbox - Gaussian pillbox straddling the boundary between two different dielectrics.

B.C. 4. $(\epsilon_e \mathbf{E}_e - \epsilon_i \mathbf{E}_i) \cdot \hat{\mathbf{n}} = 0$

Proof:

By definition, in a linear, homogeneous, isotropic material $\mathbf{D} = \epsilon_o \epsilon \mathbf{E}$, where ϵ_o is the permittivity of free space and $\epsilon_{e,i}$ is the relative permittivity of the particular media. Boundary condition follows straight from B.C. 3.

■

B.C. 5. $\mathbf{E}_{etan} = \mathbf{E}_{itan}$

Proof:

Faraday's Law under electrostatic conditions reduces to

$$\nabla \times \mathbf{E} = 0,$$

which by Stokes theorem is equivalent to

$$\oint \mathbf{E} \cdot d\mathbf{l} = 0.$$

Using the line integral along the loop defined in figure A.2 we have,

$$\int_{top} \mathbf{E}_e \cdot d\mathbf{l}_{top} + \int_{side} \mathbf{E} \cdot d\mathbf{h} + \int_{btm} \mathbf{E}_i \cdot d\mathbf{l}_{btm} + \int_{side} \mathbf{E} \cdot d\mathbf{h} = 0,$$

where the definitions of the line segments and field are as noted in the figure. Now consider reducing the height of the loop. As we reduce the height, the contribution from the sides become negligible and can be ignored. Hence,

$$\int_{top} \mathbf{E}_e \cdot d\mathbf{l}_{top} + \int_{btm} \mathbf{E}_i \cdot d\mathbf{l}_{btm} = 0.$$

As the line segments face opposite directions, $d\mathbf{l}_{top} = -d\mathbf{l}_{btm}$. Denoting this quantity by $d\mathbf{l}$, we find,

$$\int_{top} (\mathbf{E}_e - \mathbf{E}_i) \cdot d\mathbf{l} = 0.$$

Noting, this equation holds for all $d\mathbf{l}$, it must be that the integrand is zero. Equivalently,

$$\mathbf{E}_{etan} = \mathbf{E}_{itan},$$

where E_{tan} is the tangential component of the electric field.

■

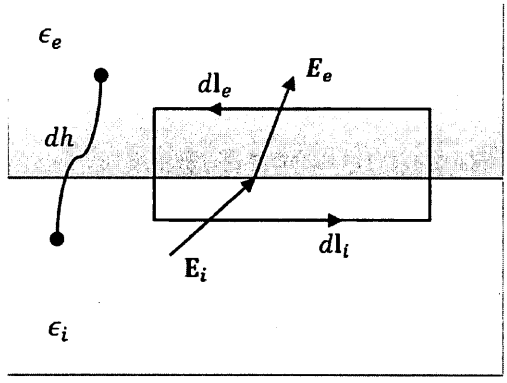

Figure A.2: Gaussian path - Gaussian path straddling the boundary between two different dielectrics.

B.C. 6. $g_e\mathbf{E}_{er} + \epsilon_e \frac{\partial \mathbf{E}_{er}}{\partial t} = g_i\mathbf{E}_{ir} + \epsilon_i \frac{\partial \mathbf{E}_{ir}}{\partial t}$

Proof:

This is simply a result of Kirchhoff's current law. The terms g are the conductivity of the particular media and E_r, the radial / normal component of the electric field. And in turn, $g\mathbf{E}_r$ is Ohm's law describing the conduction current. The

second term $\epsilon\frac{\partial \mathbf{E}_r}{\partial t}$, comprised of the dielectric constant ϵ and the time derivative of the field's normal component, describes the displacement current within the particular dielectric media.

■

B.C. 7. $\Phi_e(r,\theta) = \Phi_i(r,\theta)$ when $r = a$

Proof:

By definition,

$$\begin{aligned}\Phi(A) - \Phi(C) &= -\int_C^A \mathbf{E}\cdot d\mathbf{l}, \\ &= -\left[\int_C^{B-\epsilon} \mathbf{E}\cdot d\mathbf{l} + \int_{B-\epsilon}^{B+\epsilon} \mathbf{E}\cdot d\mathbf{l} + \int_{B+\epsilon}^{A} \mathbf{E}\cdot d\mathbf{l}\right],\end{aligned}$$

for any $\epsilon > 0$, see figure A.3. Consider the right-hand-side as we let $\epsilon \to 0$,

$$-\lim_{\epsilon\to 0}\left[\int_C^{B-\epsilon} \mathbf{E}\cdot d\mathbf{l} + \int_{B+\epsilon}^{A} \mathbf{E}\cdot d\mathbf{l}\right] - \lim_{\epsilon\to 0}\int_{B-\epsilon}^{B+\epsilon} \mathbf{E}\cdot d\mathbf{l}.$$

Unless $\mathbf{E} = \infty$ at B, the value of the third integral is 0. Since we assume that there are no free charges we may assume that $\mathbf{E} < \infty$ and hence,

$$\begin{aligned}\Phi(A) - \Phi(C) &= -\lim_{\epsilon\to 0}\left[\int_C^{B-\epsilon} \mathbf{E}\cdot d\mathbf{l} + \int_{B+\epsilon}^{A} \mathbf{E}\cdot d\mathbf{l}\right], \\ &= \lim_{\epsilon\to 0}\left[\Phi(B-\epsilon) - \Phi(C) + \Phi(A) - \Phi(B+\epsilon)\right] \\ &= \Phi(A) - \Phi(C) + \lim_{\epsilon\to 0}\left[\Phi(B-\epsilon) - \Phi(B+\epsilon)\right] \\ 0 &= \lim_{\epsilon\to 0}\left[\Phi(B-\epsilon) - \Phi(B+\epsilon)\right]\end{aligned}$$

This implies that the potential is continuous accross the boundary B.

■

Electrostatics

The boundary conditions above are used to solve for the unknown constants of the Laplace equation (A.1). We apply the subscripts i and e to indicate whether the particular measure is that in the interior or exterior of the sphere, respectively. Since,

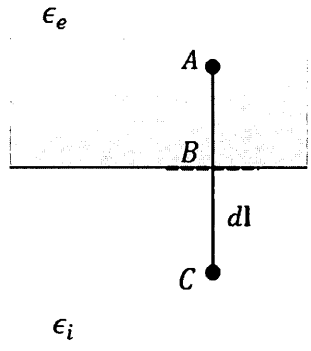

Figure A.3: Path Connecting the two media - Straight path extending from one media to the other. The boundary is marked by B.

potentials both on the inside and outside the sphere need to be solved separately, each with possibly different coefficients, we denote

$$\Phi_i(r,\theta) = \sum_{n=0}^{\infty} \left(A_n r^n + B_n \frac{1}{r^{n+1}} \right) P_n(\cos\theta) \quad \text{and} \tag{A.2}$$

$$\Phi_e(r,\theta) = \sum_{n=0}^{\infty} \left(C_n r^n + D_n \frac{1}{r^{n+1}} \right) P_n(\cos\theta) \tag{A.3}$$

Now, consider the effect of the above boundary conditions

B.C. 1. $\Phi_e(r,\theta) \to -E_o r\cos(\theta)$ as $r \to \infty$

Hence, as $r \to \infty$,

$$\Rightarrow \sum_{n=0}^{\infty} \left(C_n r^n + D_n \frac{1}{r^{n+1}} \right) P_n(\cos\theta) \to -E_o r\cos\theta,$$

$$\Rightarrow C_0 + C_1 r\cos\theta + \sum_{n=2}^{\infty} C_n r^n P_n(\cos\theta) + \sum_{n=0}^{\infty} D_n \frac{1}{r^{n+1}} P_n(\cos\theta) \to -E_o r\cos\theta.$$

As, $r \to \infty$ the first sum diverges, whereas the second converges to zero for all constants C_n and D_n. Hence it must be that,

$$C_0 = 0, \qquad C_1 = -E_o, \qquad C_n = 0,\ \forall n \geq 2.$$

Thus, the potential outside the sphere is given by

$$\Phi_e(r,\theta) = -E_o r\cos\theta + \sum_{n=0}^{\infty} D_n \frac{1}{r^{n+1}} P_n(\cos\theta).$$

B.C. 2. As $r \to 0$, $\Phi_i(r,\theta) < \infty$

Hence, as $r \to 0$

$$\Phi_i(r,\theta) = \sum_{n=0}^{\infty} \left(A_n r^n + B_n \frac{1}{r^{n+1}} \right) P_n(\cos\theta) < \infty.$$

So it must be that $B_n = 0, \forall n \geq 0$, reducing the potential inside the sphere to

$$\Phi_i(r,\theta) = \sum_{n=0}^{\infty} A_n r^n P_n(\cos\theta).$$

B.C. 7. $\Phi_e(r,\theta) = \Phi_i(r,\theta)$ when $r = a$

$$\Phi_e(a,\theta) = \Phi_i(a,\theta)$$

$$-E_o a\cos\theta + \sum_{n=0}^{\infty} D_n \frac{1}{a^{n+1}} P_n(\cos\theta) = \sum_{n=0}^{\infty} A_n a^n P_n(\cos\theta)$$

Equating the coefficients of the Legendre function:

$$P_0: \quad D_0\frac{1}{a} = A_0 \quad \Rightarrow \quad A_0 = \frac{1}{a}D_0, \tag{A.4}$$

$$P_1: \quad -E_o a + D_1\frac{1}{a^2} = A_1 a \quad \Rightarrow \quad A_1 = \frac{1}{a^3}D_1 - E_o, \tag{A.5}$$

$$P_n: \quad D_n\frac{1}{a^{n+1}} = A_n a^n \quad \Rightarrow \quad A_n = \frac{1}{a^{2n+1}}D_n,\ n \geq 2. \tag{A.6}$$

B.C. 4. $(\epsilon_e \mathbf{E}_e - \epsilon_i \mathbf{E}_i)\cdot \hat{\mathbf{n}} = 0$, when $r = a$

Using the definition, $\mathbf{E} = -\nabla\Phi$,

$$\epsilon_e \nabla\Phi_e \cdot \hat{\mathbf{n}} = \epsilon_i \nabla\Phi_i \cdot \hat{\mathbf{n}},$$

$$\epsilon_e \left.\frac{\partial \Phi_e}{\partial n}\right|_{r=a} = \epsilon_i \left.\frac{\partial \Phi_i}{\partial n}\right|_{r=a},$$

$$\epsilon_e \left.\frac{\partial \Phi_e}{\partial r}\right|_{r=a} = \epsilon_i \left.\frac{\partial \Phi_i}{\partial r}\right|_{r=a},$$

$$\epsilon_e \frac{\partial}{\partial r}\left(-E_o r\cos\theta + \sum_{n=0}^{\infty} D_n \frac{1}{r^{n+1}} P_n(\cos\theta) \right)_{r=a} = \epsilon_i \frac{\partial}{\partial r}\left(\sum_{n=0}^{\infty} A_n r^n P_n(\cos\theta) \right)_{r=a},$$

$$\epsilon_e \left(-E_o\cos\theta - \sum_{n=0}^{\infty} (n+1) D_n \frac{1}{r^{n+2}} P_n(\cos\theta) \right)_{r=a} = \epsilon_i \left(\sum_{n=0}^{\infty} n A_n r^{n-1} P_n(\cos\theta) \right)_{r=a},$$

$$\epsilon_e \left(-E_o\cos\theta - \sum_{n=0}^{\infty} (n+1) D_n \frac{1}{a^{n+2}} P_n(\cos\theta) \right) = \epsilon_i \left(\sum_{n=0}^{\infty} n A_n a^{n-1} P_n(\cos\theta) \right).$$

Now, if we equate the coefficients of the Legendre function:

$$P_0: \quad \epsilon_e\left(\frac{-1}{a^2}D_0\right) = 0 \quad \Rightarrow \quad D_0 = 0$$

$$\Rightarrow \quad A_0 = 0 \qquad \text{by A.4}$$

$$P_1: \quad \epsilon_e\left(-E_o - 2\frac{1}{a^3}D_1\right) = \epsilon_i A_1 \quad \Rightarrow \quad A_1 = \frac{\epsilon_e}{\epsilon_i}\left(\frac{-2}{a^3}D_1 - E_o\right)$$

$$= \frac{1}{a^3}D_1 - E_o \qquad \text{by A.5}$$

$$\Rightarrow D_1 = E_o a^3 \frac{\epsilon_i - \epsilon_e}{\epsilon_i + 2\epsilon_e}, \qquad A_1 = -E_o \frac{3\epsilon_e}{\epsilon_i + 2\epsilon_e}$$

$$P_n: \quad -\epsilon_e(n+1)\frac{1}{a^{n+2}}D_n = \epsilon_i n a^{n-1} A_n \quad \Rightarrow \quad A_n = -\frac{\epsilon_e}{\epsilon_i}\frac{n+1}{n}\frac{1}{a^{2n+1}}D_n$$

$$= \frac{1}{a^{2n+1}}D_n \qquad \text{by A.6}$$

$$\Rightarrow D_n = 0, \qquad A_n = 0, \ \forall n \geq 2$$

Substituting the coefficients into the potential equation (A.1), we find

$$\Phi_i(r,\theta) = -E_o \frac{3\epsilon_e}{\epsilon_i + 2\epsilon_e}\cos\theta, \tag{A.7}$$

$$\Phi_e(r,\theta) = -E_o r\cos\theta + E_o a^3 \frac{\epsilon_i - \epsilon_e}{\epsilon_i + 2\epsilon_e}\frac{1}{r^2}\cos\theta,$$

$$= -E_o r\cos\theta\left[1 - \frac{a^3}{r^3}\frac{\epsilon_i - \epsilon_e}{\epsilon_i + 2\epsilon_e}\right]. \tag{A.8}$$

The first term in the equation (A.8) is the original (unperturbed) potential in the absence of the dielectric sphere. Therefore, the second term represents the perturbation that results when the dielectric sphere is introduced into the uniform field. Hence, the potential which constitutes the formation of an electric image on the fish surface is of the form,

$$\partial\Phi(r,\theta) = \frac{E_o a^3\cos\theta}{r^2}\frac{\epsilon_i - \epsilon_e}{\epsilon_i + 2\epsilon_e}. \tag{A.9}$$

Electrodynamic

The case of a spatially uniform field with temporally oscillating magnitude is similar as above. Starting with solutions of the Laplace equation given in spherical coordinates

$$\Phi_i(r,\theta) = \sum_{n=0}^{\infty}\left(A_n r^n + B_n \frac{1}{r^{n+1}}\right) P_n(\cos\theta) \quad \text{and}$$
$$\Phi_e(r,\theta) = \sum_{n=0}^{\infty}\left(C_n r^n + D_n \frac{1}{r^{n+1}}\right) P_n(\cos\theta),$$

we assume that $\Phi(r,\theta,t) = \Phi(r,\theta)e^{i\omega t}$, where ω is the angular frequency of the unperturbed field. Now, using the boundary conditions above, we solve for the coefficients of the Legendre functions.

B.C. 1. $\Phi_e(r,\theta) \to -E_o r\cos(\theta)$ as $r \to \infty$

Hence, as $r \to \infty$,

$$\Rightarrow \sum_{n=0}^{\infty}\left(C_n r^n + D_n \frac{1}{r^{n+1}}\right) P_n(\cos\theta) \to -E_o r\cos\theta,$$
$$\Rightarrow C_0 + C_1 r\cos\theta + \sum_{n=2}^{\infty} C_n r^n P_n(\cos\theta) + \sum_{n=0}^{\infty} D_n \frac{1}{r^{n+1}} P_n(\cos\theta) \to -E_o r\cos\theta.$$

As, $r \to \infty$ the first sum diverges, whereas the second converges to zero for all constants C_n and D_n. Hence it must be that,

$$C_0 = 0, \qquad C_1 = -E_o, \qquad C_n = 0,\ \forall n \geq 2.$$

Thus, the potential outside the sphere is given by

$$\Phi_e(r,\theta) = -E_o r\cos\theta + \sum_{n=0}^{\infty} D_n \frac{1}{r^{n+1}} P_n(\cos\theta).$$

B.C. 2. As $r \to 0$, $\Phi_i(r,\theta) < \infty$

Hence, as $r \to 0$

$$\Phi_i(r,\theta) = \sum_{n=0}^{\infty}\left(A_n r^n + B_n \frac{1}{r^{n+1}}\right) P_n(\cos\theta) < \infty.$$

So it must be that $B_n = 0, \forall n \geq 0$, reducing the potential inside the sphere to

$$\Phi_i(r,\theta) = \sum_{n=0}^{\infty} A_n r^n P_n(\cos\theta).$$

B.C. 6. $g_e\mathbf{E}_{er} + \epsilon_e\frac{\partial \mathbf{E}_{er}}{\partial t} = g_i\mathbf{E}_{ir} + \epsilon_i\frac{\partial \mathbf{E}_{ir}}{\partial t}$

Noting that

$$\mathbf{E}_r = \mathbf{E}\cdot\hat{\mathbf{n}} = -\nabla\Phi\cdot\hat{\mathbf{n}} = -\frac{\partial\Phi}{\partial r}, \quad \text{and} \quad \frac{\partial\Phi}{\partial t} = i\omega\Phi.$$

We find,

$$\begin{aligned} g_i\frac{\partial\Phi_i}{\partial r} + \epsilon_i\frac{\partial^2\Phi_i}{\partial t\partial r} &= g_e\frac{\partial\Phi_e}{\partial r} + \epsilon_e\frac{\partial^2\Phi_e}{\partial t\partial r}, \\ (g_i + i\omega\epsilon_i)\left.\frac{\partial\Phi_i}{\partial r}\right|_{r=a} &= (g_e + i\omega\epsilon_e)\left.\frac{\partial\Phi_e}{\partial r}\right|_{r=a}, \\ \xi_i\left.\frac{\partial\Phi_i}{\partial r}\right|_{r=a} &= \xi_e\left.\frac{\partial\Phi_e}{\partial r}\right|_{r=a}, \end{aligned}$$

where we have denoted $g + i\omega\epsilon = \xi$ for simplicity. Hence,

$$\xi_i\sum_{n=0}^{\infty} nA_n a^{n-1}P_n(\cos\theta) = \xi_e\left(-E_o\cos\theta - \sum_{n=0}^{\infty}(n+1)D_n\frac{1}{a^{n+2}}P_n(\cos\theta)\right).$$

Equating the Legendre coefficients:

$$\begin{aligned} P_0: &\quad 0 = -D_0\frac{1}{a^2}\xi_e && \Rightarrow \quad D_0 = 0 \\ P_1: &\quad \xi_i A_1 = \xi_e\left(-E_o - 2D_1\frac{1}{a^3}\right) && \Rightarrow \quad A_1 = \frac{\xi_e}{\xi_i}\left(-E_o - 2D_1\frac{1}{a^3}\right) \\ P_{n\geq 2}: &\quad \xi_i n A_n a^{n-1} = -\xi_e(n+1)D_n\frac{1}{a^{n+2}} && \Rightarrow \quad A_n = -\frac{\xi_e}{\xi_i}\frac{(n+1)}{n}D_n\frac{1}{a^{2n+1}}. \end{aligned} \tag{A.10}$$

B.C. 5. $\mathbf{E}_{etan} = \mathbf{E}_{itan}$

This boundary condition is equivalent to

$$\frac{\partial\Phi_e}{\partial\theta} = \frac{\partial\Phi_i}{\partial\theta}.$$

Now,

$$\begin{aligned} \frac{\partial\Phi_e}{\partial\theta} &= -E_o r P_1'(\cos\theta) + \sum_{n=0}^{\infty} D_n\frac{1}{r^{n+1}}P_n'(\cos\theta), \\ &= -E_o r P_1'(\cos\theta) + \sum_{n=1}^{\infty} D_n\frac{1}{r^{n+1}}P_n'(\cos\theta), \\ \frac{\partial\Phi_i}{\partial\theta} &= \sum_{n=0}^{\infty} A_n r^n P_n'(\cos\theta), \\ &= \sum_{n=1}^{\infty} A_n r^n P_n'(\cos\theta), \end{aligned}$$

where, we have denoted $\frac{d}{d\theta}P(\cos\theta) = P'$ and noted that $P'_0 = 0$. Hence, by the boundary condition, when $r = a$ we must have

$$\sum_{n=1}^{\infty} A_n r^n P'_n(\cos\theta) = -E_o r P'_1(\cos\theta) + \sum_{n=1}^{\infty} D_n \frac{1}{r^{n+1}} P'_n(\cos\theta).$$

We now equate the coefficients of the derivatives of the Legendre function:

$$\begin{aligned} P'_1: \qquad & A_1 a = -E_o a + D_1 \frac{1}{a^2} \qquad \Rightarrow \qquad A_1 = -E_o + D_1 \frac{1}{a^3} \\ P'_{n\geq 2}: \qquad & A_n a^n = D_n \frac{1}{a^{n+1}} \qquad \Rightarrow \qquad A_n = D_n \frac{1}{a^{2n+1}}. \end{aligned}$$

Using this result along with that found in equation (A.10) to solve for the coefficients, we find

$$D_1 = a^3 E_o \left(\frac{\xi_i - \xi_e}{\xi_i + 2\xi_e}\right), \qquad A_1 = -E_o + E_o \left(\frac{\xi_i - \xi_e}{\xi_i + 2\xi_e}\right)$$

and

$$D_n = 0, \qquad A_n = 0 \qquad \forall n \geq 2.$$

Substituting the coefficients into the potential equation (A.1), we find

$$\begin{aligned} \Phi_e(r,\theta) &= \sum_{n=0}^{\infty} \left(C_n r^n + D_n \frac{1}{r^{n+1}}\right) P_n(\cos\theta), \\ &= -E_o r\cos\theta + \left(\frac{\xi_i - \xi_e}{\xi_i + 2\xi_e}\right) E_o \frac{a^3}{r^2}\cos\theta. \end{aligned} \tag{A.11}$$

The first term in the equation (A.11) is the original (unperturbed) potential in the absence of the dielectric sphere. Therefore, the second term represents the perturbation that results when the dielectric sphere is introduced into the uniform field. Hence, the perturbation of a spatially uniform field with temporally oscillating magnitude by a dielectric sphere is given by

$$\begin{aligned} \partial\Phi(r,\theta) &= \left(\frac{\xi_i - \xi_e}{\xi_i + 2\xi_e}\right) E_o \frac{a^3}{r^2}\cos\theta, \\ &= \frac{\rho_e - \rho_i + i\omega\rho_e\rho_i(\epsilon_i - \epsilon_e)}{\rho_e + 2\rho_i + i\omega\rho_e\rho_i(\epsilon_i + 2\epsilon_e)} E_o \frac{a^3}{r^2}\cos\theta. \end{aligned} \tag{A.12}$$

where $\xi = g + i\omega\epsilon = 1/\rho + i\omega\epsilon$ and ρ is the resistivity of the particular dielectric media.

Appendix B

Perturbation by General Dielectric Object

Theory

The electric potential ψ, of a uniform electrostatic field in a medium with dielectric constant ϵ_e at any point P must obey Poisson's Equation,

$$\nabla^2\psi(P) = -\frac{\rho}{\epsilon_e\epsilon_0}. \tag{B.1}$$

Consider an imaginary boundary surface S dividing the medium into two regions V and V', interior and exterior to S, respectively. We denote measures taken interior to S by the subscrip i and exterior by the subscript e.

Boundary conditions for the unperturbed potential ψ on the surface S are

$$\lim_{P_i\to q}\psi(P_i) = \psi(q) = \lim_{P_e\to q}\psi(P_e), \text{ and} \tag{B.2a}$$

$$\lim_{P_i\to q}\frac{\partial\psi(P_i)}{\partial n_i} \equiv \frac{\partial\psi(q)}{\partial n_i} = \frac{\partial\psi(q)}{\partial n_e} \equiv \lim_{P_e\to q}\frac{\partial\psi(P_e)}{\partial n_e}, \tag{B.2b}$$

where $\partial/\partial n$ represents the derivative along the normal just interior or just exterior to S, P are field points interior and exterior to S and q is a point on the surface S.

We now consider filling the imaginary boundary surface S by a dielectric body of relative permittivity ϵ_i. The resulting potential ϕ must still satisfy Poisson's Equation

at all points:

$$\nabla^2\phi(P_i) = -\frac{\rho}{\epsilon_i\epsilon_0}, \qquad \forall P_i \text{ inside } S, \tag{B.3}$$

$$\nabla^2\phi(P_e) = -\frac{\rho}{\epsilon_e\epsilon_0}, \qquad \forall P_e \text{ outside } S. \tag{B.4}$$

Boundary conditions for the now perturbed potential ϕ are

$$\lim_{P_i\to q}\phi(P_i) = \phi(q) = \lim_{P_e\to p}\phi(P_e), \text{ and} \tag{B.5a}$$

$$\epsilon_i \lim_{P_i\to q}\frac{\partial\phi(P_i)}{\partial n_i} \equiv \epsilon_i\frac{\partial\phi(q)}{\partial n_i} = \epsilon_e\frac{\partial\phi(q)}{\partial n_e} \equiv \epsilon_e \lim_{P_e\to q}\frac{\partial\phi(P_e)}{\partial n_e}. \tag{B.5b}$$

Equation (B.5a) is due to the continuity of potential across the boundary owing to the absence of free charges there. Equation (B.5b) is derived by considering the normal component of the electric field across the boundry, and follows directly from $(\epsilon_e\mathbf{E}_e - \epsilon_i\mathbf{E}_i)\cdot\hat{\mathbf{n}} = 0$.

Consider Green's Identity,

$$\begin{aligned}\iiint_D \left(\alpha\nabla^2\beta - \beta\nabla^2\alpha\right)\,\mathrm{d}v &= \iint_{\partial D}\left(\alpha\nabla\beta - \beta\nabla\alpha\right)\,\mathrm{d}s,\\ &= \iint_{\partial D}\left(\alpha\frac{\partial\beta}{\partial n} - \beta\frac{\partial\alpha}{\partial n}\right)\,\mathrm{d}s,\end{aligned} \tag{B.6}$$

where the volume D is bounded by the closed surface ∂D, and $\partial/\partial n$ is the directional derivative in the direction of the outward pointing normal to the surface element $\mathrm{d}s$.

We begin by letting

$$\alpha = \frac{1}{|\bar{r} - \bar{r}_P|}, \qquad \beta_i = \epsilon_i\phi_i - \epsilon_e\psi_i \qquad \text{and} \qquad \beta_e = \phi_e - \psi_e. \tag{B.7}$$

It can be varified [60] that

$$\begin{aligned}&\nabla^2\frac{1}{|\bar{r} - \bar{r}_P|} = -4\pi\delta(\bar{r} - \bar{r}_P), \qquad \nabla^2\beta_{i,e} = 0, \text{ and}\\ &\frac{\partial}{\partial n_i}\frac{1}{|\bar{r} - \bar{r}_P|} = \frac{\partial}{\partial n_e}\frac{1}{|\bar{r} - \bar{r}_P|}.\end{aligned} \tag{B.8}$$

Let us first consider Green's Identity (B.6), in region V' exterior to S. Substituting equations (B.7) into (B.6), we have

$$\begin{aligned}
&\iiint_{V'} \left[\frac{1}{|\bar{r}-\bar{r}_P|}\nabla^2(\phi_e-\psi_e)-(\phi_e-\psi_e)\nabla^2\frac{1}{|\bar{r}-\bar{r}_P|}\right] \mathrm{d}v \\
&\quad = -\iint_S \left[\frac{1}{|\bar{r}_q-\bar{r}_P|}\frac{\partial}{\partial n_e}(\phi_e-\psi_e)-(\phi_e-\psi_e)\frac{\partial}{\partial n_e}\frac{1}{|\bar{r}_q-\bar{r}_P|}\right] \mathrm{d}s \qquad \text{(B.9)} \\
&\qquad + \iint_\Sigma \left[\frac{1}{|\bar{R}-\bar{r}_P|}\frac{\partial}{\partial R}(\phi_e-\psi_e)-(\phi_e-\psi_e)\frac{\partial}{\partial R}\frac{1}{|\bar{R}-\bar{r}_P|}\right] \mathrm{d}\Sigma
\end{aligned}$$

where Σ is a sphere of infinite radius R, S is the surface separating the region V and V' and $\bar{r}_q-\bar{r}_P$ is the directed distance from the field point P to the point q on the surface. In this way, region V' is completly enclosed by the surface that is comprised of Σ and S.

Now, as we increase R, both $|\bar{R}-\bar{r}_P|^{-1}$ and $\phi_e-\psi_e$ decrease at least as R^{-1} and $\frac{\partial}{\partial R}(\phi_e-\psi_e)$ and $\frac{\partial}{\partial R}|\bar{R}-\bar{r}_P|^{-1}$ decrease at least R^{-2}, while $\mathrm{d}\Sigma$ only increases by R^2, (surface element in spherical coordinates: $\mathrm{d}\Sigma_R = R^2\sin\theta\mathrm{d}\theta\mathrm{d}\phi$). Hence, the integral $\iint_\Sigma [\cdot]\ \mathrm{d}\Sigma$ in equation (B.9) decreases at least as R^{-1}, and can be discarded as it vanishes with increasing R. Using (B.8) to simplify

$$\begin{aligned}
&\iiint_{V'} 4\pi(\phi_e-\psi_e)\delta(\bar{r}-\bar{r}_P)\,\mathrm{d}v \\
&\quad = -\iint_S \left[\frac{1}{|\bar{r}_q-\bar{r}_P|}\frac{\partial}{\partial n_e}(\phi_e-\psi_e)-(\phi_e-\psi_e)\frac{\partial}{\partial n_e}\frac{1}{|\bar{r}_q-\bar{r}_P|}\right] \mathrm{d}s. \qquad \text{(B.10)}
\end{aligned}$$

In a similar way Green's Identity in the interior V, of S is

$$\begin{aligned}
&\iiint_{V} \left[\frac{1}{|\bar{r}-\bar{r}_P|}\nabla^2(\epsilon_i\phi_i-\epsilon_e\psi_i)-(\epsilon_i\phi_i-\epsilon_e\psi_i)\nabla^2\frac{1}{|\bar{r}-\bar{r}_P|}\right] \mathrm{d}v \\
&\quad = \iint_S \left[\frac{1}{|\bar{r}_q-\bar{r}_P|}\frac{\partial}{\partial n_i}(\epsilon_i\phi_i-\epsilon_e\psi_i)-(\epsilon_i\phi_i-\epsilon_e\psi_i)\frac{\partial}{\partial n_i}\frac{1}{|\bar{r}_q-\bar{r}_P|}\right] \mathrm{d}s. \qquad \text{(B.11)}
\end{aligned}$$

Again, using (B.8) to simplify,

$$\begin{aligned}
&\iiint_{V} 4\pi(\epsilon_i\phi_i-\epsilon_i\psi_i)\delta(\bar{r}-\bar{r}_P)\,\mathrm{d}v \\
&\quad = \iint_S \left[\frac{1}{|\bar{r}_q-\bar{r}_P|}\frac{\partial}{\partial n_i}(\epsilon_i\phi_i-\epsilon_i\psi_i)-(\epsilon_i\phi_i-\epsilon_i\psi_i)\frac{\partial}{\partial n_i}\frac{1}{|\bar{r}_q-\bar{r}_P|}\right] \mathrm{d}s. \qquad \text{(B.12)}
\end{aligned}$$

Consider the case where the field point P is located exterior to the surface S, that is $P = P_e$. Taking advantage of the sifting property of the δ-function, integration of equations (B.10) and (B.12) yield

$$\phi(P_e) - \psi(P_e) = -\frac{1}{4\pi} \iint_S \left[\frac{1}{|\bar{r}_q - \bar{r}_{P_e}|} \frac{\partial}{\partial n_e} (\phi_e - \psi_e) - (\phi_e - \psi_e) \frac{\partial}{\partial n_e} \frac{1}{|\bar{r}_q - \bar{r}_{P_e}|} \right] \mathrm{d}s, \text{ and} \tag{B.13}$$

$$0 = \frac{1}{4\pi} \iint_S \left[\frac{1}{|\bar{r}_q - \bar{r}_{P_e}|} \frac{\partial}{\partial n_i} (\epsilon_i \phi_i - \epsilon_e \psi_i) - (\epsilon_i \phi_i - \epsilon_e \psi_i) \frac{\partial}{\partial n_i} \frac{1}{|\bar{r}_q - \bar{r}_{P_e}|} \right] \mathrm{d}s, \tag{B.14}$$

respectivly. Upon multiplying equation (B.13) by ϵ_e and adding equation (B.14) we find

$$\begin{aligned}
\epsilon_e \phi(P_e) - \epsilon_e \psi(P_e) = & -\frac{1}{4\pi} \iint_S \left[\frac{1}{|\bar{r}_q - \bar{r}_{P_e}|} \frac{\partial}{\partial n_e} (\epsilon_e \phi_e - \epsilon_e \psi_e) - (\epsilon_e \phi_e - \epsilon_e \psi_e) \frac{\partial}{\partial n} \frac{1}{|\bar{r}_q - \bar{r}_{P_e}|} \right] \mathrm{d}s \\
& + \frac{1}{4\pi} \iint_S \left[\frac{1}{|\bar{r}_q - \bar{r}_{P_e}|} \frac{\partial}{\partial n_i} (\epsilon_i \phi_i - \epsilon_e \psi_i) - (\epsilon_i \phi_i - \epsilon_e \psi_i) \frac{\partial}{\partial n} \frac{1}{|\bar{r}_q - \bar{r}_{P_e}|} \right] \mathrm{d}s \\
= & \frac{1}{4\pi} \iint_S \left\{ \frac{1}{|\bar{r}_q - \bar{r}_{P_e}|} \left(\frac{\partial}{\partial n_i} (\epsilon_i \phi_i - \epsilon_e \psi_i) - \frac{\partial}{\partial n_e} (\epsilon_e \phi_e - \epsilon_e \psi_e) \right) \right. \\
& \left. - \frac{\partial}{\partial n} \frac{1}{|\bar{r}_q - \bar{r}_{P_e}|} (\epsilon_i \phi_i - \epsilon_e \psi_i - \epsilon_e \phi_e + \epsilon_e \psi_e) \right\} \mathrm{d}s \\
= & \frac{1}{4\pi} \iint_S \left\{ \frac{1}{|\bar{r}_q - \bar{r}_{P_e}|} \left(\epsilon_i \frac{\partial \phi_i}{\partial n_i} - \epsilon_e \frac{\partial \phi_e}{\partial n_e} + \epsilon_e \frac{\partial \psi_e}{\partial n_e} - \epsilon_e \frac{\partial \psi_i}{\partial n_i} \right) \right. \\
& \left. + (\epsilon_e \phi_e - \epsilon_i \phi_i + \epsilon_e \psi_i - \epsilon_e \psi_e) \frac{\partial}{\partial n} \frac{1}{|\bar{r}_q - \bar{r}_{P_e}|} \right\} \mathrm{d}s
\end{aligned}$$

Applying our boundary conditions, (B.2) and (B.5), we arrive at

$$\boxed{\phi(P_e) = \psi(P_e) + \frac{1}{4\pi} \frac{\epsilon_e - \epsilon_i}{\epsilon_e} \iint_S \phi(q) \frac{\partial}{\partial n} \frac{1}{|\bar{r}_q - \bar{r}_{P_e}|} \mathrm{d}s,} \tag{B.15}$$

describing the electrostatic potential at an exterior point P_e of S, [61]. As the integral in equation (B.15) is evaluated for q ranging over the entire surface S, it is clear that the potential at any point exterior to S is dependent on the surface potential distribution.

Consider the value of the integral as the point P_e approaches a particular point q_0

on the surface S.

$$\lim_{P_e \to q_0} \iint_S \phi(q) \frac{\partial}{\partial n} \frac{1}{|\bar{r}_q - \bar{r}_{P_e}|} \, \mathrm{d}s = \iint_S \phi(q) \frac{\partial}{\partial n_q} \frac{1}{|\bar{r}_q - \bar{r}_{q_0}|} \, \mathrm{d}s_q + 2\pi\phi(q_0).^{1} \tag{B.16}$$

Thus,

$$\lim_{P_e \to q_0} \phi(P_e) = \lim_{P_e \to q_0} \psi(P_e) + \lim_{P_e \to q_0} \frac{1}{4\pi} \frac{\epsilon_e - \epsilon_i}{\epsilon_e} \iint_S \phi(q) \frac{\partial}{\partial n} \frac{1}{|\bar{r}_q - \bar{r}_{P_e}|} \, \mathrm{d}s$$

$$\implies \phi(q_0) = \psi(q_0) + \frac{1}{4\pi} \frac{\epsilon_e - \epsilon_i}{\epsilon_e} \iint_S \phi(q) \frac{\partial}{\partial n_q} \frac{1}{|\bar{r}_q - \bar{r}_{q_0}|} \, \mathrm{d}s_q + \frac{\epsilon_e - \epsilon_i}{2\epsilon_e} \phi(q_0),$$

$$\implies \phi(q_0) \left(1 - \frac{\epsilon_e - \epsilon_i}{2\epsilon_e}\right) = \psi(q_0) + \frac{1}{4\pi} \frac{\epsilon_e - \epsilon_i}{\epsilon_e} \iint_S \phi(q) \frac{\partial}{\partial n_q} \frac{1}{|\bar{r}_q - \bar{r}_{q_0}|} \, \mathrm{d}s_q.$$

Hence,

$$\boxed{\phi(q_0) = \frac{2\epsilon_e}{\epsilon_e + \epsilon_i} \psi(q_0) + \frac{\epsilon_e - \epsilon_i}{2\pi(\epsilon_e + \epsilon_i)} \iint_S \phi(q) \frac{\partial}{\partial n_q} \frac{1}{|\bar{r}_q - \bar{r}_{q_0}|} \, \mathrm{d}s_q.} \tag{B.17}$$

Equation (B.17) describes the potential at the point q_0 on the surface S.

[1] [62]

References

[1] H. W. Lissmann and K. E. Machin. **The mechanism of object location in Gymnarchus niloticus and similar fish.** *J Exp Biol*, **35**:451–486, 1958. 1

[2] A. J. Kalmijn. **The detection of electric fields from inanimate and animate sources other than electric organs.** In A. Fassard, editor, *Handbook of Sensory Physiology*, pages 147–200. Springer-Verlag, Berlin, 1974. 2

[3] T. H. Bullock. **Electroreception.** *Annu Rev NeuroSci*, **5**:121–170, 1982. 2

[4] W. Heiligenberg and J. Bastian. **The electric sense of weakly electric fish.** *Annu Rev Physiol*, **46**:561–583, 1984. 2

[5] H. W. Lissmann. **Continuous electrical signals from the tail of a fish, *Gymnarchus niloticus*.** *Nature*, **167**:201–202, 1951. 2

[6] M. V. L. Bennett. **Electric organs.** In W. S. Hoar and D. J. Randall, editors, *Fish physiology*, **5**, pages 347–491. Academic Press, London, 1971. 3

[7] J. S. Albert and W. G. R. Crampton. **Electroreception and Electrogenesis.** In D. H. Evans and J. B. Claiborn, editors, *The Physiology of Fishes, 3rd Edition*, pages 431–472. Taylor & Francis Group, Boca Raton, FL, 2006. 3, 25

[8] A. A. Caputi, B. A. Carlson, and O Macadar. **Electric organs and their control.** In T. H. Bullock, C. D. Hopkins, A. N. Popper, and R. R. Fay, editors, *Electroreception*, pages 410–451. Springer Science + Business Media Inc, New York, NY, 2005. 4

[9] C. Assad, B. Rasnow, and P. K. Stoddard. **Electric Organ Discharges and Electric Images During Electrolocation.** *J Exp Biol*, **202**:1185–1193, 1999. 4, 11, 15, 16, 26, 27, 28, 38, 63, 64, 99

[10] E. I. Knudsen. **Spatial Aspects of the Electric Fields Generated by Weakly Electric Fish.** *J Comp Physiol*, **99**:103–118, 1975. 4, 19, 28, 29, 38

[11] B. Rasnow. **Electric Fish Behavior**, April 2013. 5

[12] G. von der Emde. **Active Electrolocation of Objects in Weakly Electric Fish.** *J Exp Biol*, **202**:1205–1215, 1999. 6, 16, 17, 20, 22, 56, 63, 64, 97, 99

[13] T. H. Bullock, K. S. Hagiwara, K. Kusano, and K. Negishi. **Evidence for a category of electroreceptors in lateral line of gymnotid fishes.** *Science*, **134**:1426–1427, 1961. 6

[14] A. Fessard and T. Szabo. **Mise evidence dun recepteur sensible a' lelectricite dans la peau dun mormyre.** *Seanc Acad Sci Paris*, **253**:1859–1860, 1961. 6

[15] E. S. Olson and L. D. Smullin. **Frequency Tuning in the Electroreceptive Periphery.** *Biophys J*, **55**(6):1191–1204, 1989. 7

[16] M. V. L. Bennett. **Mechanisms of electroreception.** In P. Cahn, editor, *Lateral line detectors*, pages 313–393. Indiana University Press, Bloomington, IN, 1967. 7

[17] M. V. L. Bennett. **Electroreception.** In W. S. Hoar and D. J. Randall, editors, *Fish Physiology*, **5**, pages 493–574. Academic Press, New York, NY, 1971. 7

[18] C. E. Carr, L. Maler, and E. Sas. **Peripheral Organization and Central Projections of the Electrosensory Nerves in Gymnotiform Fish.** *J Comp Neuro*, **211**:139–153, 1982. 7, 11, 39, 44, 57, 63

[19] J. M. Jorgensen. **Morphology of Electroreceptive Sensory Organs.** In T. H. Bullock, C. D. Hopkins, A. N. Popper, and R. R. Fay, editors, *Electroreception*, pages 47–67. Springer Science + Business Media Inc, New York, NY, 2005. 8

[20] S. Hagiwara and H. Morita. **Coding mechanisms of electroreceptor fibers in some electric fish.** *J Neurophysiol*, **26**:551–567, 1963. 8

[21] J. Bastian. **Frequency response characteristics of electroreceptors in weakly electric fish (Gymnotoidei) with pulse discharge.** *J Comp Physiol*, **112**:165–180, 1976. 8, 9, 55

[22] T. H. Bullock and S. Chichibu. **Further analysis of sensory coding in electroreceptors of electric fish.** In *Proc Natl Acad Sci*, **54**, pages 422–329, USA, 1965. 9

[23] Y. X. Guo and M. Kawasaki. **Representation of accurate temporal information in the electrosensory system of the African electric fish, *Gymnarchus niloticus*.** *J Neurosci*, **17**:1761–1768, 1997. 9

[24] C. D. Hopkins. **Stimulus filtering and electroreception: tuberous electroreceptors in three species of gymnotoid fish.** *J Comp Physiol*, **111**:171–207, 1976. 9, 10

[25] M. Kawasaki. **Physiology of Tuberous Electrosensory Systems.** In T. H. Bullock, C. D. Hopkins, A. N. Popper, and R. R. Fay, editors, *Electroreception*, pages 154–194. Springer Science + Business Media Inc, New York, NY, 2005. 9, 11, 12

[26] J. Bastian. **Variations in the frequency response of electroreceptors dependent on receptor location in weakly electric fish (Gymnotoidei) with a pulse discharge.** *J Comp Physiol*, **121**:53–64, 1977. 9

[27] W. Heiligenberg and J. Dye. **Labeling of electroreceptive afferents in gymnotid fish by intracellular injection of HRP: the mystery of multiple maps.** *J Comp Physiol*, **148**:287–296, 1982. 11

[28] J. E. Lewis and L. Maler. **Neuronal population codes and the perception of object distance in weakly electric fish.** *J Neurosci*, **21**:2842–2850, 2001. 11, 13, 26, 64

REFERENCES

[29] B. Bratton and J. Bastian. **Descending control of electroreception. II. Properties of nucleus praeeminentialis neurons projecting directly to the electrosensory lateral line lobe.** *J Neurosci*, **10**:1241–1253, 1990. 11

[30] E. Sas and L. Maler. **The nucleus praeeminentials: a Golgi study of a feedback center in the electrosensory system of gymnotiform fish.** *J Comp Neurol*, **221**:127–144, 1983. 12

[31] G. von der Emde, S. Schwarz, L. Gomez, R. Budelli, and K. Grant. **Electric fish measure distance in the dark.** *Nature*, **395**:890–894, 1998. 15, 16, 17, 20, 22, 25, 56, 61, 63, 64, 97, 98, 99, 101

[32] B. Rasnow. **The effects of simple objects on the electric field of Apteronotus.** *J Comp Physiol (A)*, **178**:397–411, 1996. 15, 17, 20, 21, 23, 25, 27, 41, 63, 64, 66, 97, 98, 99, 103

[33] B. Rasnow and J. M. Bower. **Imaging with electricity: How weakly electric fish might perceive objects.** In *Proceedings of Computational Neuroscience: Trends in Research*, New York, NY, 1997. Plenum Press. 15, 21, 63, 64, 99

[34] S. Schwarz and G. von der Emde. **Distance Discrimination During Active Electrolocation in the Weakly Electric Fish Gnathonemus petersii.** *J Comp Physiol (A)*, **186**:1185–1197, 2001. 16, 17, 22, 25, 52, 56, 63, 64, 96, 99

[35] M. J. Toerring and P. Belbenoit. **Motor programmes and electroreception in mormyrid fish.** *Behav Ecol Sociobiol*, **4**:369–379, 1979. 18, 26

[36] S. A. Stamper, E. Roth, N. J. Cowan, and E. S. Fortune. **Active sensing via movement shapes spatiotemporal patterns of sensory feedback.** *J Exp Biol*, **215**:1567–1574, 2012. 18

[37] W. F. Heiligenberg. **Theoretical and experimental approaches to spatial aspects of electrolocation.** *J Comp Physiol*, **103**:247–272, 1975. 18

[38] M. J. Lannoo and S. J. Lannoo. **Why do electric fishes swim backwards? An hypothesis basied on gymnotiform foraging behavior interpreted through sensory contstraints.** *Environ Biol Fishes*, **36**:157–165, 1993. 18

[39] M. MacIver. *The computational neuroethology of weakly electric fish: body modeling, motion analysis, and sensory signal estimation.* PhD thesis, University of Illinois, Urbana-Champaign, US, 2001. 18

[40] M. Sim and D. Kim. **Electrolocation based on tail-bending movements in weakly electric fish.** *J Exp Biol*, **214**:2443–2450, 2011. 18, 23, 25, 27, 63, 64, 98, 99

[41] V. Hofmann, J. I. Sanguinetti-Scheck, L. Gomez-Sena, and J. Engelmann. **From static electric images to electric flow: Toward dynamic perceptual cues in active electroreception.** *J Physiol Paris*, pages –, 2012. 18, 25, 26, 63, 64, 98, 99

[42] L. Chen, J. L. House, R. Krahe, and M. E. Nelson. **Modeling signal and background components of electrosensory scenes.** *J Comp Physiol A*, **191**:331–345, 2005. 19, 27, 28, 30, 43, 49

[43] D. Babineau, J. L. Lewis, and A. Longtin. **Spatial acuity and Prey detection in weakly electric fish.** *PLoS Comput Biol*, **3**(3):402–411, 2007. 19

[44] B. Rasnow and J. M. Bower. **The electric organ discharges of the gymnotiform fishes: I. Apteronotus leptorhynchus.** *J Comp Physiol (A)*, **178**:383–396, 1996. 20, 28, 38, 39, 43, 71

[45] M. J. Toerring and P. Moller. **Locomotor and electric displays associated with electrolocation during exploratory behavior in mormyrid fish.** *Behav. Brain Res.*, **12**:291–306, 1984. 26

[46] K. Behrend. **Cerebellar influence on the time structure of movement in the electric fish Eigenmannia.** *Neuroscience*, **13**(1):171–178, 1984. 26

[47] J. R. Solberg, K. M. Lynch, and M. A. MacIver. **Robotic electrolocation: Active underwater object localization with electric fields.** In *IEEE International Conference on Robotics and Automation*, Rome, Italy, 2007. 27

[48] J. R. Solberg, K. M. Lynch, and M. A. MacIver. **Active Electrolocation for Underwater Target Localization.** *Int J Robot Res*, **27**(5):529–548, 2008. 27

[49] J. Bastian. **Gain control in the electrosensory system: a role for the descending projections to the electrosensory lateral line lobe.** *J Comp Physiol A*, **158**(4):505–515, 1986. 28

[50] M. E. Nelson and M. A. MacIver. **Prey capture in the weakly electric fish *Apteronotus albifrons*: sensory acquisition strategies and electrosensory consequences.** *J Exp Biol*, **202**(10):1195–1203, 1999. 28

[51] J. V. Stewart. *Intermediate Electromagnetic Theory.* World Scientific Publishing Co., Singapore, 2001. 30

[52] G. B. Arfken, H. J. Weber, and F. E. Harris. *Mathematical Methods for Physicists: A Comprehensive Guide*, chapter 15. Elsevier Inc., Oxford, UK, seventh edition, 2012. 34

[53] D. Bodznick and J. C. Montgomery. **The physiology of Low-Frequency Electrosensory Systems.** In T. H. Bullock, C. D. Hopkins, A. N. Popper, and R. R. Fay, editors, *Electroreception*, pages 132–153. Springer Science + Business Media Inc, New York, NY, 2005. 49, 64

[54] J. A. Freund, L. Schimansky-Geier, B. Beisner, A. Neiman, D. F. Russell, T. Yakusheva, and F. Moss. **Behavioral Stochastic Resonance: How the Noise from a Daphnia Swarm Enhances Individual Prey Capture by Juvenile Paddlefish.** *J Theor Biol*, **214**:71–83, 2002. 51, 53

[55] B. Kramer. **Waveform Discrimination, Phase Sensitivity and Jamming Avoidance in Wave-type Electric Fish.** *J Exp Biol*, **202**:1387–1389, 1999. 52

[56] D. F. Russell, L. A. Wilkens, and F. Moss. **Use of behavioural stochastic resonance by paddlefish for feeding.** *Nature*, **402**:291–294, 1999. 54, 55, 99

[57] E. S. Fortune and M. J. Chacron. **Physiology of Tuberous Electrosensory Systems**. In A. P. Farrell, editor, *Encyclopedia of Fish Physiology: From Genome to Environment*, pages 366–374. Academic Press, San Diego, CA, 2011. 55

[58] T. W. Edwards. *Perturbation of a Uniform Electrostatic Field by a Dielectric Cube*. Master's thesis, University of Wisconsin, Madison, US, 1961. 56

[59] M. Mohan, K. Mayekar, R. Zhou, G. von der Emde, and H. Bousack. **Investigation of a Bubble Detector based on Active Electrolocation of Weakly Electric Fish**. *J. Phys.: Conf. Ser.*, **434**(1), 2013. 101

[60] J. D. Jackson. *Classical Electrodynamics*, chapter 1. John Wiley & Sons, Inc., New York, NY, second edition, 1975. 116

[61] T. W. Edwards and J. van Bladel. **Electrostatic Dipole Moment of a Dielectric Cube**. *Appl Sci Res (B)*, **9**:151–155, 1961. 118

[62] O. D. Kellogg. *Foundations of Potential Theory*. J. Springer, New York, NY, 1929. 119

Declaration

I herewith declare that I have produced this paper without the prohibited assistance of third parties and without making use of aids other than those specified; notions taken over directly or indirectly from other sources have been identified as such. This paper has not previously been presented in identical or similar form to any other Canadian or foreign examination board.

The thesis work was conducted from 2007 to 2013 under the supervision of Drs. Huaxiong Huang and Greg Lewis at York University.

Toronto,